EPOXIDIZED SUCROSE SOYATE AND DERIVATIVES AS BIODERIVED

CROSSLINKERS IN VARIOUS THERMOSETS

A Dissertation
Submitted to the Graduate Faculty
of the
North Dakota State University
of Agriculture and Applied Science

By

Samantha Danielle Silbert

In Partial Fulfillment of the Requirements
for the Degree of
DOCTOR OF PHILOSOPHY

Major Department:
Coatings and Polymeric Materials

October 2019

Fargo, North Dakota

North Dakota State University
Graduate School

Title

EPOXIDIZED SUCROSE SOYATE AND DERIVATIVES AS BIODERIVED
CROSSLINKERS IN VARIOUS THERMOSETS

By

Samantha Danielle Silbert

The Supervisory Committee certifies that this ***disquisition*** complies with North Dakota

State University's regulations and meets the accepted standards for the degree of

DOCTOR OF PHILOSOPHY

SUPERVISORY COMMITTEE:

Dean Webster

Chair

Andriy Voronov

Stuart Croll

Siew Lim

Approved:

10-3-2019	Dean Webster
Date	Department Chair

ABSTRACT

Throughout the world, alternatives to petrochemically-derived materials are being sought. Aside from petrochemical feedstocks with precarious futures, materials that are derived from renewable resources such as crops are attractive. Epoxidized sucrose soyate is a material made from soybean oil and sucrose. Its rigid sucrose core, flexible aliphatic chains, and many modifiable epoxy sites make it an attractive candidate to replace petrochemically derived materials in a multitude of thermosets. This dissertation encompasses studies of ESS and its derivatives for the development of thermosets in a variety of processes. Namely, ESS-derived polycarbamates for use in ambient-curing polyurethane coatings produced via carbamate-dialdehyde crosslinking, ESS-derived acrylic resins for their use in stereolithographic printing, and UV-curable epoxy coatings from both ESS and adhesion-promoting derivatives. The incorporation and effect of strengthening and/or processing additives were also assessed in the mentioned ESS-containing thermosets. Each topic involves a unique area where formulations use resins derived from petrochemicals; several posing health and/or environmental concerns. Investigations to match or exceed the performances of conventional formulations with alternatives made with ESS further demonstrate the remarkable tunability and versatility of this material, as well as the assets available to lessen reliance on petrochemicals with the use of a renewable resource.

ACKNOWLEDGEMENTS

me as a Summer Journeyman fellow in your group. It was a fantastic experience and I learned so much. Among Dr. Escarsega's group, a thank you to Maria, Fred, Dan, Heather, Raven and Felicia. It was amazing to spend the summer in the Aberdeen Proving Ground and learn from you all! I wish you all the best.

To Dr. Michelle Francl, thank you for your encouragement in my pursuit of a higher education.

To my dear friends and family, thank you for helping me accomplish my goals and always being there for me.

Lastly, thank you to my husband, Eric. I look forward to our future and growing old by your side. You are the best thing that ever happened to me and I will spend the rest of my life doing all that I am able to thank you properly. For a long and happy voyage.

DEDICATION

For Mom & Dad, Jim & Wendy, and my husband Eric.

PREFACE

"Spallanzani began fumblingly to learn how to grow wee beasts, and how to use a microscope. He cut his hands and broke large expensive flasks. He forgot to clean his lenses and sometimes saw his little animals dimly through his fogged glasses—just as you can faintly make out minnows in the water riled up by your net. He raved at his blunders; he was not the dogged worker that Leeuwenhoek had been—but despite his impetuousness he was persistent—he must prove that these yarns about the animalcules were yarns, nothing more. But wait! *"If I set out to prove something, I am no real scientist—I have to learn to follow where the facts lead me—I have to learn to whip my prejudices…"* And he kept on learning to study little animals, and to observe with a patient, if not an unprejudiced eye, and gradually he taught the vanity of his ideas to bow to the hard clearness of his facts."

—Paul De Kruif on Lazzarro Spallanzani, *The Microbe Hunters*, 1926.

TABLE OF CONTENTS

ix

LIST OF TABLES

LIST OF FIGURES

xvii

LIST OF EQUATIONS

LIST OF ABREVIATIONS

UV…………………………..……………………………………………………Ultraviolet

ESS……………………………………………………………….Epoxidized Sucrose Soyate

MSSP………………………………………………………...Methoxy Sucrose Soyate Polyol

ESSP………………………………………………………...Ethoxy Sucrose Soyate Polyol

PSSP……………………………………………………….Propoxy Sucrose Soyate Polyol

AP…………………………..…………………………………………………Alkyd Polyol

TCAP…………………………………………………...Transcarbamoylated Alkyd Polyol

CMSSP………………………………………...Transcarbamoylated Methoxy Sucrose Soyate Polyol

CESSP……………………………………..Transcarbamoylated Ethoxy Sucrose Soyate Polyol

CPSSP……………………………………………Transcarbamoylate Ethoxy Sucrose Soyate Polyol

EEW………………………………………………………….Epoxy Equivalent Weight

AN………………………………………………………………………Acid Number

OHEW......…………………………………………………….Hydroxyl Equivalent Weight

CEW…………………………………………………………..Carbamate Equivalent Weight

NIPU……………………………………………………………...Non-Isocyanate Polyurethane

CHDA…………………………………………………...Cyclohexanedicarboxaldehyde

HMF……………………………………………………………Hydroxymethylfurfural

DFF……………………………………………………………………….Diformylfuran

SLA………………………………………………………………...Stereolithography

CAD………………………………………………………………Computer-Assisted Design

PDMS……………………………………………………………..Polydimethylsiloxane

MBSS………………………………………………...Methacrylated Butyl Sucrose Soyate

DMESS…………………………………………………….Dimethacrylated Butyl Sucrose Soyate

AESS……………………………………………………Acrylate Epoxidized Sucrose Soyate

BPAEDA…………………………………………………Bisphenol-A Ethoxylate Diacrylate

m-POSS……………………………………. Methacrylated Polyoligomeric Silsqueloxane

g-POSS……………………………………………Glycidyl Polyoligomeric Silsqueloxane

CGE……………………………………………………Cardanol Glycidyl Ether

BAESS………………………………………………Benzoic Acid Epoxidized Sucrose Soyate

MHBAESS…………………………………Monohydroxybenzoic Acid Epoxidized Sucrose Soyate

DHBAESS…………………………………..Didydroxybenzoic Acid Epoxidized Sucrose Soyate

PAESS………….…………………………………..Protocatechuic Acid Epoxidized Sucrose Soyate

PESS………………………………………………Phosphonated Epoxidized Sucrose Soyate

MEKDR…………………………………………………..Methyl Ethyl Ketone Double Rubs

DMA………………………………………………………Dynamic Mechanical Analysis

TGA……………………………………………………….Thermogravimetric Analysis

DSC……………………………………………………..Differential Scanning Calorimetry

GPC…………………………………………………....Gel-Permeation Chromatography

FTIR………………………………………………Fourier-Transform Infrared Spectroscopy

ATR-FTIR………………Attenuated Total Reflectance Fourier-Transform Infrared Spectroscopy

NMR…………………………………………….Nuclear Magnetic Resonance Spectroscopy

CHAPTER 1. INTRODUCTION

Sustainable Thermosets

Sustainability is often thought of as using available resources in a way that allows their use to be maintained for the foreseeable future. The definition can be expanded to one of *balance*; often in the context of the environment. Mankind is growing and evolving; the growth of population goes hand-in-hand with reliance on more energy and materials. Petrofuels and petrochemical-based materials have provided numerous benefits and petrochemically-derived plastics and energy are dominant in our daily lives. However, their increased use has posed issues such as environmental damage upon extraction and refining of petrofuels, nondegradable plastic waste, poor air quality and climate change from fossil fuel combustion. Further there stands the precarious future of this finite resource. The use and reliance of petrochemicals is undoubtedly an example where there is a severe lack of balance with the environment.

It is these reasons that there has long been a push for renewable alternatives to petrochemical fuels and chemical feedstocks. If well managed, bioderived feedstocks can be regrown and replaced; their future does not have a finiteness like petrochemicals. However, challenges are posed through the use of bioderived feedstocks for materials. Among them are harvest, refining, and modification that may for companies be more challenging or expensive to switch from processes that use petrochemicals. Material properties that can rival that of conventional petro-products are the first step to make bioderived alternatives more attractive.

This thesis investigates the use of epoxidized sucrose soyate; a material made from soybean oil and sugar. Modifications of this multifunctional material were explored as sustainable crosslinking alternatives to petrochemically-derived materials in a variety of thermosets. Specifically, these thermosets are for polyurethane coatings, epoxy coating, and

acrylic, 3D-printable inks. Whether it is through making a coating or 3D-printed material more bioderived or making a process less toxic, using a renewable material can better balance mankind's ever-growing and changing material demands now and in the future.

Thermosetting Resins

A thermoset is an irreversible polymer network formed by crosslinking reactions of polymers or prepolymers. Unlike a thermoplastic, where material properties come from intermolecular forces between entangled chains, thermoset properties arise from covalent bonds at crosslinks. The number and density of these linkages can be correlated to properties such as chemical resistance, strength, and durability. An understanding of these structure-property relationships and ability to tune properties makes apparent the value of thermosetting materials in industrial applications. These industries range from food packaging, protective coatings, electrical insulators, foams, fabrics, composites, and innumerable others.[1-5]

While the goal of a finished product is to meet or exceed determined performance parameters, much more must be considered in the design of a thermosetting material. Aspects of the synthesis and processing must be considered. Among them, safety, suitable viscosity for the application method, other additives for the speed, efficiency, and stability of the crosslinking reaction (initiators, light stabilizers), additives to lessen cost or strengthen the network, and even compatibility of cosmetic additives (dispersed pigments, surfactants).[6]

The previously-mentioned considerations did not bring up concerns of recent times, namely, sustainability of materials, energy utilization, dependence on non-renewable resources, waste production and disposal, toxicity, use of heavy metals, and volatile organic compounds.[7-10] It is these reasons among many others that consumers, governmental organizations, and industry have been eyeing alternatives to petrochemically-derived materials that come from biobased

sources. The ultimate challenges with the feasibility of replacements come from whether they meet or exceed the properties of their counterparts and are not out of reach due to cost. Only until very recently have bioderived alternatives reached a lower average of being 2-4 times the cost of petrochemical options.[11] It is a factor why bioplastics amount to less than one percent of all plastics manufactured worldwide.[12]

Plant Derivatives and Modifications for Use in Thermosets

There are a large variety of bio-derived sources in consideration for thermoset applications. Plant oils are attractive candidates for starting materials given their commercial availability, low cost, and low toxicity.[13,14] Wood, starches, sugars, and other biomass further expand the arsenal of bio-derived starting materials for thermosets.[15]

Plant oils are triglycerides, or esters of 3 fatty acids and glycerol. The degree of unsaturation on the fatty acid chains influence their structures and ultimately how one may further tune their structures. Plant oils with high amounts of unsaturation, such as tung, linseed, walnut, and soybean are able to crosslink under exposure to air through the process of autoxidation. This property of what is classified as *drying oils* led to their cultivation and use as some of the oldest known paint binders and varnishes. The representative structure of a soybean oil triglyceride is seen in **Figure 1.1**.[16]
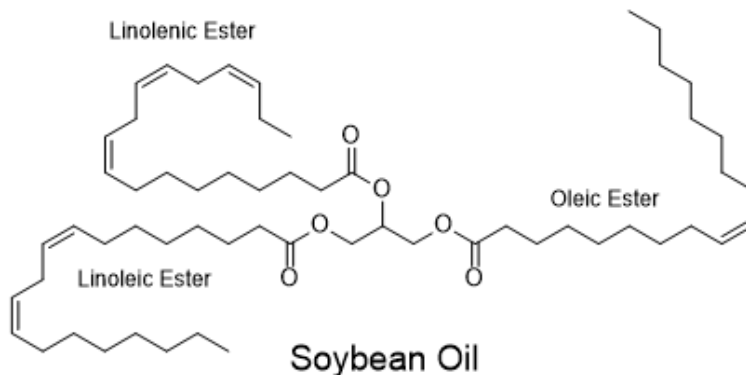
Figure 1.1. Representative Structure of a Soybean Oil Triglyceride

Modifications of plant oils have had a long history and continue to be pursued in a variety of methods today. An example from the early 20th century was alkyd resins developed in the 1920s.[14,17] These resins involved a transesterification of a triglyceride with petrochemically-derived polyols and carboxylic acids and anhydrides (**Figure 1.2**). The resulting resins were able to be cured in contact with air like drying oils, however the esterified acids and anhydrides (particularly phthalate acids and anhydrides) both greatly increased the molecular weight of the resin and imparted valuable rigid properties.[14]
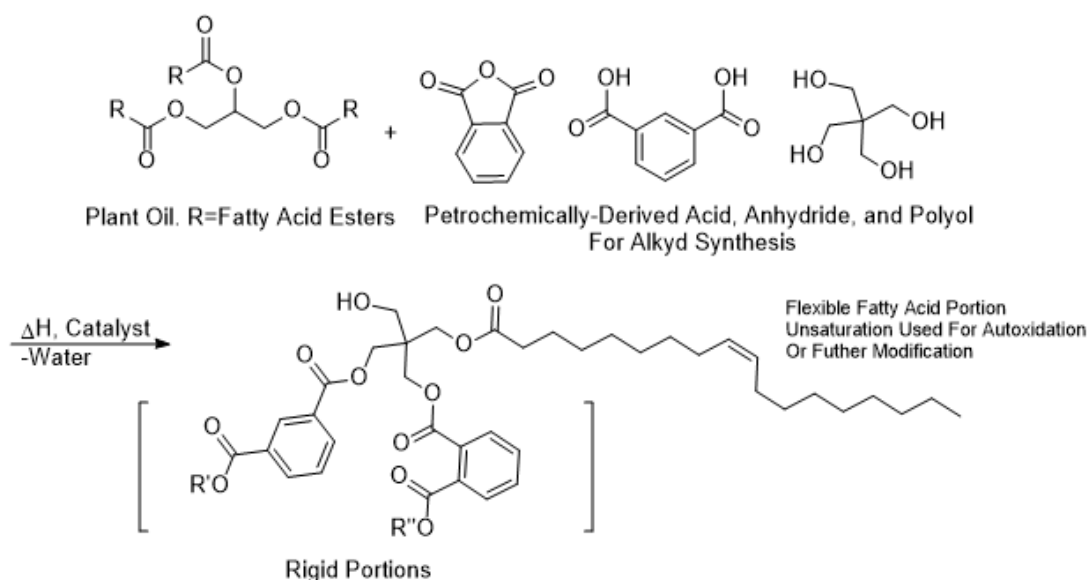
Figure 1.2. Representative Synthesis and Structure of an Alkyd Polyol from a Plant Oil Triglyceride

Subsequently discovered modifications allow tuning of bioderived materials with unsaturation. One such method is through thiol-ene chemistry, where a thiol reacts with an alkene. This method is touted for its high yield, rate, and stereoselectivity, however there are issues with certain plant oils being modified this way. These are primarily due to hindrances with conversion of highly unsaturated fatty acids, the necessitation to use large amounts of mercaptans, and the notoriously unpleasant odor of mercaptans.[18-20] Another method is by epoxidizing the unsaturation of the plant oil with peroxyacids, peroxides, catalysts, and/or

enzymes. Epoxy, or oxirane groups are reactive and can be crosslinked with themselves or modified further by ring-opening the epoxide with alcohols or acids.[21,22] Many epoxidized plant oils are commercially available, and while they are primarily used as plasticizers, coatings and plastics are also produced from these starting materials. While modification of the fatty acids of the plant oil triglycerides is well known, the number of crosslinking sites available on plant oil chains can be limited and the produced thermosets are soft. This limits them as strong alternatives to petrochemically-derived counterparts. However, like alkyds, modification of plant oil triglycerides through transesterification of the fatty acids with a highly functional polyol can increase the number of fatty acid esters present in a single molecule instead of 3 in the triglyceride. More fatty acid esters with unsaturation mean more sites to epoxidize, and more oxirane means more sites able to crosslink/be modified for crosslinking. Epoxidized sucrose soyate (ESS) is a bio-derived material that uses this logic of establishing more crosslinking sites to produce easily modifiable and high-performance materials.

Lignin has likewise received attention and been modified to be a thermosetting resin. It has many modifiable sites and is an inexpensive biproduct, however issues with its inherently dark color and differences in irregularities in structure hinder wider adoption.[23] However, lignin has remained of interest as a material feedstock given procedures have been developed to produce smaller molecular derivatives from lignin.[24] Lignin is a biopolymer produced by plants that acts as a structural support. Derivatives of its rigid, aromatic structures that aid in its structure-supporting behavior have been proposed for use as replacements for petrochemicals in applications such as reactive diluents and coating crosslinkers.[25] The representative structure of lignin and some smaller molecular derivatives of interest, guaiacol and syringol, can be seen in **Figure 1.3**.
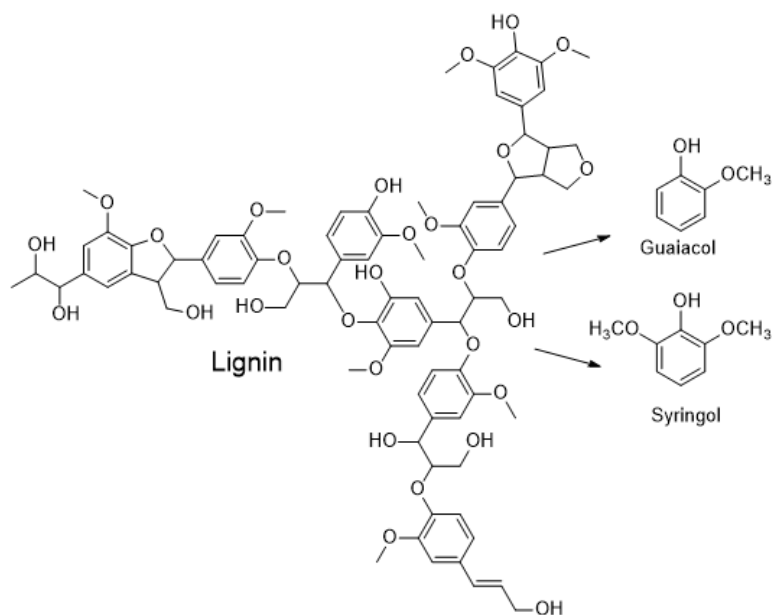
Figure 1.3. Lignin and Derivatives of Interest

Hydroxymethylfurfural (HMF) is another notable biobased material. Specific sugars that undergo acid-catalyzed polycondensation produce HMF.[26,27] HMF has been functionalized for use in a variety of thermosets.[28-30] Its rigid structure and ease of production at large scale have made its derivatives of interest as alternatives to petrochemicals such as 2,5-furandicarboxylic acid replacing terephthalic acid in the production of polyesters and 2,5-diformylfuran replacing cyclohexanedicarboxaldehyde as a non-isocyanate polyurethane crosslinker.[31]

Epoxidized Sucrose Soyate

Sucrose, or table sugar, is a disaccharide composed of fructose and glucose. Polyesters of unsaturated fatty acids and sucrose have been around since the 1960s, however highly substituted sucrose-fatty acid polyester have only been around the past couple of decades.[32] Procter and Gamble in 2003 released a highly substituted (7.7 out of 8 sites) polyester of sucrose and soybean oil under the trade name SEFOSE.[33] The fatty acids primarily present in soybean oil include linolenic (7-10%), linoleic (51%), and oleic acid (23%).[34] Thus, a highly substituted polyester of sucrose combined with mono or polyunsaturated fatty acid chains creates a sucrose

soyate material with many sites to functionalize. SEFOSE, sucrose, and the fatty acids of soybean oil are seen in **Figure 1.4**. Using peroxide, highly reactive oxirane could be generated at each unsaturated site on the molecule. The resultant material, *epoxidized sucrose soyate* (**Figure 1.4**) is completely bioderived, facile to tune and modify, and can be scaled up to pilot scale amounts.[35] It is straightforward that ESS derivatives have been used in a large variety of thermosets. Among them are thermosets formed from mono and dimethacrylates, epoxy-anhydrides, polyurethanes, non-isocyanate polyurethanes, UV-curable epoxy, and epoxy-diacids.[36-40] Further, thermosets are prized for their mechanical properties where their strength can be traced to dense crosslinking. ESS contains both a rigid sucrose core and many crosslinking sites. These traits coupled with the modifiability, enable ESS to be a valuable tool to produce strong thermosets through multitudinous crosslinking chemistries.
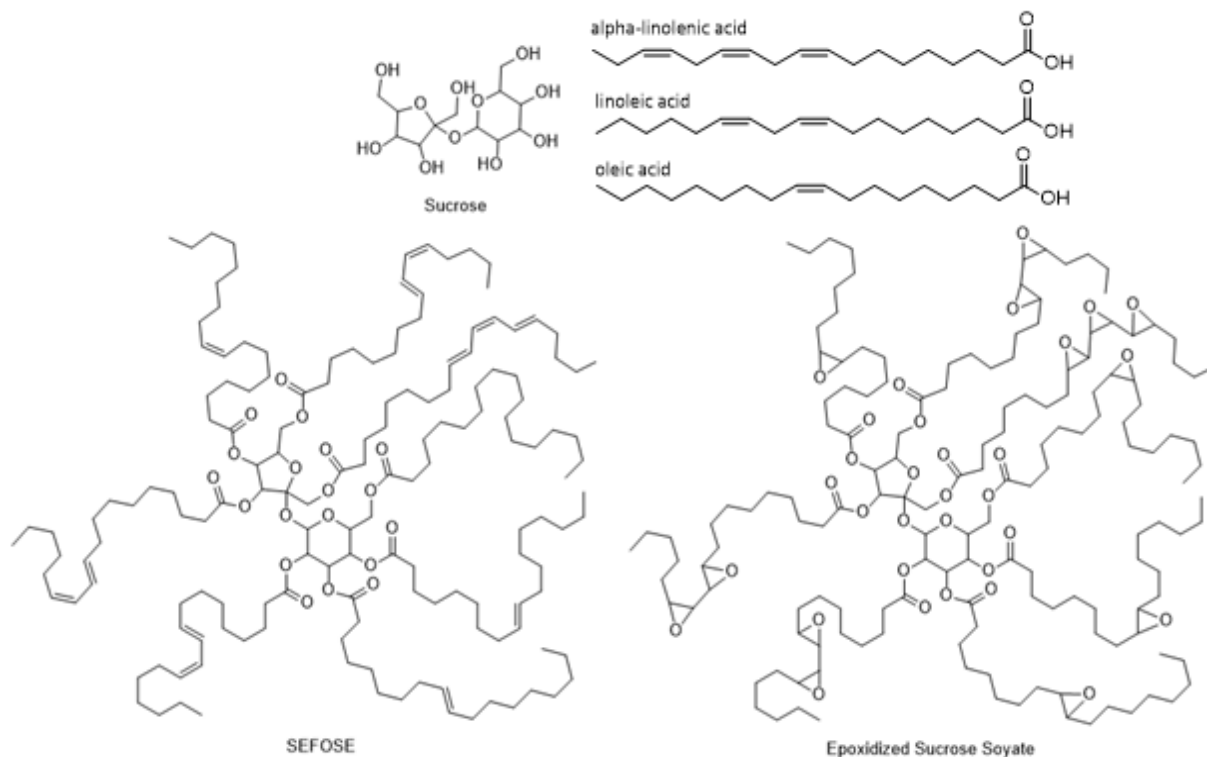
Figure 1.4. Sucrose, Primary Fatty Acids of Soybean Oil (Alpha-Linolenic, Linoleic, Oleic), SEFOSE, and Epoxidized Sucrose Soyate

7

Notable Applications for Bio-Derived Alternatives

There is an enormous amount of thermoset applications where bio-derived resins may be able to substitute petrochemical ones. ESS and its derivatives are being considered due to their polyfunctionality and ease of tuning. Derivatives of lignin and HMF are considered as crosslinkers or diluents for ESS thermosets to increase or make a thermoset almost completely bioderived. The following categories of thermosets were investigated for this dissertation.

Non-Isocyanate Polyurethanes

Polyurethane is an important thermoset that is used in coatings, foams, and molded thermosets. It is valuable for its chemical resistance, weatherability, and toughness that arise from hydrogen bonding. Typically, polyurethane is formed by the reaction of a polyol and a polyisocyanate (**Figure 1.5**). Concerns arise from the exposure to isocyanate given they are sensitizers, or materials that produce an allergic response after repeat exposure. In some instances, such as those with automotive painters spraying isocyanate, exposure has been fatal.[42,43] These concerns have been an impetus for researchers to find routes that can produce polyurethane thermosets without the use of isocyanates. Many approaches exist, however hindrances to these routes include toxic starting materials, production of the starting materials using toxic reagents, mediocre mechanical properties, and poor reactivity under similar conditions in comparison to conventional hydroxyl-isocyanate reactions.[44]
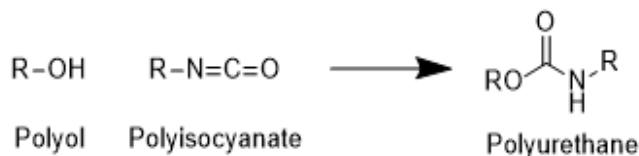
Figure 1.5. Formation of Polyurethane by Hydroxyl-Isocyanate Crosslinking

Cornille et al reviewed a multitude of non-isocyanate polyurethane routes. Each were classified by the type of reaction; ring opening polymerization (cyclic carbamate-aziridine

8

crosslinking), polyadditions (cyclic carbonate-amine crosslinking), rearrangements (carboxamide-polyol crosslinking, azides), and polycondensations (carbonate-amine, polycarbamate-polyol, carbamate-aldehyde crosslinking). Many of the crosslinkers mentioned necessitate the use of toxic phosgene.

Cyclic carbonate-amine and carbamate-aldehyde crosslinking do not require phosgene. Benefits of cyclic carbonates are that they do not have moisture sensitivity like isocyanate where reacting with water produces CO_2 and urea, nor do they release volatile organic compounds during crosslinking. This relieves concerns involving both storage and application. While there is an impressive amount of literature on this route, a commonly cited hindrance is the poor procession of the reaction with 5 and 6-membered cyclic carbonate rings at room temperature. However, recent publications found the use of 8-membered cyclic carbonate rings to proceed both at room temperature and without a catalyst.[45]

Carbamate-aldehyde crosslinking also poses more advantages than the lack of phosgene. This method (**Figure 1.6**) is touted for curing rapidly at ambient temperatures and having a long potlife. A fairly new method, this technology is limited in that there are few multifunctional aldehyde crosslinkers available for purchase. Most commonly, the aldehyde crosslinker is a mixture of 1,4 and 1,3-cyclohexane dicarboxaldehyde (CHDA). This material is sold under the trade name PARALOID EDGE by DOW Chemical and is crosslinked with resins which are acrylic and alkyd-derived polycarbamates. Alternative crosslinkers that are derived from lignin or HMF can introduce new architectures; thus, introducing far more crosslinking options to this method. Rigidity is often imparted by cyclic structures and these derivatives are rich sources of aromatic structures. CHDA and lignin/HMF dialdehyde crosslinkers are seen in **Figure 1.7**.[46-48]
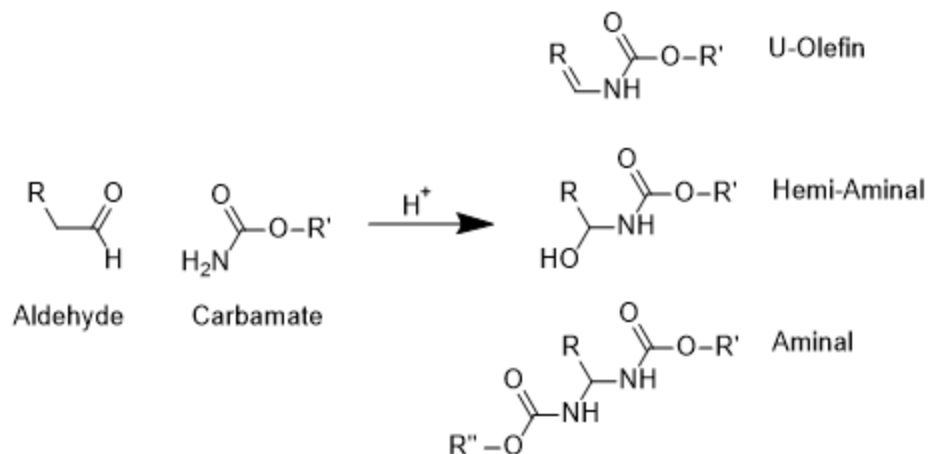
Figure 1.6. Formation of Polyurethane Linkages Via Aldehyde and Carbamate Crosslinking
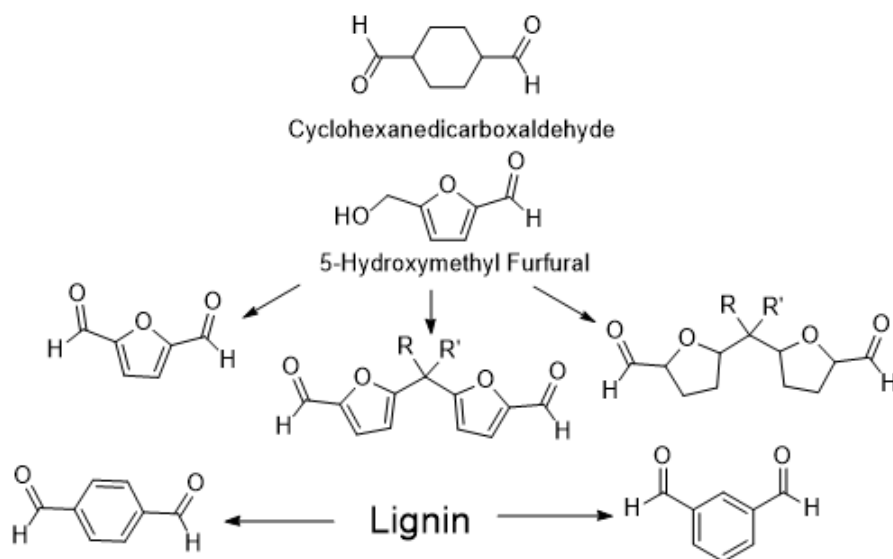
Figure 1.7. CHDA and Dialdehyde Crosslinkers Derived from HMF and Lignin

The polycarbamate component is flexible in that it is produced through the modification of a polyhydroxyl resin through the process of transcarbamoylation. There are many bioderived polyhydroxyls available for modification. ESS is an excellent candidate to form a polycarbamate resin given there are established protocols to turn ESS into a polyhydroxyl compound. Pan et al. determined an alkoxylation method by ring-opening ESS with various alcohols and an acid catalyst.[49] A secondary hydroxyl can then be transcarbamoylated and make a polyfunctional

carbamate resin. ESS and bioderived dialdehydes thus have the potential to make a highly bioderived, non-isocyanate polyurethane system.

3D-Printable Resins

3D printing is a technique where a 3-dimensional structure is built by printing layer by layer. This technique is also termed *additive manufacturing*.[50] There are an enormous variety of 3D-printing techniques. They are usually differentiated by the materials used or the way the layer is added. Specifically, techniques categorized by materials are those that build plastic or metal structures while techniques categorized by layer addition are those by stereolithographic or extrusion methods. Metal 3D-printed structures involve a powder bed where layers of metal powder are sintered together. This method is limited in that is uses a large amount of power and the set-up is prohibitively expensive. However, it is rapidly improving and becoming more accessible to non-commercial users. Notably, there is a large amount of interest in the aircraft industry to develop airplane parts by metal 3D printing.[51] Plastic methods can involve thermoplastics, which are commonly seen in the extrusion methods, or prepolymers that become thermosets when using stereolithographic methods.[52]

The applications of 3D printed materials are enormous. Rapid prototyping for product development, agile tooling, and research are some of the most common justifications for those in industry. However, since several additive manufacturing methods have become cheaper and more open-source, 3D-printing hobbyists are now a major segment. Other markets of interest for 3D printing include food, medical care, automotive, construction, apparel, computers, robotics, aerospace, and art among others.[53]

Stereolithography or *vat* polymerization is a type of 3D printing where there is a build platform that lowers into a vat of prepolymer formulation. This vat is usually coated with a low

surface energy polymer like polydimethysiloxane (PDMS) or fluoropolymers. The oxygen

content of PDMS further aids by inhibiting the free radical curing of the polymer so it does not

cure on the vat. Exposure to a laser through the bottom of the vat cures a small layer of

prepolymer to the build platform. The platform then moves away from the vat before lowering

again, re-wetting, and repeating another layer. Each of these layers correspond to a slice of a

CAD file (STL).[54] Eventually, a 3D thermoset is formed. This process is illustrated in **Figure
1.8**.
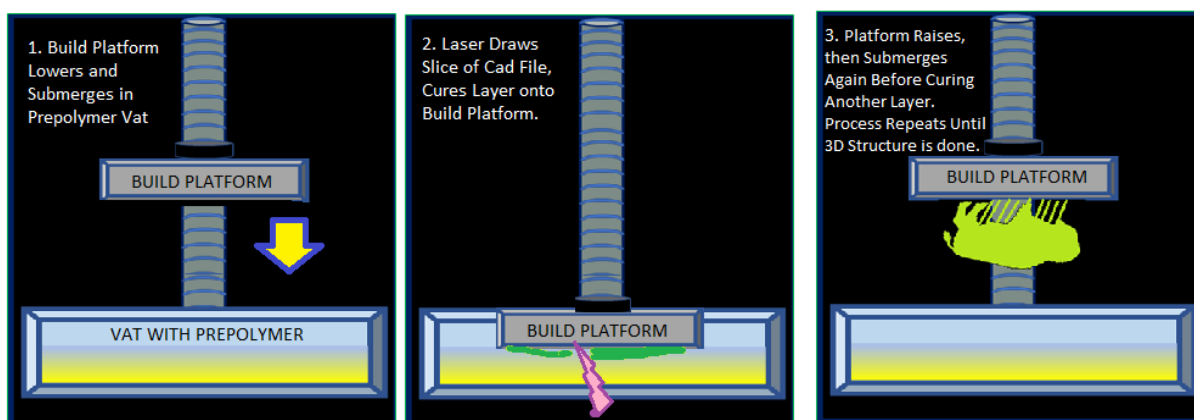
Figure 1.8. Process of Stereolithographic Printing

     For a formulation to be successful as a printable ink through stereolithography, many

formulation parameters must be met. First, the formulation needs to be able to precisely cure

under the brief exposure to a laser of specific wavelength and power respective of the printer

utilized. It needs to cure well enough and build upon itself, but not cure *too well* so that it does

not risk damaging the vat or the printer when it repeatedly separates from the vat. An

understanding of the actinic wavelengths of the photoinitiator in the formulation as well as how

the functional groups participating in covalent bond formation cure is imperative. The glass

transition of the final thermoset is also of importance during material selection given one does

not want a polymer so weak that it fragments/breaks during the printing process or again, harm

the printer. Additives such as pigments can also impact scattering and adsorption of laser light meant for specified curing, so adjustments may need to be made for formulations whose only difference is color. Some printers allow modification of laser power to aid in under-curing so a strong enough thermoset can be printed without harming the printer, while a post-cure regime in an oven or under lights can fully cure the structure. Next, there are diluents and crosslinkers which can be absorbed into the vat's PDMS layer and warp it, risking the print as well as the printer. Further, the formulation needs to be low enough viscosity that the platform is sufficiently rewetted each time it moves away. A high viscosity formulation also puts the print at risk given it may cause a print to fall off the platform when it pulls back. Lastly, removal from the platform can break the print itself or impart a stress on the print which can influence a property of interest, such as if it is a flexural or tensile sample. It is extremely common, and in most cases necessary, to add structural supports to ease removal, protect the print, as well as allow prints in different orientations. This can be completed by using a supplemental software such as XYZ Nobel to rotate/move the structure and add supports.

In this software approach, one can *lift* an object in the Z-axis before supports are added. These supports can be both manually added (which may be necessary for delicate structures) or automatically generated. The appearance of different orientations in XYZ Nobel software as well as their appearance after auto-generated supports are added can be seen in **Figure 1.9**. While supports are vital, they do (sometimes drastically) increase the time to complete a print as well as consume resin.
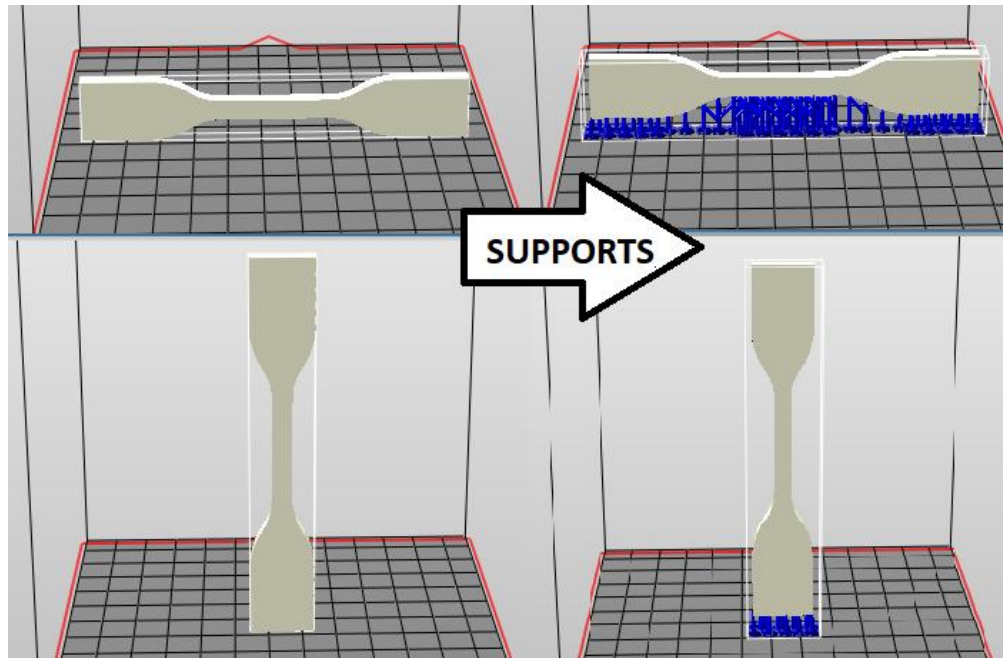
Figure 1.9. Appearance of Tensile Samples in Different Orientations and Autogenerated Supports in XYZ Nobel Software

Formulations used for SLA printing are composed of resins, reactive diluents, and photoinitiators that are actinic under the laser conditions of the printer. Most commonly, these thermosets are built upon the crosslinking of acrylate functionalities by free-radical polymerization. As an example, the Peopoly Moai Blue formulation for printing on a Peopoly Moai SLA Printer contains a urethane acrylate, a rigid acrylic monomer such as bisphenol-A ethoxylate diacrylate (BPAEDA), the diluent hexanedioldiacrylate (HDDA), and the photoinitiator benzophenone. This formulation analyzed by gel-permeation chromatography in **Figure 1.10** showed a urethane acrylate content of ~42%, ~12% BPAEDA, and ~45% HDDA. Modifying ESS to become a polyacrylic that can be used in an SLA ink involves juggling processing parameters alongside the compatibility of ESS with other components to ensure a successful printing process.
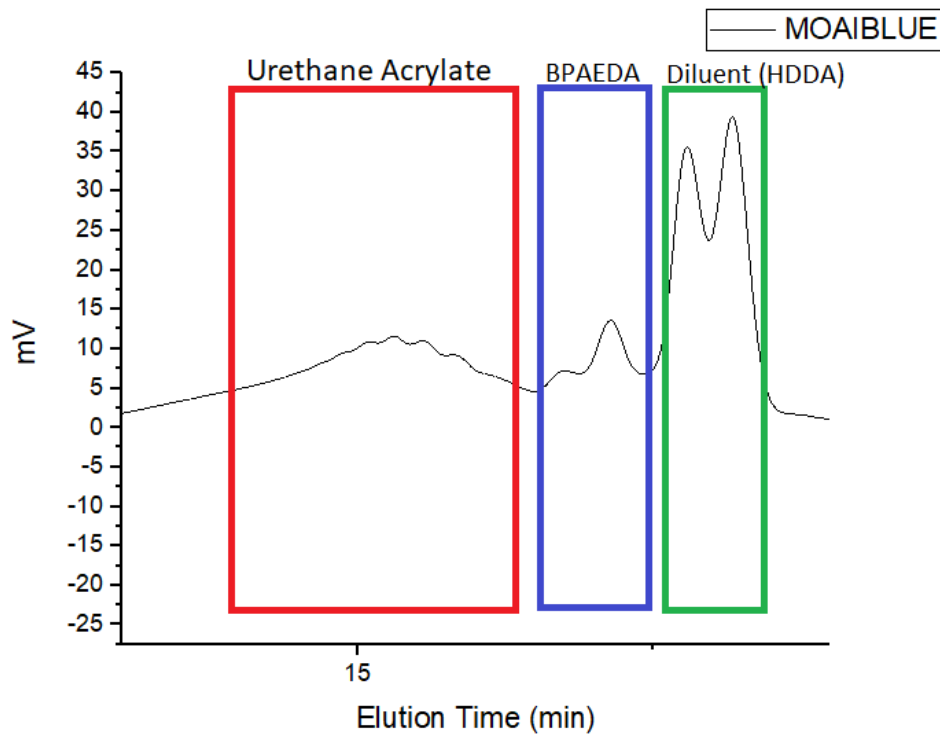
Figure 1.10. Gel Permeation Chromatographic Analysis of Peopoly Moai Blue Formulation

UV-Curable Epoxy Coatings

UV-curable epoxy coatings, sealants, and adhesives can crosslink through UV cationic polymerization. Cationic UV-curing can be broken down into steps of initiation and propagation. The first part of initiation is when the photoinitiator decomposes into an acid upon exposure to UV wavelengths at which it is actinic. The second part is this acid reacting with a nearby epoxy and turning them into reactive cationic species. Propagation is when these cationic species react with nearby epoxies and spread the reaction.[55] A schematic comparing free-radical and cationic curing processes is seen in **Figure 1.11**. ESS, with between 9-14 oxirane per molecule, introduces an opportunity for dense crosslinking in a UV-curable epoxy coating.
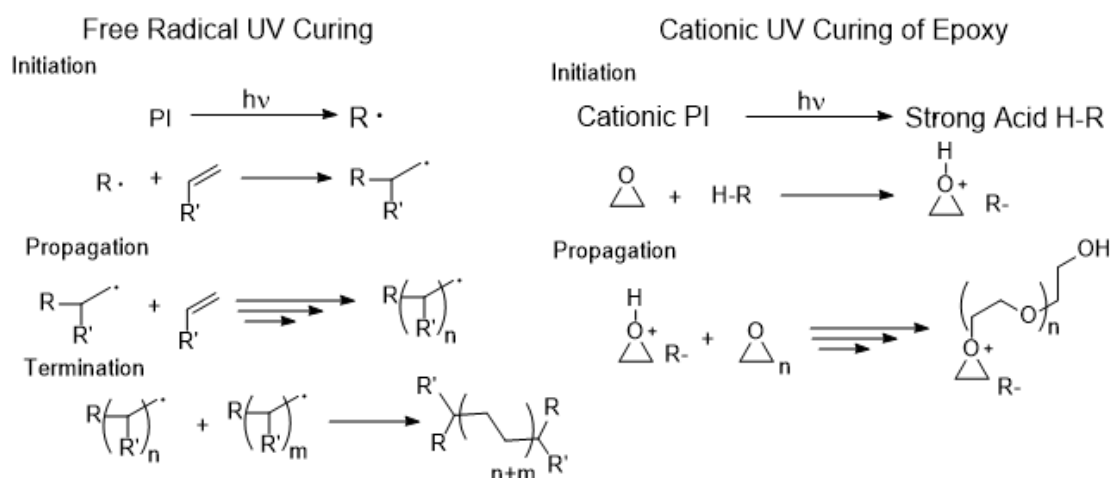
Figure 1.11. Schematic of Free Radical and Cationic UV-Curing Processes

Additives to Bioderived UV-Curable Epoxies and SLA Inks

Polyoctahedral Silsqueloxane (POSS) Additives

Polyoctahedral silsqueloxanes (POSS) are organosilicons which have a cage-like

structure. While it contains inorganic silica centers, modifications of the organic portions allow

functional groups that can react and form polymeric networks. The silica centers are then able to

confer their rigid and thermally stable properties to the network. Further, there is interest that

POSS nanoparticles may confer unique durability to a polymeric network due to crack

propagation taking a more circuitous route because of the rigid POSS structures.[56] Glycidyl

POSS (g-POSS) has been utilized in UV-curable epoxy coatings previously, however they have

not been assessed as an additive in a bioderived epoxy system. Similarly, methacrylated POSS

(m-POSS) has not been assessed as an additive in a bioderived methacrylated SLA formulation.

If small amounts of POSS can both lower the viscosity of a formulation while also impart

thermomechanical advantages, POSS may be further shown as a strengthening diluent in

bioderived systems. The structure of POSS, glycidyl POSS, and methacrylated POSS are seen in

Figure 1.12 and **1.13**.
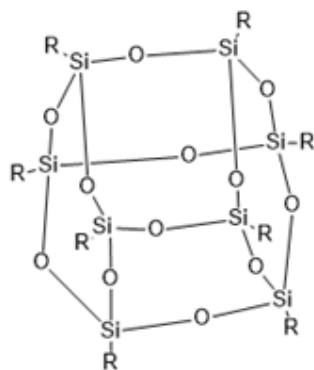
Figure 1.12. Structure of Polyoligomeric Silsqueloxane (POSS)
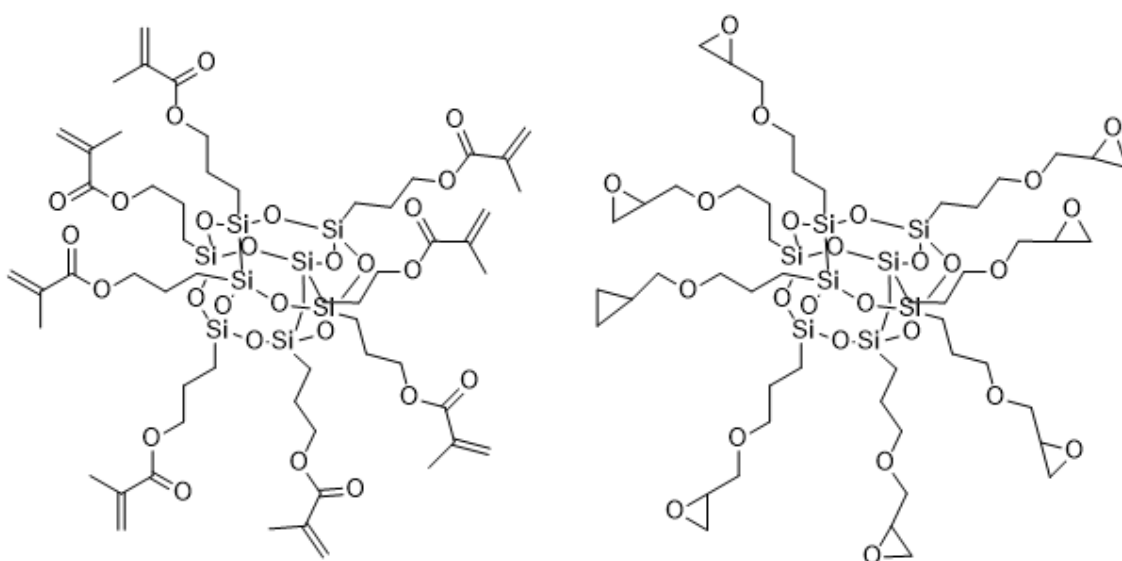
Figure 1.13. Methacrylated POSS (m-POSS) and Glycidylated POSS (g-POSS)

Cardanol-Derived Additives

Cardanol is a biorenewable material that is gaining great interest. It is a material retrieved from the industrial biproduct cashew nutshell liquid. This liquid is as its name implies, from the cashew plant *Anacardium occidentale L.* Around 18-27% of the post-processing of cashews is this liquid depending on the method utilized. This liquid, once its content of anacardic acid is removed/minimized by decarboxylation through heating or base treatment, is composed of predominantly cardanol (~60%), the diphenolic cardol (10-15%), polymeric products, and

methylcardol. The cardanol is subsequently separated and collected by vacuum distillation.

Cardanol is not a singular compound given its side chain has differing degrees of unsaturation.

5% is the completely saturated pentadecyl chain, 49% monounsaturated at the 8C site, 17%

diunsaturated at the 8C and 11C sites, and 29% triunsaturated at the 8C, 11C, and 14C sites.[57]

The production and structures of a cardanol mixture upon processing cashew nutshell liquid is

seen in **Figure 1.14**.
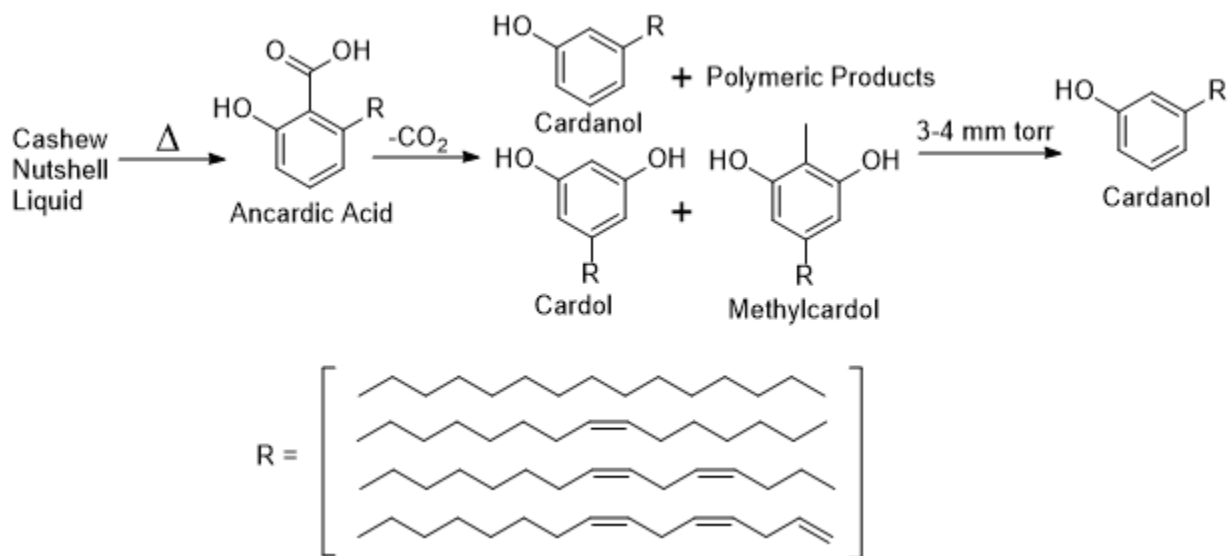
Figure 1.14. Processing of Cashew Nutshell Liquid to Produce Cardanol

Cardanol is of great interest for a variety of reasons. On top of being an easily produced

and bioderived material, its structure lends it potential for a wide variety of applications. Its polar

hydroxyl functionality and nonpolar aliphatic chain give it amphiphilic character which has been

exploited for use as a bioderived surfactant. This same aliphatic chain is noted for providing

flexibility, viscosity-lowering character, and pot-life extension to formulations. Its aromatic ring

is touted for chemical and thermal resistance. Both the chain unsaturation and the hydroxyl

functionality of cardanol have been modified for further expand its use into specialty chemicals

and applications. Currently cardanol has found use in coatings for marine, industrial, concrete,

and food applications, adhesives for transportation, electronics, and construction materials, and as a modifier for many composites.[58]

Reactive diluents are an important additive in many coatings and composites. Lowering viscosity is important to meet processing parameters and diluents can do so in a way superior to solvents. Reactive diluents, given they become part of the network lower VOCs unlike many solvents. Their structures can be chosen to tune properties of a formulation such as to make it more rigid or flexible. Also, especially with coatings, there are less issues and defects such as cratering arising with surface tension inhomogeneities that an evaporating solvent may cause. Many common diluents in UV-curing of epoxies and acrylates are petrochemically derived. Reactive diluents from card0anol derivatives may improve upon properties of ESS-containing formulations when substituting for petrochemically derived diluents and simultaneously increase the bio-derived content of the thermoset.

Modifications of ESS for Adhesion Promotion of UV-Curable Epoxy Coatings

Adhesion to substrates is a complicated, multifaceted issue. Efforts to improve adhesion can involve modification of a substrate by mechanical (ablation, etching) or chemical (acid treatment) means to change the surface so that a cured coating is less likely to delaminate. Alternatively, strategies can involve modification of the coating with functional groups that either chemically link or are more attracted to the substrate than the coating.

Millet et al discovered that by phosphonating an epoxidized fatty acid and adding to UV-curable methacrylate coating, corrosion protection of their steel substrates greatly improved. This was attributed to the adhesion promotion and improved barrier effects of the phosphonate.[54] Phosphonates are a functionality which have not been investigated with ESS thermosets. Specifically, phosphonating the oxirane of ESS with phosphoric acid produces phosphonate

esters that can bond to a pretreated substrate. A schematic of this is seen in **Figure 1.15**. The

multifunctionality of ESS allows some oxirane to be phosphonated while allowing remaining

epoxy to crosslink via UV-initiated cationic polymerization.

Phosphonate Functionality Adhering to Pretreated Substrate
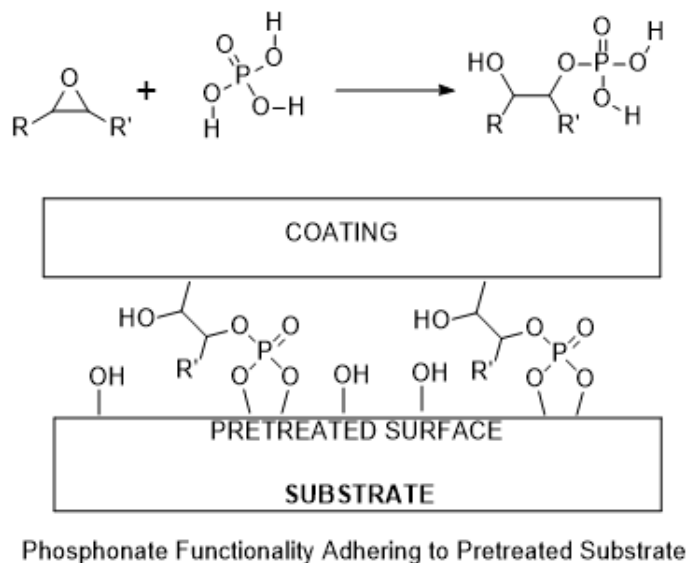
Figure 1.15. Phosphonate Functionalization of an Epoxy Polymer and its Adherence to a
Pretreated Substrate

In many applications, scientists have been inspired by processes seen in nature. Adhesion

strategies have especially been sought among those occurring naturally. Strong adhesives have

been developed based upon the structure of gecko feet which enables them to climb walls with

ease or mussel glue that lets them remain on fast-moving ships. Mussel glue adhesion was

elucidated by the high concentration of *L*-DOPA amino acid present in the glue's proteins. This

amino acid contains a catechol functionality which has a variety of surface interactions.[59] These

may include hydrogen bonding of the catechol OH groups to acceptors on the substrate,

coordination bonding of the OH groups to the substrate, and sometimes aromatic interactions of

the phenol depending on the substrate composition. Incorporation of this moiety on ESS may

also improve metal adhesive ability. The structure of *L*-DOPA and its catechol moiety as well as

a strategy to incorporate said moiety onto ESS is seen in **Figure 1.16**.
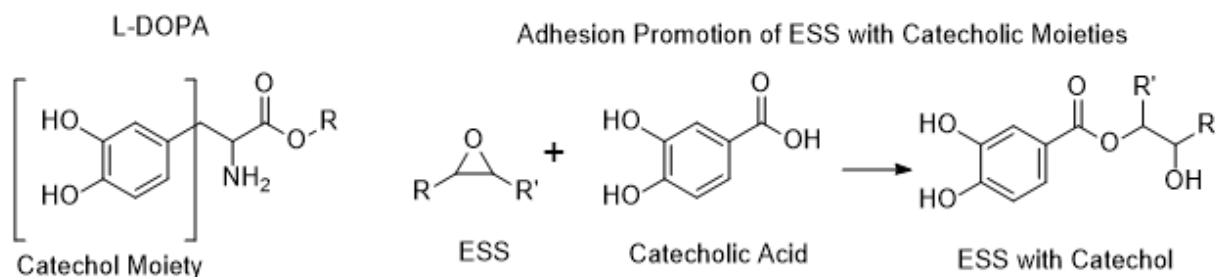
Figure 1.16. L-DOPA Amino Acid from Mussel Glue Protein as its Adhesion-Promoting Catechol Moiety and Incorporation of the Moiety onto ESS

This thesis involves investigations of how to modify ESS and incorporate it into various thermosets as well as screening additives to investigate processing and thermoset performance improvements. First, ESS was transformed into a polyol and then a polycarbamate and was crosslinked with petrochemically and bioderived dialdehydes to form a series of non-isocyanate polyurethane coatings. Next, ESS-derived acrylates were synthesized and formulated to be stereolithographic inks. Prints from these formulations were assessed for how their mechanical properties compared to commercial resins and formulations. This study was followed by an additive study where POSS derivatives were screened in an ESS-derived stereolithographic formulation to investigate improvements to processing, and thermo-mechanical properties of the prints. Next, ESS was evaluated in a UV-curable epoxy coating study when bio-derived glycidyl cardanol plasticizers were incorporated. Lastly, UV-curable epoxy coatings containing ESS modified with adhesion-promoting phosphonate and catechol functional groups were formulated and evaluated.

References

1. Dodiuk, H., & Goodman, S. H.*Handbook of thermoset plastics*. William Andrew, 2013.

2. Raquez, J. M., Deléglise, M., Lacrampe, M. F., & Krawczak, P.*Prog. Pol. Sci.,* **2010**, *35.4*, 487-509.

3. Silvestre, Clara, Donatella Duraccio, and Sossio Cimmino. *Prog. Pol. Sci.*, **2011**, *36.12*, 1766-1782.

4. Mo, H., Huang, X., Liu, F., Yang, K., Li, S., & Jiang, P. *IEEE Transactions on Dielectrics and Electrical Insulation,* **2015**, *22.2,* 906-915.

5. Pickering, Steve J. *Composites Part A: applied science and manufacturing,* **2006**, *37.8*, 1206-1215.

6. Zonatti, W. F., Guimarães, B. M. G., Duleba, W., & Ramos, J. B *Text. Cloth. Sust.,* **2015**, *1.1*, 1.

7. Crawford, Shaun, and Claudiu T. Lungu. *Sci. Tot. Env.,* **2011,** *409*, 3403-3408.

8. Senophiyah-Mary, J., R. Loganath, and P. Mohamed Shameer. *J. Env. Chem. Eng.* **2018**, *6.2*, 3185-3191.

9. Zini, Elisa, and Mariastella Scandola. *Poly. Comp*, **2011**, *32.12*, 1905-1915.

10. La Rosa, A. D., et al. *J. Clean. Prod.* **2013**, *44*, 69-76.

11. Iles, Alastair, and Abigail N. Martin. *J. Clean Prod.,* **2013**, *45*, 38-49.

12. Song, J. H., Murphy, R. J., Narayan, R., & Davies, G. B. H.*Philosophical transactions of the royal society B: Biological sciences,* **2009**, *364,* 2127-2139.

13. Standeven, Harriet AL. *J. Am. Inst. Cons.* **2013**, *52.3*, 127-139.

14. Stingley, Dale V. *Indust. Eng. Chem.,* **1940**, *32.9,* 1217-1220.

15. Ragauskas, Arthur J., et al. *Sci*, **2006**, *311*, 484-489.

16. Mosiewicki, Mirna A., and Mirta I. Aranguren. *Eur. Pol. J.*, **2013**, *49.6*, 1243-1256.

17. Scholz, H. A. *Indust. & Eng. Chem.,* **1953**, *45.4,* 709-711.

18. Türünç, Oğuz, and Michael AR Meier. *Eur. J. Lip. Sci. & Tech.,***2013**, *115.1*, 41-54.

19. Türünç, Oğuz, and Michael AR Meier. *Macro. Rap. Comm.*, **2010**, *31.2*, 1822-1826.

20. Desroches, M., Caillol, S., Lapinte, V., Auvergne, R., & Boutevin, B.*Macromol.*, **2011**, *44.8*, 2489-2500.

21. Hilker, I., Bothe, D., Prüss, J., & Warnecke, H. J.*Chem. Eng. Sci.*, **2001**, *56.2*, 427-432.

22. Kim, Joo Ran, and Suraj Sharma. *Indust. Cr. & Prod.,* **2012**, *36.1*, 485-499.

23. Zhao, Shou, and Mahdi M. Abu-Omar. *ACS Sus. Chem. & Eng.,* **2017**, *5.6*, 5059-5066.

24. Guigo, N., Mija, A., Vincent, L., & Sbirrazzuoli, N. *Eur. Pol. J.,* **2010**, *46.5*, 1016-1023.

25. Ragauskas, Arthur J., et al. *Sci.,* **2014**, *344*, 1246843.

26. Markwart, K. U. N. Z. "Hydroxymethylfurfural, a possible basic chemical for industrial intermediates." *Studies in Plant Science*. Vol. 3. Elsevier, 1993. 149-160.

27. Li, Yuan, et al. *Biores. Tech.*, **2013**, *133*, 347-353.

28. Lilga, Michael A., Richard T. Hallen, and Michel Gray. *Topics in Catalysis,* **2010**, *53.15*, 1264-1269.

29. Vijjamarri, Srikanth, et al. *ACS Sus. Chem. & Eng.,* **2018**, *6.2*, 2491-2497.

30. Fan, W., Verrier, C., Queneau, Y., & Popowycz, F. *Curr. Org. Synth.,* **2019**, *16.4*, 583-614.

31. Van Putten, R. J., Van Der Waal, J. C., De Jong, E. D., Rasrendra, C. B., Heeres, H. J., & de Vries*Chem. Rev.,* **2013**, *113.3*, 1499-1597.

32. Rizzi, George Peter, and Harry Madison Taylor. U.S. Patent No. 3,963,699. 15 Jun. 1976.

33. Pan, Xiao, and Dean C. Webster. *Macr. Rap. Comm.,* **2011**, *32.17*, 1324-1330.

34. Ivanov, Dušica S.; Lević, Jovanka D.; Sredanović, Slavica A. *J. Inst. F. Tech.,* **2013**, *37*, 65–70.

35. Monono, Ewumbua M., Dean C. Webster, and Dennis P. Wiesenborn. *Indust. Cr. & Prod.*, **2015**, *74*, 987-997.

36. Pan, Xiao, Partha Sengupta, and Dean C. Webster. *Biomacr.,* **2011**, *12.6*, 2416-2428.

37. Amiri, A., Hosseini, N., Ulven, C., & Webster, D."Advanced bio-composites made from methacrylated epoxidized sucrose soyate resin reinforced with flax fibers." *Proceedings of the 20th International Conference on Composite Materials, Copenhagen, Denmark.* 2015.

38. Pan, Xiao, and Dean C. Webster. *Chem. Sus. Chem.,* **2012**, *5.2*, 419-429.

39. Yan, Jingling, and Dean C. Webster. *Green Mat.,* **2014**, *2.3*, 132-143.

40. Ma, Songqi, Dean C. Webster, and Farukh Jabeen. *Macromol.* **2016**, *49.1,* 3780-3788.

41. Glasser, W. G., Barnett, C. A., Rials, T. G., & Saraf, V. P.., et al. *J. App. Pol. Sci.,* **1984**, *29.5*, 1815-1830.

42. Guan, Jing, et al. *Indus. & Eng. Chem. Res.,* **2011**, *50.11*, 6517-6527.

43. Chester, D. A., Hanna, E. A., Pickelman, B. G., & Rosenman, K. D. *Am. J. Ind. Med.,* **2005**, *48.1*, 78-84.

44. Cornille, A., Auvergne, R., Figovsky, O., Boutevin, B., & Caillol, S*Eur. Pol. J.*, **2017**, *87*, 535-552.

45. Yuen, Alexander, et al. *Pol. Chem.*, **2016**, *7.11*, 2105-2111.

46. Anderson, Jeffrey R., et al. "Ambient temperature curable isocyanate-free compositions for preparing crosslinked polyurethanes." U.S. Patent No. 8,653,174. 18 Feb. 2014.

47. Argyropoulos, John N., et al. "Ambient temperature curable isocyanate-free compositions for preparing crosslinked polyurethanes." U.S. Patent Application No. 15/068,823.

48. Anderson, Jeff R., et al. "Crosslinkable composition, a method of making the same and a crosslinked composition produced therefrom." U.S. Patent No. 9,580,622. 28 Feb. 2017.

49. Pan, Xiao, and Dean C. Webster. *ChemSusChem*, **2012**, *5.2*,Seifi, M., Salem, A., Beuth, J., Harrysson, O., & Lewandowski, J. J.*Jom,* **2016**, *68.3*, 747-764.

50. Schubert, Carl, Mark C. Van Langeveld, and Larry A. Donoso. *Brit. J. Opht.*, **2014**, *98.2*, 159-161.

51. Conner, Brett P., et al. *Add. Man.,* **2014**, *1*, 64-76.

52. Brown, Andrew C., and Deon De Beer. "Development of a stereolithography (STL) slicing and G-code generation algorithm for an entry level 3-D printer." *2013 Africon*. IEEE, 2013.

53. Wang, X., Jiang, M., Zhou, Z., Gou, J., & Hui, D*Composites Part B: Engineering,* **2017**, *110*, 442-458.

54. Millet, F., Auvergne, R., Caillol, S., David, G., Manseri, A., & Pébère, N, *Prog. Org. Coat.* **2014**, *77.2,* 285-291.

55. Thames, Shelby F., and H. Yu. *Surf. & Coat. Tech.,* **1999**, *115*, 208-214.

56. Abad, M. J., Barral, L., Fasce, D. P., & Williams, R. J*Macro.*, **2003**, *36.9*, 3128-3135.

57. Liu, R., Zhang, X., Zhu, J., Liu, X., Wang, Z., & Yan, J. *ACS Sus. Chem. & Eng.*, **2015**, *3.7*, 1313-1320.

58. Voirin, C., Caillol, S., Sadavarte, N. V., Tawade, B. V., Boutevin, B.,*Pol. Chem.,* **2014**, *5.9*, 3142-3162.

59. Guardingo, Mireia, et al. *Small,* **2014**, *10.8*, 1594-1602.

CHAPTER 2. BIOBASED, NON-ISOCYANATE, 2K POLYURETHANE COATINGS PRODUCED FROM POLYCARBAMATE AND DIALDEHYDE CROSSLINKING

Introduction

This project involved the development of a carbamate-aldehyde non-isocyanate polyurethane system produced from a bio-derived polycarbamate and bio-derived dialdehyde crosslinkers. The goal was to explore how bio-derived architectures of both components may impact coating performance in terms of cure and mechanical properties. Further, this study looked to expand upon the limited dialdehyde crosslinking options for this NIPU route.

Epoxidized sucrose soyate was explored as a bioderived polycarbamate given there are previously established methods to alkoxylate via acid catalysis the epoxy sites with aliphatic alcohols of different lengths. The resultant secondary alcohol can then be transcarbamoylated with a carbamate such as methyl carbamate, a stannate catalyst, and elevated temperatures. ESS polyols made with methanol, ethanol, and 1-propanol were explored given the introduction of hydroxyl and then carbamate groups substantially increase the viscosity due to hydrogen bonding; a longer alcohol was hypothesized to lower the viscosity of the polycarbamate. A comparison soybean oil alkyd polycarbamate like DOW's PARALOID™ resin was synthesized as a control.

The dialdehyde components were developed from bio-derived sources such as hydroxymethyl furfural and lignin derivatives as well as the petrochemically-derived cyclohexanedicarboxaldehyde (CHDA) which is conventionally used in this crosslinking method under the trade name PARALOID EDGE XL™ (**Figure 2.1**). A screening of the many crosslinking candidates with the characterized polycarbamate resins were performed with a standard formulation. While many candidates were dialdehydes, others contained single

26

aldehyde functionalities, protecting groups, and other functionalities to see how they impacted the processing and reaction. The most promising coatings (good dry times, adhesion, solvent resistance, etc) were characterized further.
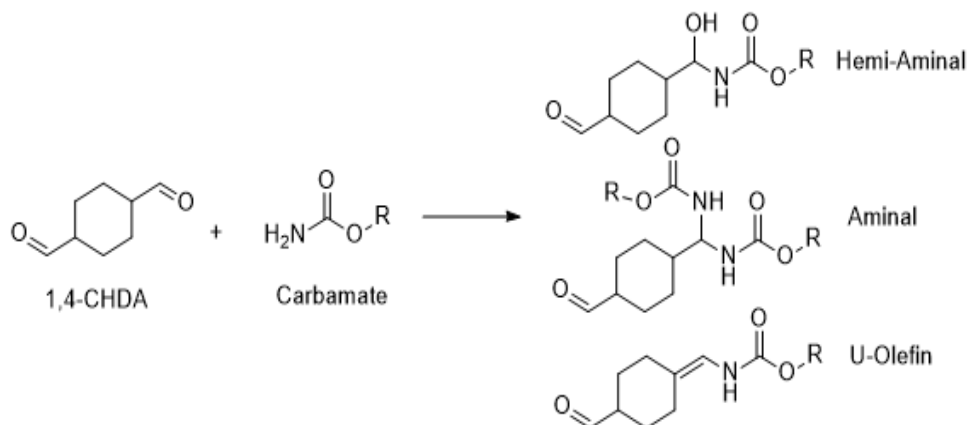
Figure 2.1. Reaction between 1,4-CHDA and a Carbamate

Experimental Section

Raw Materials

Epoxidized sucrose soyate was synthesized as previously reported.[24,25] It was received with an epoxy equivalent weight of 253 g/eq as determined by ASTM D 1652. Refined, bleached, deodorized, soybean oil was obtained from Cargill. Methyl carbamate, 2-nitrophenol, dibutyltin oxide, 2-chloro-1,3,2-dioxaphospholane, chromium (III) acetylacetonate, pyridinium chlorochromate (PCC) and 1,4-cyclohexane diol were obtained from Sigma Aldrich. Isophthalic acid, phthalic anhydride, pentaerythritol, tetrafluoroboric acid solution (TFBA), and solvents were obtained from VWR International. K-Cure 1040 *para*-toluenesulfonic acid solution (40% in IPA) was obtained from King Industries. 5-Hydroxymethyl furfural (HMF) was purchased from AvaBiochem. Manganese dioxide was purchased from Acros Organics. All noted low-molecular, bioderived crosslinkers specified were synthesized by members of the Sibi group at NDSU and used as received.

Synthesis of Sucrose Soyate Polyols

The ring-opening of ESS with methanol to produce methoxy sucrose soyate polyol (MSSP) was completed using a method reported in *Nelson et al*. The same method but by using ethanol or 1-propanol respectively produced ethoxy sucrose soyate polyol (ESSP) and propoxy sucrose soyate polyol (PSSP).

In a one liter, 3-neck round bottom flask equipped with thermocouple, overhead mechanical stirrer, and addition funnel, 215 g methanol, 3.75 g of 48% wt TFBA solution, and 13.4 g DI water were added. The mixture was heated to 50 °C and dropwise addition of 200 g of epoxidized sucrose soyate dissolved in 100 g of chloroform commenced at a rate of 2 mL/min. After completing the addition, the temperature was held for 20 more minutes and then cooled to room temperature. Sodium bicarbonate solution was added and the mixture stirred for 20 more minutes. Stirring was then halted and the mixture phase separated overnight. The following day, the top layer in the flask was removed and the resin was diluted with dichloromethane and transferred to a 1 L separatory funnel. The mixture was washed 8 times with DI water or until a pH strip placed into the removed water post-separation read a neutral pH. Solvent was removed via rotary evaporation and the transparent resin stored. The resins' OH equivalent weights (OHEW) were assessed by ^{31}P-NMR Method described in "^{31}P-NMR Procedure to Determine Hydroxyl Content of Resins."

Synthesis of Soybean Oil Alkyd Polyol (AP)

In a 1 L resin kettle with overhead mechanical stirring, thermocouple, a Dean-Stark trap, reflux condenser, and N_2 inlet, 347.2 g of soybean oil, 178.4 g pentaerythritol and 0.63 g of dibutyltin dioxide were added. The mixture was heated to 220 °C under a gentle N_2 blanket. The methanol test (dissolving one part resin in 3 parts MeOH to note monoglyceride formation) was

performed every 2 hours and upon passing (by dissolving) the resin was let to cool to 100 °C. Then, 89.75 g isophthalic acid, 134.63 g phthalic anhydride, and 4% wt xylenes (based on charge) were then added to the kettle. The temperature of the mixture was gradually increased 10 °C at a time before reaching 220 °C. Acid number was collected when little/no water was being collected in the Dean-Stark trap. When acid number titration showed a value of ≤8 mg KOH/g the heating was turned off and, upon cooling, the resin was poured into a glass jar with N_2 blanketed on top. Hydroxyl Equivalent Weight (OHEW) was assessed by ^{31}P-NMR Method described in "^{31}P-NMR Procedure to Determine Hydroxyl Content of Resins."

Transcarbamoylation of Polyol Resins

In a 250 mL round bottom flask equipped with overhead mechanical stirrer, Dean-Stark trap, thermocouple, reflux condenser, and N_2 inlet, the respective polyol, methyl carbamate (1.5 eq carbamate: OH content of resin), and dibutyltin oxide at 0.6% wt of the added solids were charged. Next, the added mixture was diluted to 70% solids with xylenes and heating commenced to 150 °C. The reaction was held at this temperature for 8 hours before being allowed to cool at RT overnight. Methanol was collected and monitored in the Dean-Stark trap. The following day, the reaction was reheated to 150 °C and held for another 8 hours. The reaction was stopped and allowed to cool to RT before being dissolved in dichloromethane and transferred to a 1 L separatory funnel. The resin was then washed 5 times with DI water before rotary evaporation. The disappearance of excess methyl carbamate was confirmed with ^{13}C-NMR and the carbamate equivalent weight (CEW) was determined using the ^{31}P-NMR method by assessing the change in OH content. Transcarbamoylated alkyd polyol (TCAP) and transcarbamoylated methoxy sucrose soyate polyol (CMSSP) are the designations of the polycarbamates produced.

Percent Solids of the Resin

In aluminum pans of known weight, 0.5-1 g of resin was added and recorded before being covered with ~3 g of toluene. This was then placed in an oven for 2 hours at 120 °C. The pans were reweighed and the % solids calculated using Equation 1. 3 samples for each resin were completed and their values averaged.

$$Percent\ Solids = \frac{Weight\ Resin\ After\ Heating}{Weight\ Resin\ Before\ Heating} \qquad \text{(Equation 1)}$$

Rheological Analysis of the Resins and Formulations

Rheological analysis was completed on a parallel plate, TA Instruments ARES Rheometer. Sample was deposited on the cleaned bottom plate before the plate gaps were set to 1 mm and residual sample dribbling off the sides wiped away. A steady rate sweep test was completed with viscosity measured from 0.1 rotation/sec to 100 rotation/sec. The viscosity vs rate were recorded.

^{31}P-NMR Procedure to Determine Hydroxyl Content of Resins

The procedure was developed from a method stated in *Lambrini et al.*[27] In a glass vial, 15-20 mg of resin was weighed out. To this vial, 500 µL of a 50/50 by weight Pyr/CDCl$_3$ mixture was added. The internal standard, 2-nitrophenol, was dissolved in a separate vial at 10-16 mg in 1 mL Pyr/CDCl$_3$ mixture to make the internal standard solution. Of this solution, 100 µL was then added to the sample vial. In another separate vial, 11.4 mg of chromium (III) acetylacetonate was added and dissolved in 1 mL weight Pyr/CDCl$_3$ mixture and 50 µL of this solution added to the sample vial. 2-Chloro-1,3,2-dioxaphospholane (CDP) was added to the sample vial at 3:1 by volume reagent:estimated hydroxyl content of resin to ensure complete reaction of OH groups. Contents of the vial was transferred by micropipet into a Wilmad^{TM} NMR sample tube of outer and inner diameters of 5 mm and 4 mm respectively and 7" length.

^{31}P-NMR analysis was completed on an ECA Series 400 MHz NMR Spectrometer with lock on

No Solvent before running analysis. Samples were completed in duplicate and values averaged.

The reaction of the phosphorous reagent to the internal standard is seen in **Figure 2.2**. Equation 2

shows the calculation of the integral corresponding to the OH content (v_{OH}) of the internal

standard reacted with the phosporous reagent. Equation 3 shows how v_{OH} is then used to

determine the OH number of the resin assessed, while Equation 4 calculates the hydroxyl

equivalent weight of the resin. Equation 5 determines the carbamate equivalent weight from the

change in hydroxy signal from the polyol to the carbamate while Equation 6 uses that value to

calculate the carbamate equivalent weight of the resin.
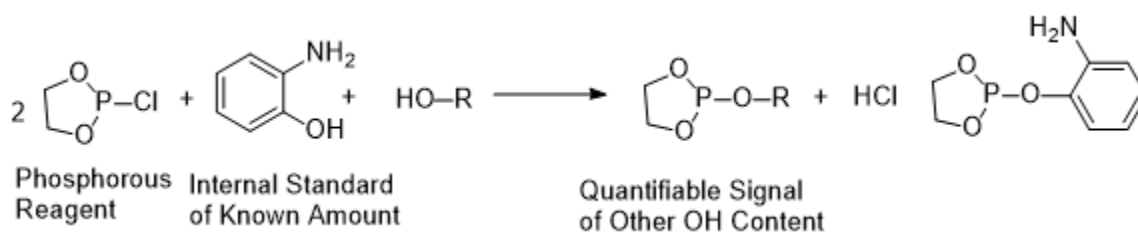
Figure 2.2. ^{31}P-NMR Process to Determine Hydroxyl Content of a Resin

Hydroxyl Equivalent Weight

$$v_{OH\ Content} = \frac{\int OH_{Resin}}{\int OH_{Internal\ Standard}} \times mmol\ Internal\ Standard \qquad \text{(Equation 2)}$$

$$OH\ \#_{Resin} = \frac{v_{OH\ Content}}{g\ Sample} \times 56.1 \left(\frac{g}{mol}\right) = \frac{mg\ KOH}{g\ Sample} \qquad \text{(Equation 3)}$$

$$OHEW_{Resin} = \frac{56100\ \frac{mg}{mol}}{OH\ \#} \qquad \text{(Equation 4)}$$

$$Carbamate\ Conversion = \frac{OH\ \#_{Polyol} - OH\ \#_{Polycarbamate}}{OH\ \#_{Polyol}} \qquad \text{(Equation 5)}$$

$$Carbamate\ Equivalent\ Weight = \frac{OHEW_{Polyol} + (43 \times Carbamate\ Conversion)}{Carbamate\ Conversion} \qquad \text{(Equation 6)}$$

Preparation of Non-Isocyanate Polyurethane Coatings

In a glass vial, the respective dialdehyde, ethanol (1.5 eq. ethanol:aldehyde), and K-CURE 1040 (40% paratoluensulfonic acid in IPA, 3% wt of formulation solids) was added. The mixture was vortexed until the aldehyde fully dissolved. The polycarbamate resin (1:1 aldehyde:carbamate) dissolved in ethyl acetate (~45% solids) was then added to the vial and the formulation vortexed until transparent. The mixture was sonicated for 10 minutes to remove bubbles (1,4-CHDA crosslinked too rapidly so it was drawn down immediately). The formulations were drawn down at 6 mils wet film thickness on Q-Panel aluminum substrates pre-cleaned with IPA and cured under laboratory ambient conditions for 3 months. Concurrently, the same formulations were made and underwent an expedited cure regime of 120 °C for 2 hours for comparison to the ambient-cured networks on both Q-Panel aluminum and pretreated steel substrates. Due to issues with formulation at a 1:1 carbamate:aldehyde ratio with TCAP, specifically involving DFF phase separating after being drawn-down, TCAP was formulated at 1.5:1 carbamate:aldehyde.

Gel Permeation Chromatography (GPC)

GPC analysis of the resins was completed on an EcoSEC HLC-8320GPC from Tosoh Bisocience with a differential refractometer detector. Around 10 mg of sample was dissolved in 1.5-2 mL of tetrahydrofuran (THF). This was then filtered through a 0.45 mm PTFE filter before being run. THF was used to elute the samples at flow rate of 0.35 mL/min. An EasiVial polystyrene standard obtained from Agilent was utilized for calibration.

Spectroscopic Analysis of the Resins and Cured Formulations

Fourier Transform Infrared Spectroscopy (FTIR) were run on a ThermoScientific Nicolet 8700 in transmission using a spectroscopic-grade KBr crystal or via Attenuated Total

Reflectance Spectroscopy (ATR) with a Thermo Fisher Scientific single reflection diamond ATR and HP clamp attachment. Resolution was 4 cm^{-1}. Proton, Carbon and Phosphorous Nuclear Magnetic Spectroscopy (^{1}H-NMR, ^{13}C-NMR, ^{31}P-NMR) were run on a 400 MHz JEOL ECA Series Nuclear Magnetic Resonance Spectrometer (JEOL USA, Peabody, MA, USA) with CDCl$_3$ as the solvent for proton and carbon, and a 50/50 CDCl$_3$/anhydrous pyridine mixture for phosphorous.

Coating Characterization

König pendulum hardness, % solids, pencil hardness, crosshatch adhesion, impact resistance, and solvent resistance were carried out in accordance with ASTM D2369, ASTM D4366, ASTM D3363, ASTM D4541, ASTM D2794, and ASTM D5402, respectively. Tack free time was determined by placing a cleanly-gloved thumb onto the coating, holding for 30 seconds, and time noted when no resistance was felt when pulling the glove away and no mark was left on the coating. Gel content was determined by taking three 1 g samples of the respective formulations, wrapping them individually in filter paper and placing adjacent to each other in an extraction thimble. The thimble was then placed in a Soxhlet extractor and extracted by dichloromethane reflux at 60 °C for 24 hours. The samples were then dried for several hours in a vacuum oven before being weighed. Final weight/Initial weight of the sample was recorded as the Gel % average of the 3 samples.

Thermal Analysis

Differential Scanning Calorimetry (DSC) was run on a TA Instruments Q1000 Modulated Differential Scanning Calorimeter. ~ 5 mg of coating was placed in a standard aluminum pan and run under a Heat-Cool-Heat regime first equilibrating at 30 °C, heating at 10 °C/min to 150 °C, cooling 10 °C/min to 20 °C, then reheating at 10 °C/min to 150 °C. Dynamic

Mechanical Analysis (DMA) was run on a TA-Instruments Q800 Dynamic Mechanical Analyzer. Film samples of around 17 mm length, 7 mm width, and 0.05 mm thickness were prepared and locked in the calibrated tension DMA clamps at 2 lbs with a torque wrench. Samples were equilibrated at 40 °C before heating at 2 °C/min to 150 °C. This was increased to 200 °C if the amplitude of the tan δ signal was near or surpassed that limit. Instrument was set at 1 Hz oscillating frequency, 0.02 oscillating strain, 0.01 static force, and 125% force track.

Results and Discussion

Synthesis and Characterization

The epoxy ring-opening of ESS with alcohols to yield MSSP, ESSP, and PSSP is shown in **Figure 2.3**. The transcarbamoylation procedure of the polyols is seen in **Figure 2.4**. OH #, OHEW, Carbamate conversion, CEW, as well as % solids of the resins are seen in **Table 2.1**. The ESS-derived polyols showed similar OH content, as well as depletion of the OH signal seen in the FTIR overlay in **Figure 2.5**. AP showed the highest hydroxyl content and TCAP had a similar carbamate conversion to CMSSP. Gel permeation chromatographic analysis (GPC) of the ESS-derived polyols seen in **Figure 2.6** notes an increase in molecular weight when a larger alcohol is used during alkoxylation. Rheological analysis in **Figure 2.7** demonstrates that the larger the alcohol utilized, the lower the viscosity of the resultant polyol. However, due to the poor carbamate conversions of CESSP and CPSSP, only CMSSP and TCAP were pursued for further analysis and crosslinking with aldehydes.
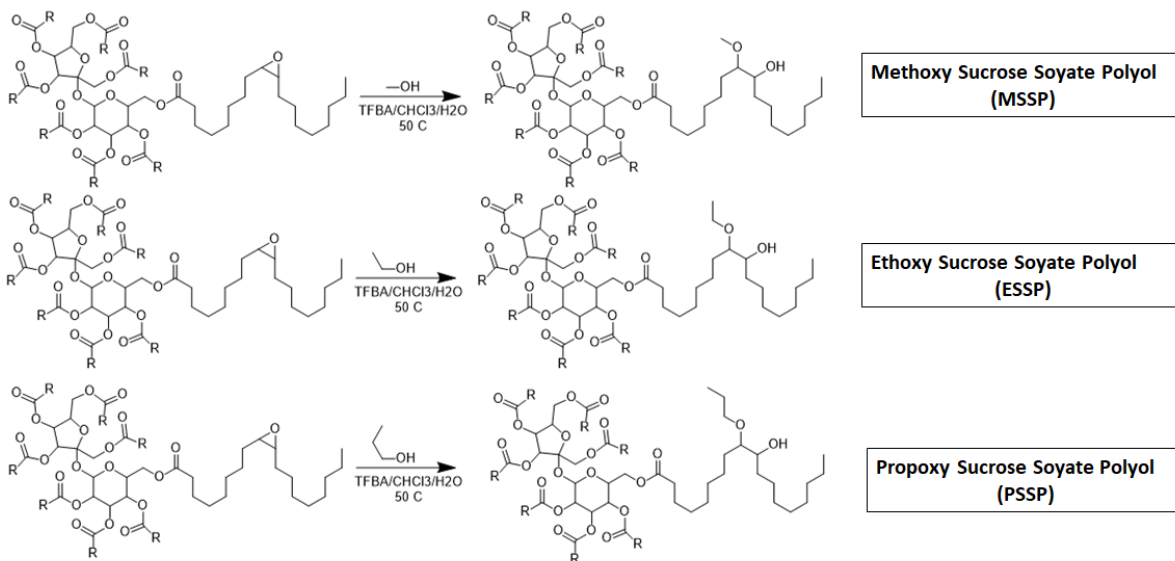
Figure 2.3. Alkoxylation of ESS to Produce MSSP, ESSP, and PSSP
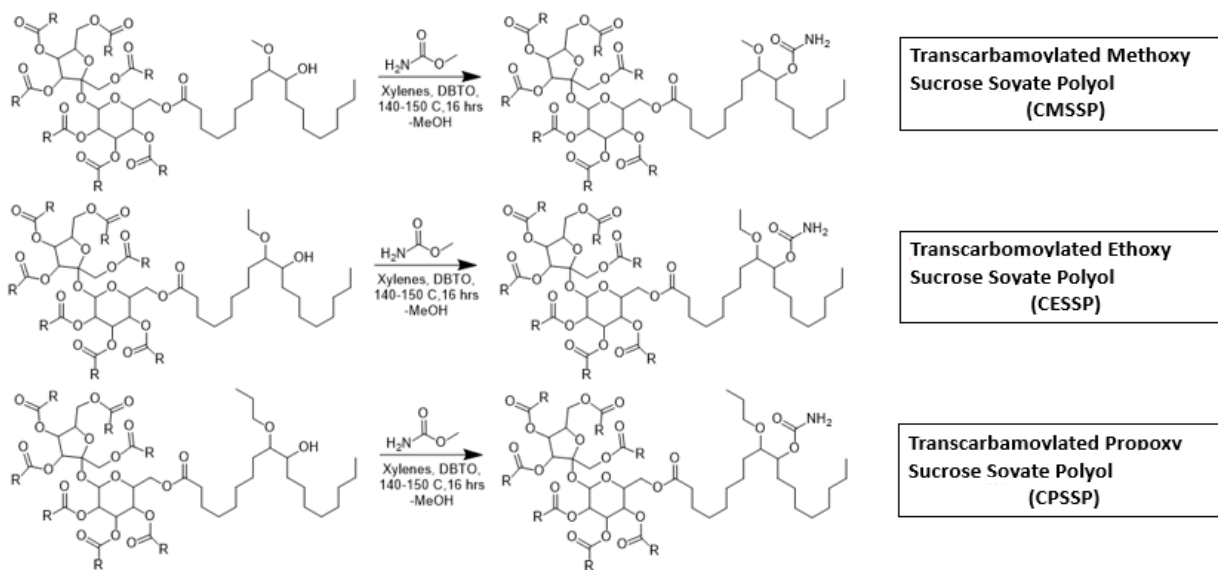
Figure 2.4. Transcarbamoylation of ESS-Derived Polyols to Yield CMSSP, CESSP, and CPSSP

35

Table 2.1. Percent Solids, Viscosity, OHEW, CEW, and % Carbamate Conversion of Resins

Resin	% Solids	OHEW (g/eq)	CEW (g/eq)	% Carbamate Conversion
MSSP	99.4	216	N/A	N/A
ESSP	98.9	236	N/A	N/A
PSSP	99.0	243	N/A	N/A
AP	98.4	119	N/A	N/A
CMSSP	93.9	2200	282	90.4
CESSP	90.2	307	2000	24.7
CPSSP	93.8	513	480	54.0
TCAP	96.1	950	181	87.9
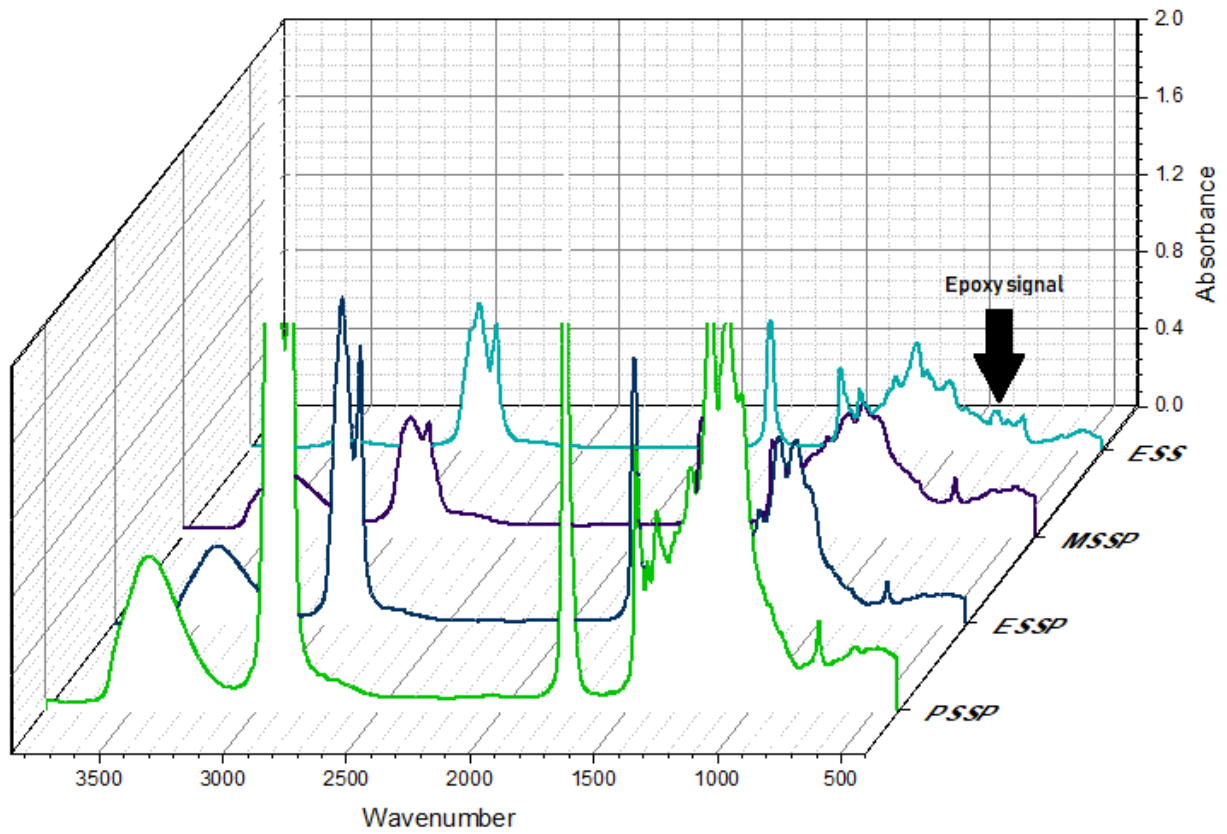
Figure 2.5. FTIR Analysis of the ESS-Derived Polyols

Resin	M_n	M_w	PDI
ESS	2717	2736	1.007
MSSP	1098	3336	3.039
ESSP	3489	4097	1.174
PSSP	3538	4102	1.160
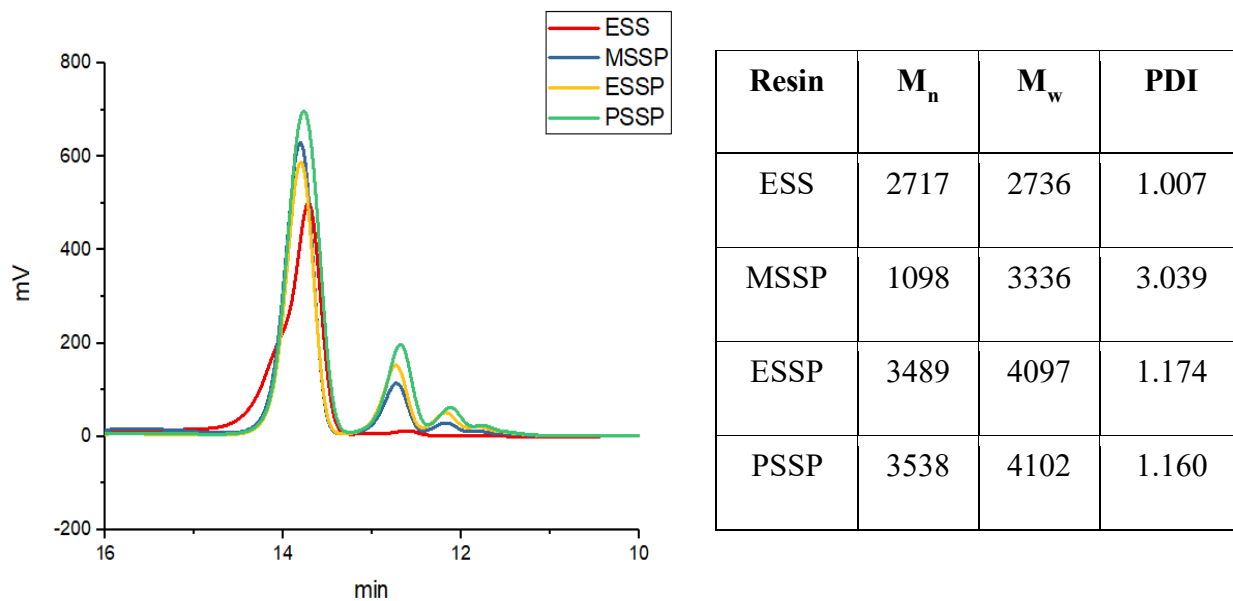
Figure 2.6. Gel Permeation Chromatographic Analysis of ESS-Derived Polyols
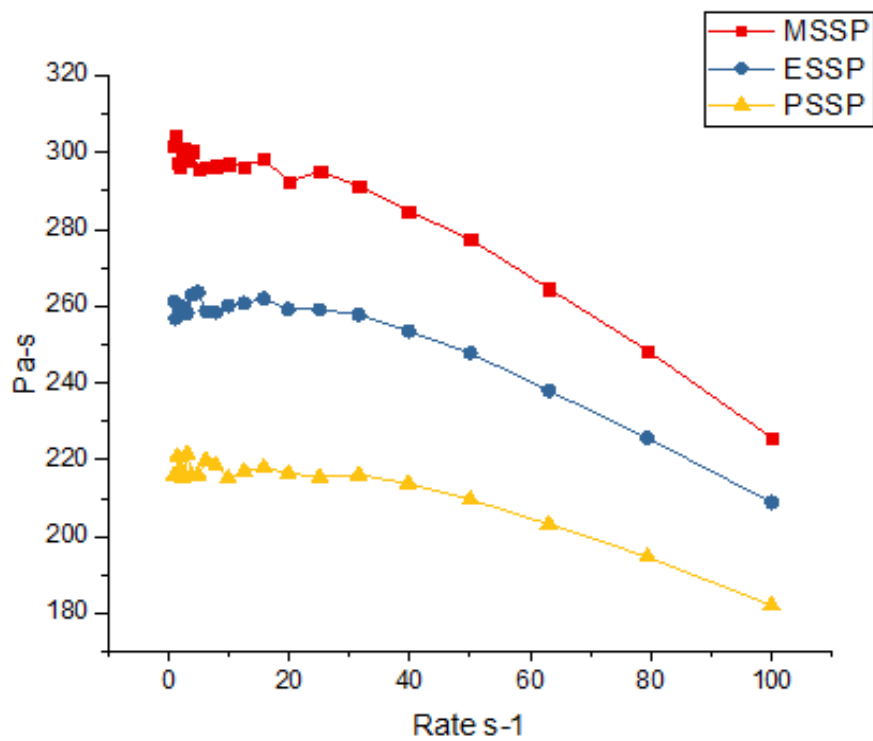
Figure 2.7. Rheological Analysis of ESS-Derived Polyols

The appearances of the resins are seen in **Figure 2.8**. ESS, MSSP, and soybean oil all had a clear and colorless appearance. The SBO-alkyd polyol took on a slightly amber appearance which greatly darkened after transcarbamoylation as seen in TCAP. CMSSP also took on an amber appearance. Gel permeation chromatographic analysis overlays are seen in **Figure 2.9** and determined values of molecular weight averages are shown in **Table 2.2**. MSSP shows a distinct increase of weight and Z-average molecular weights compared to ESS. The larger molecular weight signals seen in MSSP are the result of oligomeric side reactions with alcohol. CMSSP shows further M_w and M_z increases compared to MSSP and retains the same higher molecular weight signals, however, a low molecular weight signal appears. This may be due to transesterification of the esters of the sucrose core with the fatty acids with methyl carbamate. The alkyd polyol and polycarbamate show broad signals in **Figure 2.10** and high PDIs in **Table 2.2** which are attributed to the statistical reactions between multifunctional species. The high viscosity of the resins necessitated dilution to 50% solids with ethyl acetate before assessment. It is very apparent that transcarbamoylation greatly increases the viscosity of the resins. This may be due to hydrogen bonding from the carbamate functionality more so than the hydroxyl functionality of the polyol.
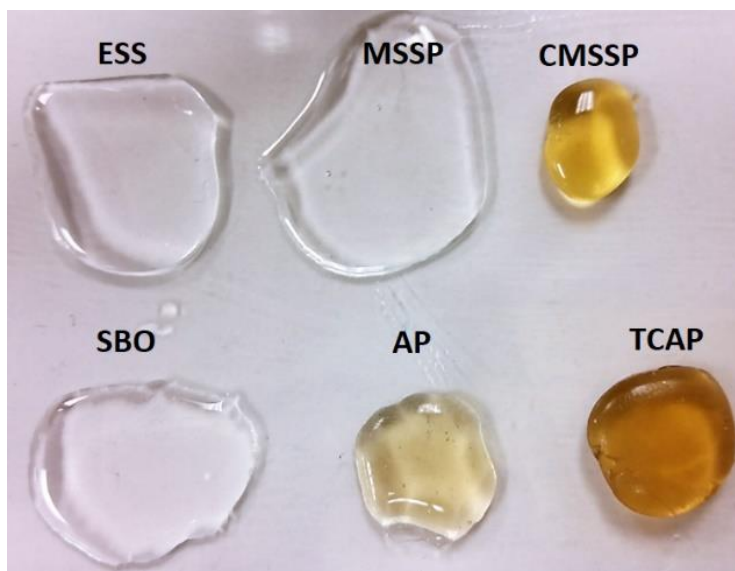
Figure 2.8. Appearances of the Resins Deposited on a Glass Plate
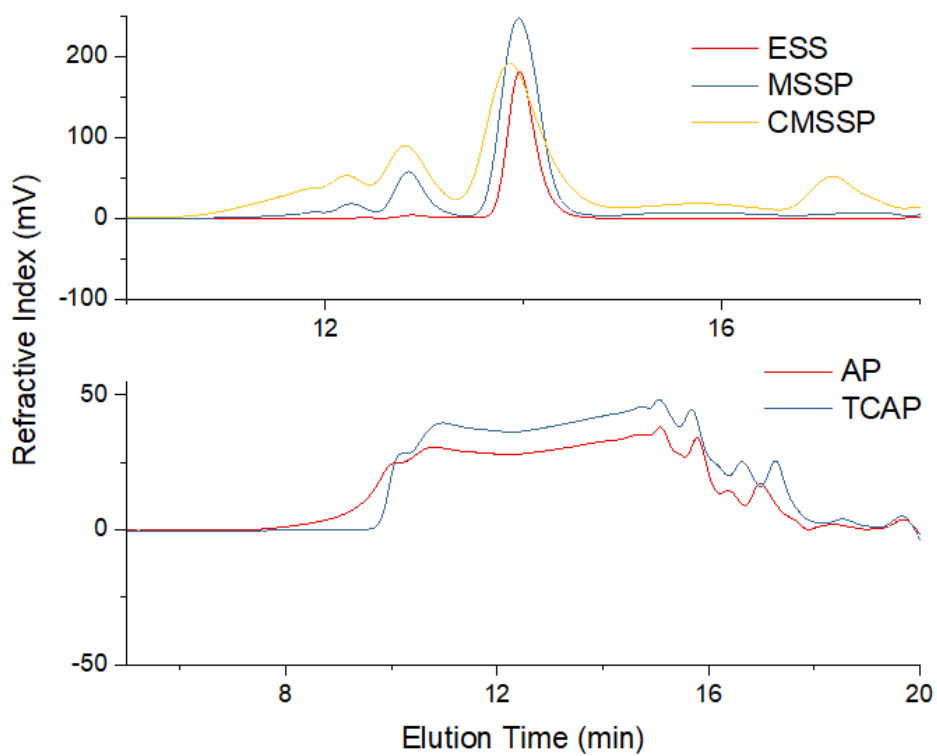
Figure 2.9. GPC Analysis of ESS-Derived Polyol and Polycarbamate to SBO-Alkyd Derived Polyol and Polycarbamate

Table 2.2. Gel Permeation Chromatographic and Rheological Analysis of ESS-Derived Polyol and Polycarbamate to SBO-Alkyd Derived Polyol and Polycarbamate

Resin	M_n	M_w	M_z	PDI	Viscosity at 50% solids (cP)
ESS	2717	2736	2754	1.007	150
MSSP	1098	3336	5245	3.039	290
CMSSP	1638	4422	8332	2.699	32600
AP	1003	4623	13932	4.61	16900
TCAP	1785	9049	26266	5.07	89400

Infrared spectroscopic analyses seen in **Figure 2.10** of the respective resins show the loss of the 826 cm^{-1} oxirane stretching of ESS[33] and the appearance of a broad, ~3300 cm^{-1} hydroxyl signal in MSSP. Upon transcarbamoylation, stretches between ~3200-3500 cm^{-1} appear which indicate amine hydrogens stretching from the carbamate groups. A new carbonyl signal ~1640 cm^{-1} is also present and indicates carbamate carbonyl stretching. The alkyd polyol also shows a broad, 3300 cm^{-1} hydroxyl signal as well as 1500-1630 cm^{-1} signals which indicate the aromatic hydrogens of the phthalates. TCAP demonstrates the ~3200-3500 cm^{-1} N-H and ~1640 cm^{-1} carbamate carbonyl signals as well, however the aromatic signals are no longer visible post-transcarbamoylation.

Screening of Dialdehyde Crosslinkers

The Sibi group and Army Research Laboratory collaborators graciously provided a large array of bio-derived dialdehydes seen in **Table 2.3**. Preliminary screenings were completed by formulating the dialdehydes and assessing whether they were able to remain stable in solution and make a crosslinked network with CMSSP and TCAP. 5-methyl-2-furaldehyde, 2-furaldehyde, 5-hydroxymethyl-2-furaldehyde, 4-hydroxy-3-methoxy-5-ethenbenzaldehyde, and vanillin contain only a single aldehyde functionality given the potential to form a full aminal by reacting 2 carbamate functionalities with 1 aldehyde. This potential was investigated to see if

only 1 present aldehyde is necessary on a crosslinker to form a carbamate-aldehyde network. 5-formyl-2-furoic acid also contains an aldehyde functionality as well as a carboxylic acid to investigate whether the acid group may autocatalyze the reaction. However, none of crosslinkers except 5-hydroxymethyl-2-furaldehyde were able to form a sufficiently crosslinked network (MEK Double Rubs >20). This may be due to the aromatic character of the monoaldehydes preventing the reaction from occurring. This was also seen with dialdehydes that had aliphatic bridges (5,5'-[Oxybis(methylene)]di(2-furaldehyde), 5,5'-(1,1-Cyclohexanediyl)di(2-furaldehyde), 5,5'-(2,2-methyl)di(2-furaldehyde), 5,5'-(2,2-methyl)di(2-furaldehyde), 5,5'-(2,2-methylbutanoate)di(2-furaldehyde)), 3,3'-Propane-2,2-diylbis(6-hydroxybenzaldehyde). These larger molecular weight dialdehydes also showed more issues dissolving in the first place or a tendency to crash out of solution. Other dialdehydes looked at capping of the dialdehydes with groups that would leave upon crosslinking that also aided with dissolving in the formulation. These included 2,2'-(2,5-Furandiyl)bis(1,3-dioxolane), 2,5-dimethoxydivinylfuran, 5-(Dimethoxymethyl)-2-furaldehyde, and 1,4-dimethoxydivinylbenzene. These derivatives easily dissolved and cured similarly to diformylfuran while diformylfuran required enough agitation and presence of acid catalyst. 1,4-benzenediamine, N,N'-bis[(1E)-2-furanylmethylene] was a curiosity to see whether a *direct-to-aminal* crosslinker was possible however this failed to dissolve. Overall, due to the constraints of batch size necessary for further assessment of the formulations as well as performances of the crosslinker candidates, diformylfuran was chosen to be compared to 1,4-CHDA when reacted with the bio-derived polycarbamates.
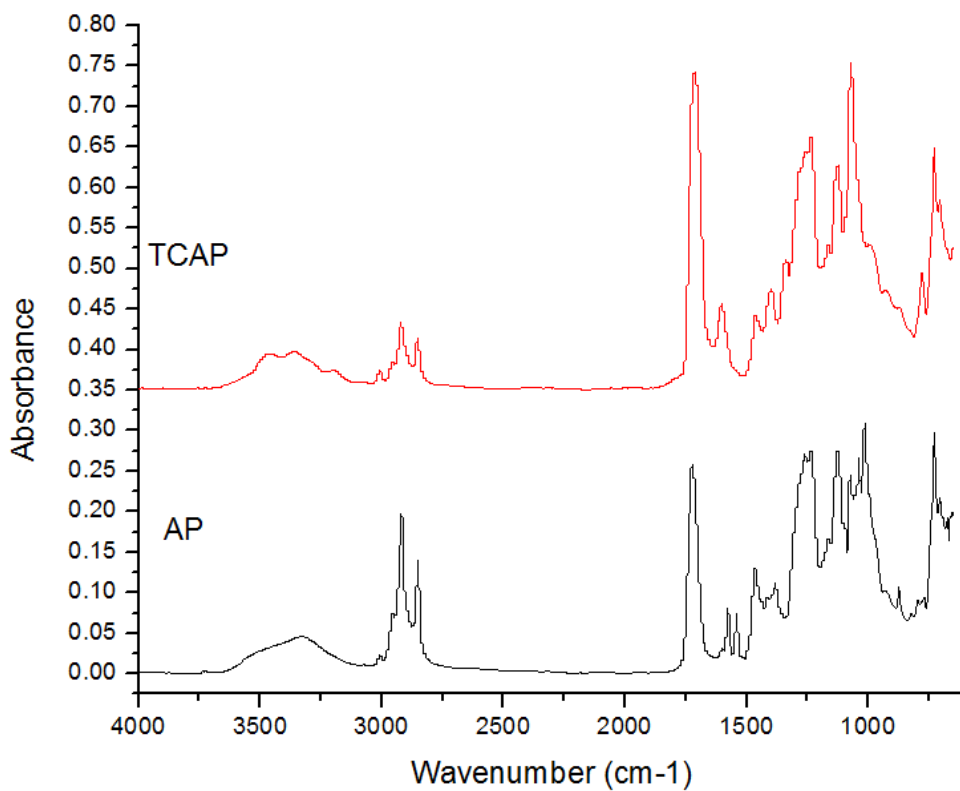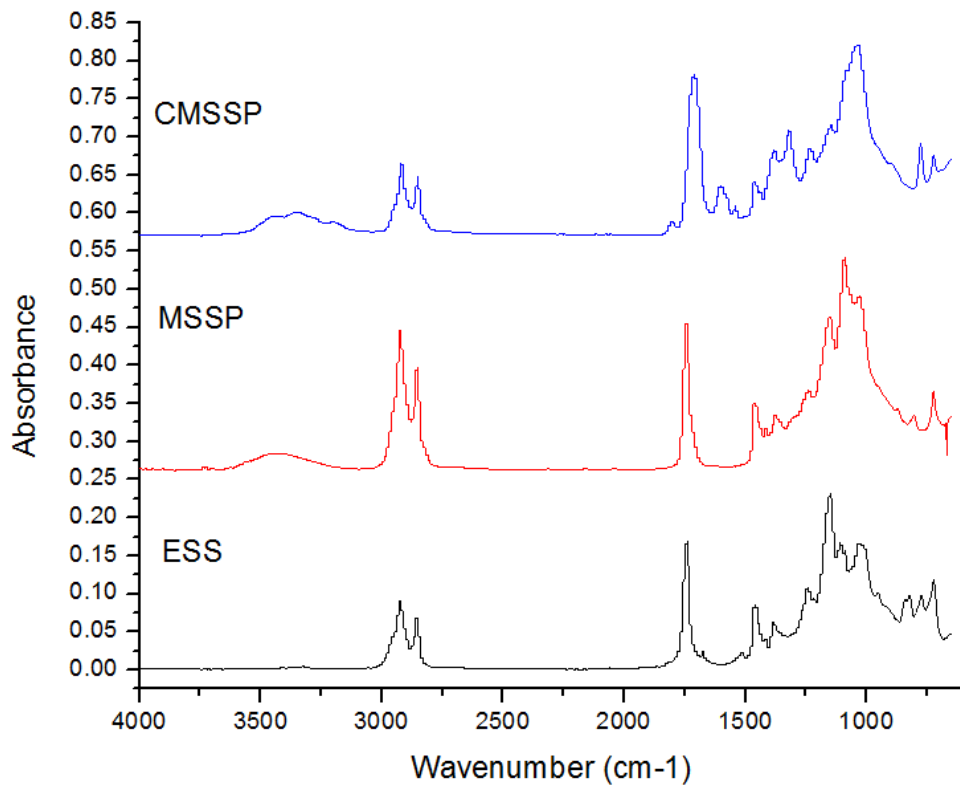
Figure 2.10. FTIR Analysis of the MSSP, CMSSP, AP, and TCAP

Table 2.3. Comprehensive List of Crosslinkers Assessed for Carbamate-Aldehyde Curing
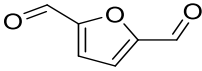
Structure of Crosslinker	Crosslinker Name	Molecular Weight (g/mol), Aldehyde Equivalent Weight (g/eq)	Attempts in NIPU Carbamate-Aldehyde Crosslinking
	Diformylfuran	124.02, 62.01	Able to disperse with acid catalyst, good cure
	5-methyl-2-furaldehyde	110.04	Unable to cure
	2-furaldehyde	96.02	Unable to cure
	5-hydroxymethyl-2-furaldehyde	126.03	Unable to cure
	5-formyl-2-furoic acid	140.01	Unable to cure
	2,2'-(2,5-Furandiyl)bis(1,3-dioxolane)	212.07, 106.04	Facile to disperse and cure
	5,5'-[Oxybis(methylene)]di(2-furaldehyde)	234.21, 117.11	Unable to cure
	5,5'-(1,1-Cyclohexanediyl)di(2-furaldehyde)	272.10, 136.05	Unable to cure
	2,5-dimethoxydivinylfuran	180.08, 90.04	Facile to disperse and cure
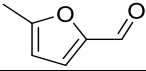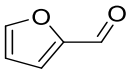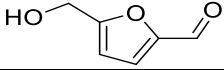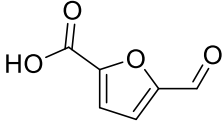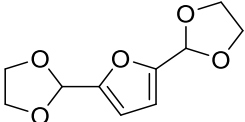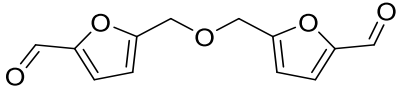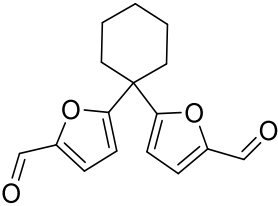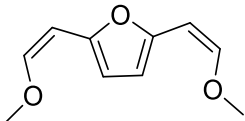
Table 2.3. Comprehensive List of Crosslinkers Assessed for Carbamate-Aldehyde Curing (continued)
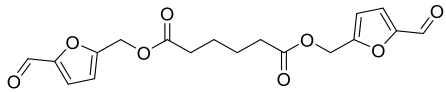
Structure of Crosslinker	Crosslinker Name	Molecular Weight (g/mol), Aldehyde Equivalent Weight (g/eq)	Attempts in NIPU Carbamate-Aldehyde Crosslinking
	5,5'-(2,2-methyl)di(2-furaldehyde)	362.1, 181.05	Unable to cure
	5,5'-(2,2-methylbutanoate)di(2-furaldehyde)	232.7, 116.04	Unable to cure
	5-(Dimethoxymethyl)-2-furaldehyde	170.06, 85.03	Facile to disperse and cure
	1,4-cyclohexanedicarboxaldehyde	140.08, 70.04	Facile to disperse, very fast cure
	1,4-pthalaldehyde	134.04, 67.02	Facile to disperse, poor cure
	1,3-pthalaldehyde	134.04, 67.02	Facile to disperse, poor cure
	1,4-benzenediamine, N,N'-bis[(1E)-2-furanylmethylene]	264.09, 132.05	Unable to cure
	3,3'-Propane-2,2-diylbis(6-hydroxybenzaldehyde)	284.1, 142.05	Facile to disperse, poor cure
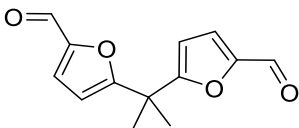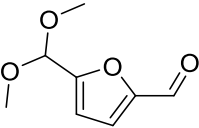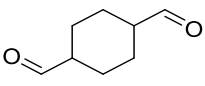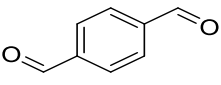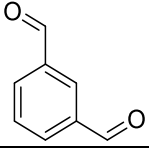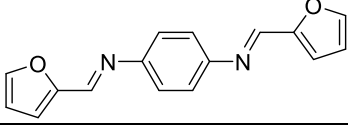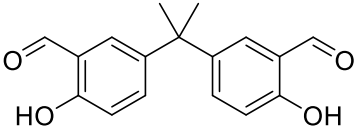
Table 2.3. Comprehensive List of Crosslinkers Assessed for Carbamate-Aldehyde Curing (continued)
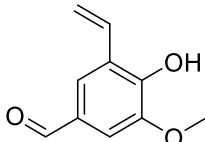
Structure of Crosslinker	Crosslinker Name	Molecular Weight (g/mol), Aldehyde Equivalent Weight (g/eq)	Attempts in NIPU Carbamate-Aldehyde Crosslinking
	4-hydroxy-3-methoxy-5-ethenbenzaldehyde	178.06	Unable to cure
	Vanillin	152.05	Unable to cure
	1,4-dimethoxydivinylbenzene	190.1, 95.05	Facile to disperse and cure
	2,3-dimethoxy-1-4-dimethylbenzaldehyde	222.09, 111.01	Unable to cure
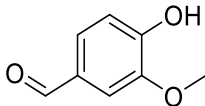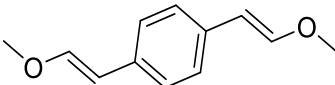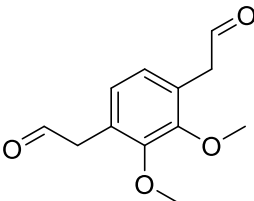
Characterization of the Coatings

Infrared spectroscopic analysis seen in **Figure 2.11** of the formulations post-ambient 3-month cure shows the disappearance of the carbamate amine stretching signals and a shifting of the carbamate carbonyl signal. Slight amine and carbamate carbonyl stretching is still seen in the TCAP formulations which were formulated at 1.5:1 carbamate:aldehyde. A broad ~3300 cm^{-1} signal remaining seen more prominently in the DFF-CMSSP formulation may indicate the presence of hydroxyls of hemiaminal linkages. The near loss of this signal in CHDA-CMSSP may indicate that either a full aminal or u-olefin network formed.[13] Both DFF formulations show a carbonyl signal around 1680 cm^{-1} which may indicate that the carbamate carbonyl is now a

polyurethane crosslink. This signal is obscured in the CHDA formulations by the carbonyls of the resins' esters at ~1700 cm^{-1}.
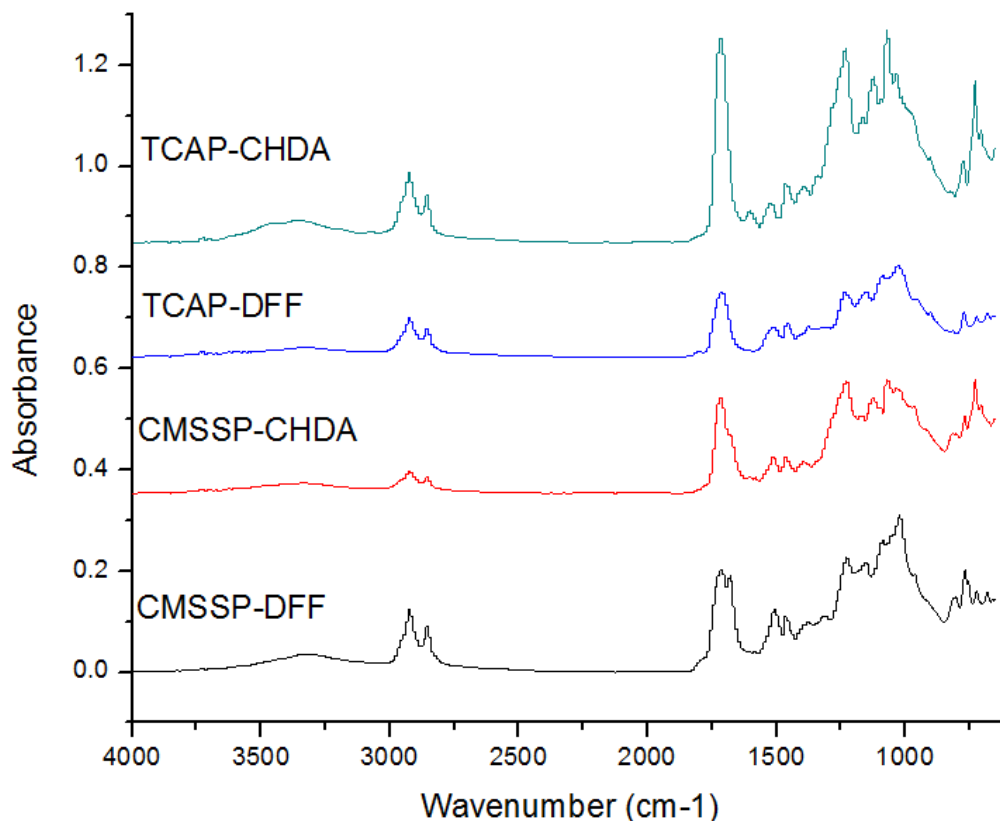
Figure 2.11. ATR Analysis of the NIPU Coating Formulations Post 3-Month Ambient Cure

The appearances of the formulations after ambient cure are seen in **Figure 2.12** and after expedited cure in **Figure 2.13**. Coatings made using DFF had notably more color development when crosslinked with both resins in comparison to the CHDA coatings. The dark brown color of DFF is much more apparent after expedited cure. DSC analysis of the ambient-cure coatings is seen in **Figure 2.14**. In the first cycle, a slight endotherm was seen from 50 °C-70 °C. This may indicate residual ethyl acetate or ethanol that was trapped in the network. After ~100 °C, a large exotherm occurs indicating that further crosslinking is occurring. The third cycle shows no sharply discernable transitions. This may be due to the further high-temperature crosslinking restricting molecular motion so much that a T_g is unable to be elucidated. Different heating rates

were likewise unsuccessful to find the step transition. DMA analysis seen in **Figure 2.15** shows the Storage Moduli generally decreasing as temperature increases, however the Loss Modulus increase, particularly seen in the CHDA formulations, may also indicate residual crosslinking. The amplitude of the *tan δ* signal demonstrates the T_gs of these ambiently-cured networks. CHDA-CMSSP showed the highest T_g from ambient cure with 91.09 °C with DFF-CMSSP providing the lowest with 67.25 °C. Tension DMA was also run on all the coatings after they had been cured for 2 hours at 120 °C right after draw-down. Their T_gs, reported in **Table 2.4**, show the lowest to be CHDA-CMSSP at 81.54 °C and the highest to be 149.9 °C with DFF-TCAP. Crosslink densities (ν_e) and the molecular weight between crosslinks (M_c) were calculated using the theory that Young's modulus, E', follows the relationship $E' = 3\nu_e RT$ and $E^{'} = 3\rho RT/M_c$ where T is the temperature, ρ is the density (assumed to be 1), and R is the gas constant.[34] The crosslink densities (ν_e) and molecular weights between crosslinks (M_c) for coatings that underwent expedited cure were in general respectively higher than the ambiently-cured coatings. This is likely due to thermal cure increasing crosslinking.
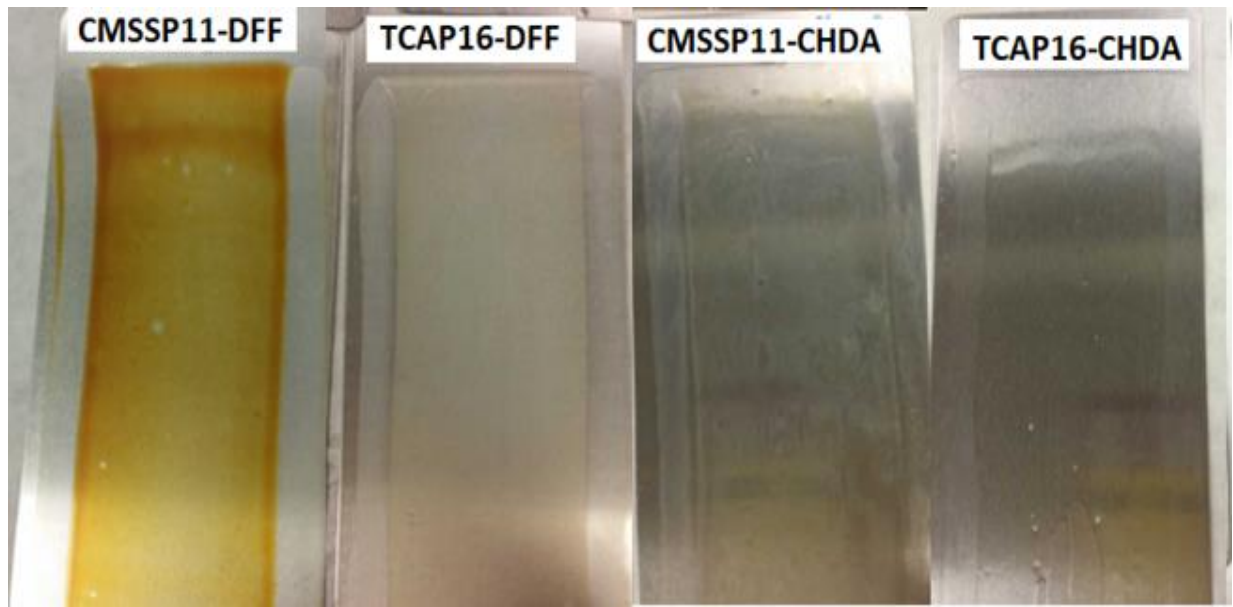
Figure 2.12. Appearance of the Formulations on Aluminum Panels After 3 Months Ambient Cure
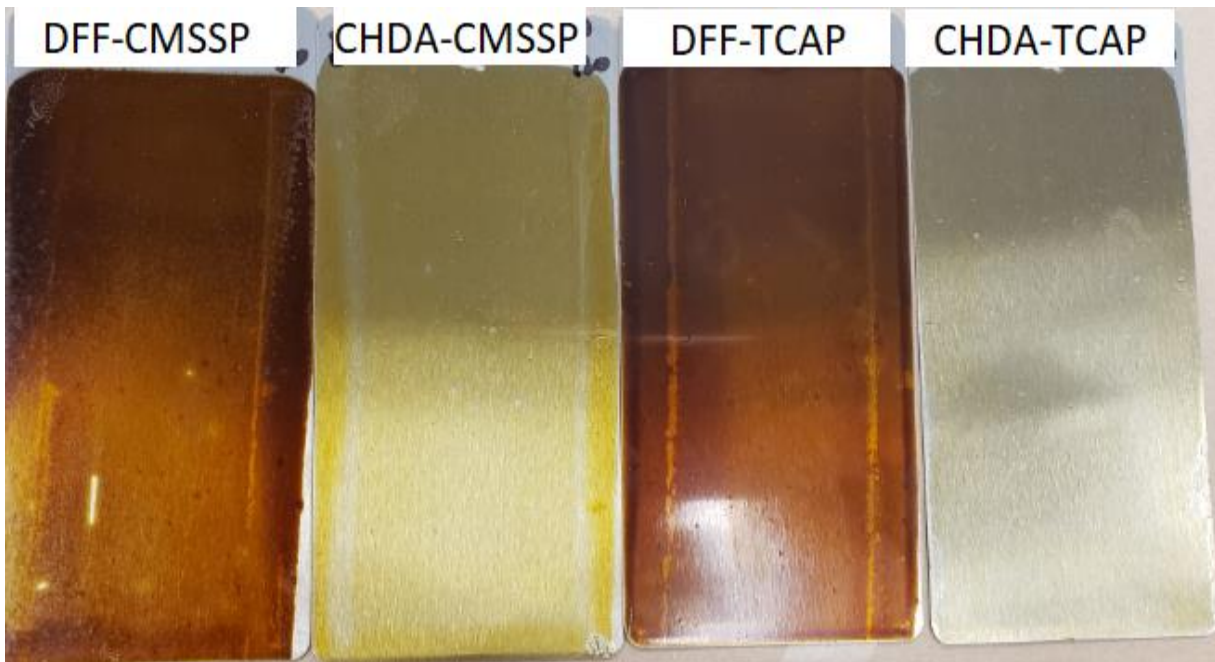
Figure 2.13. Appearance of the Formulations on Phosphate Steel Panels after Expedited Cure Conditions (2 Hours at 120 °C)
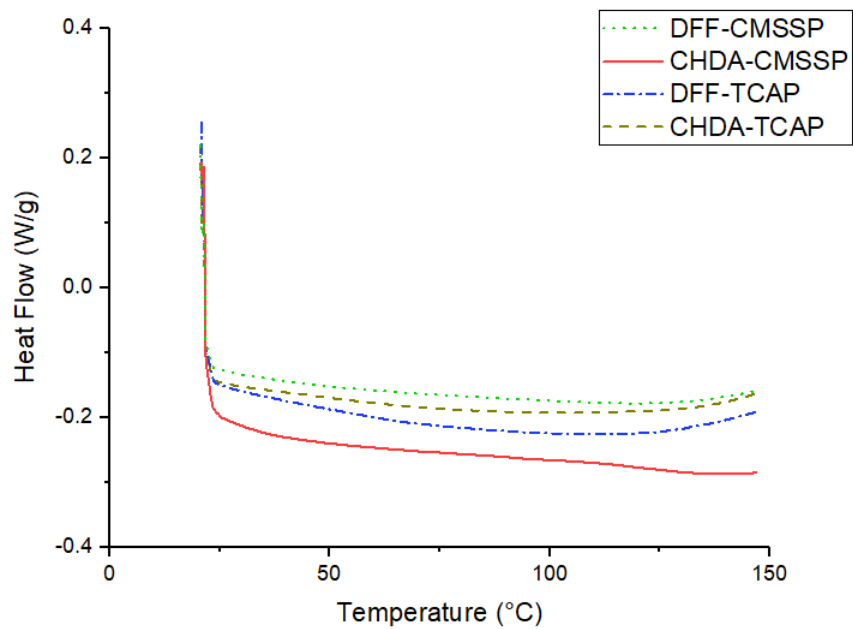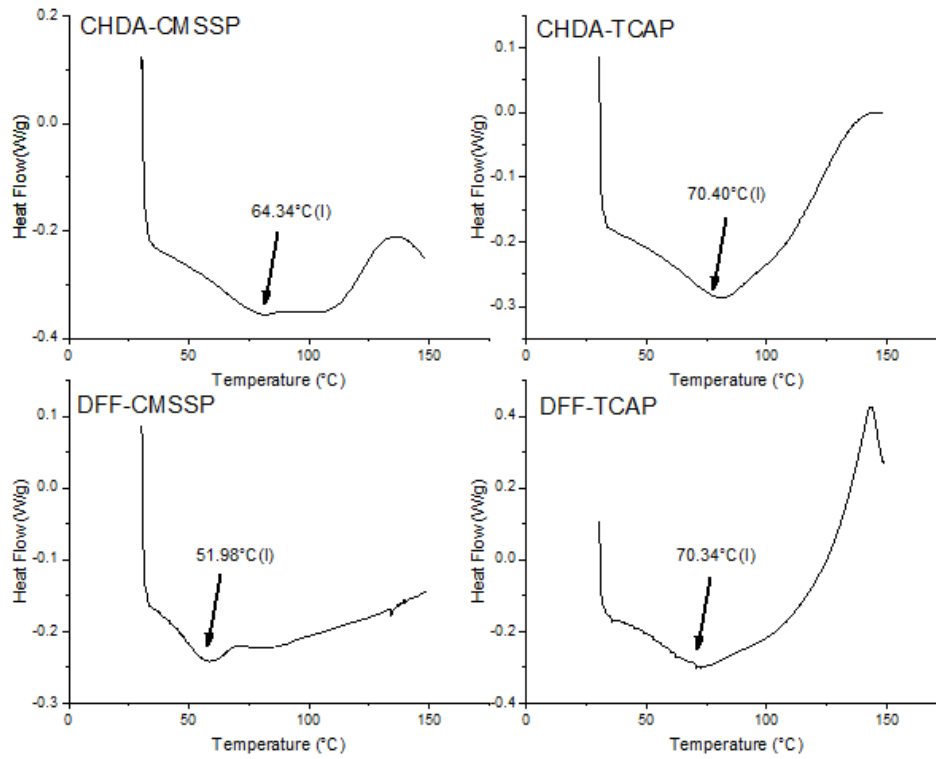
Figure 2.14. Cycle 1 (above) DSC Analysis of the Coatings. Cycle 3 (below) could not Elucidate the T_g of the Networks
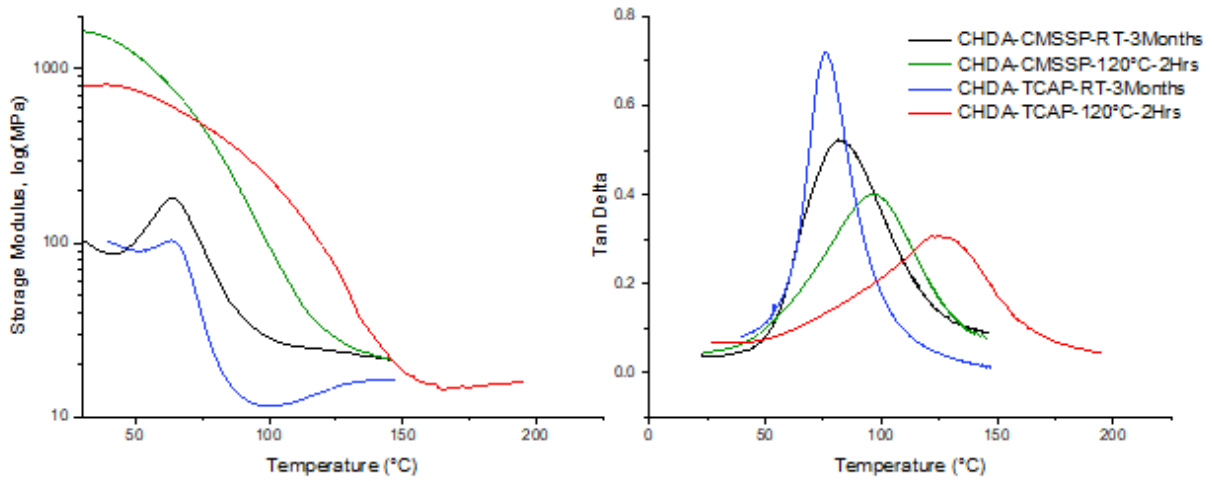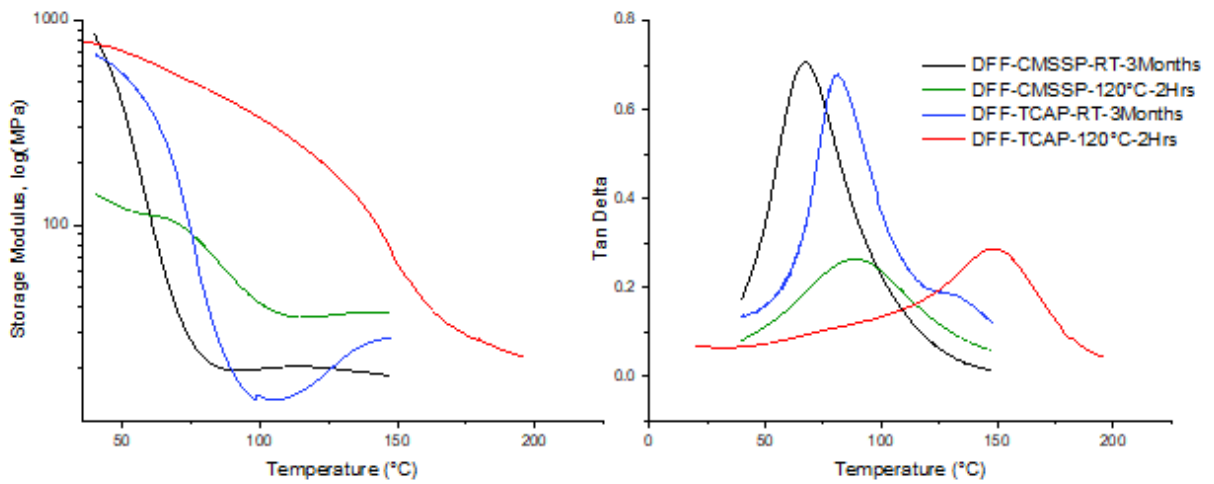
Figure 2.15. DMA Analysis of the NIPU Coatings

Table 2.4. T_gs and Crosslink Densities of the Non-Isocyanate Polyurethane Formulations

Formulation	Cure Regime	T_g (DMA, °C)	E' (MPa) at Rubbery Modulus Onset	M_c (g/mol)	v_e [x10^3 mol mm^{-3}]
DFF-CMSSP	180 days, RT	67.25	19.57	471	2.12
	120 °C, 2 hours	87.59	35.24	277	3.62
DFF-TCAP	180 days, RT	81.26	14.53	659	1.52
	120 °C, 2 hours	149.9	27.65	409	2.45
CHDA-CMSSP	180 days, RT	91.09	33.24	296	3.38
	120 °C, 2 hours	81.54	25.24	379	2.63
CHDA-TCAP	180 days, RT	75.85	11.80	801	1.25
	120 °C, 2 hours	125.4	16.37	653	1.53

Standard characterizations of the coatings (**Table 2.5**) show all the formulations were tack free rapidly under ambient conditions. It also shows across the board low impact resistances, low crosshatch adhesions, and König Hardnesses at or near 100 s indicating the networks are hard and brittle for CHDA and DFF coatings regardless of resin or cure regime. Pencil hardnesses improved over time for ambient cure from HB after one week up to F. Coatings with DFF were harder (as seen with König and Pencil hardness) than CHDA coatings and showed better solvent resistances regardless of resin. Notably, solvent resistances of the ambiently-cured DFF formulations were 3x higher than 1 week ambiently-cured CHDA formulations regardless of resin. Solvent resistances improved for the formulations after expedited cure, although the DFF formulations reached over 400 double rubs. Expedited cured formulations reached as high as H pencil hardness, yet expedited cure did not improve CHDA coatings' hardnesses. Solvent resistances improved for formulations after expedited cure. Gel % of the ambiently-cured networks showed ~30% higher extractable content for the coatings crosslinked with CHDA compared the coatings crosslinked with DFF. Expedited cure reduced the extractable content for the CHDA formulations and CMSSP-DFF, indicating further

crosslinking. Expedited-cure of TCAP-DFF showed a mild increase, however it still had less extractable content than CHDA formulations. This demonstrates that DFF is generating more crosslinks with the carbamate resins both ambiently and under thermal cure than CHDA. These results indicate that DFF networks cured under ambient or expedited cure overall perform better than CHDA regardless of polycarbamate resins used.

Table 2.5. Standard Characterizations of Non-Isocyanate Polyurethanes

Formulation	Curing Conditions	Thickness (µm)	Konig Hardness (s)	Pencil	Xhatch	Rev. Impact (in-lbs)	MEK DRs	Tack Free (min)	Gel %
DFF-CMSSP	Ambient (1 week/3 months)	37.3 ± 3	122/127	HB/F	0B/0B	<3.92	116/225	8	91.4
	120 °C	27.9 ± 3	135	H	0B	<3.92	>400	N/A	96.6
DFF-TCAP	Ambient (1 week/3 months)	38.2 ± 2	131/137	HB/F	0B/0B	<3.92	160/>400	6	94.0
	120 °C	34.6 ± 4	131	H	0B	<3.92	>400	N/A	87.3
CHDA-CMSSP	Ambient (1 week/3 months)	32.3 ± 2	70/143	2B/HB	0B/4B	<3.92	44/200	7	67.5
	120 °C	35.1 ± 2	101	2B	0B	<3.92	196	N/A	75.0
CHDA-TCAP	Ambient (1 week/3 months)	28.9 ± 3	116/115	HB/2B	0B/3B	<3.92	49/44	12	64.4
	120 °C	25.7 ± 2	81	HB	0B	<3.92	190	N/A	80.9

Conclusions

Several ESS-derived polyols were produced via acid-catalyzed alkoxylation of ESS with alcohols of different lengths. The polyols demonstrated lower viscosity with increasing alcohol size, however upon transcarbamoylation, the larger molecular weight ESS polyols showed lower conversion than MSSP to CMSSP. A soybean oil-derived alkyd polyol showed similar carbamate conversion to CMSSP and was used as a control bio-derived polycarbamate for

carbamate-aldehyde polyurethane coatings. An initial screening of a large variety of bio-derived crosslinkers was completed with the polycarbamates before diformylfuran was chosen to be compared to the conventional cyclohexanedicarboxaldehyde crosslinker. The coatings demonstrated hardness, solvent resistance, and glass transitions from 67-91 °C when cured ambiently over 3 months. Expedited cure showed increases in T_g for almost all the coatings, with the alkyd polycarbamate and DFF reaching as high as 149.9 °C. DFF-crosslinked coatings surpassed CHDA-crosslinked coatings in terms of hardness and solvent resistances regardless of resin. However, all the coatings showed brittleness and the DFF coatings imposed a color. Future work will be to improve the adhesion and reduce brittle properties of these coatings and to mitigate the imposition of color when using a biomass-derived dialdehyde. This study demonstrated that dialdehydes prepared from renewable furanics can be ambiently crosslinked with bio-derived polycarbamates to make polyurethanes that surpass the standard performance of those with a widely utilized and petrochemically-derived dialdehyde. This invites unique architectures that biomass-derived materials can provide to be used to form completely bioderived polyurethanes.

References

1. Raquez, J. M., Deléglise, M., Lacrampe, M. F., & Krawczak, P. *Prog. Polym. Sci*. **2010**, *35(4)*, 487-509.

2. Guan, Jing, et al. *Ind. Eng. Chem. Res*. **2011**, *50.11*, 6517-6527.

3. Maisonneuve, L., Lamarzelle, O., Rix, E., Grau, E., & Cramail, H." *Chem. Rev.*, **2015**, *115.22*, 12407-12439.

4. Brocas, A, Cendejas, G., Caillol, S., Deffieux, A., Carlotti, S. *J. Polym. Sci., Part A: Polym. Chem.* **2011**, *49.12*, 2677-2684.

5. Webster, DC., Crain, A. *Prog. Org. Coat.*, **2000**, *40.1-4*, 275-282.

6. Webster, DC. *Prog. Org. Coat,* **2003**, *47.*1, 77-86.

7. Datta, J.; Włoch, M. *Polym. Bull.* **2015**, *73 (5),* 1459–1496.

8. Ubaghs, L.; Keul, H.; Höcker, H. *Polym.* **2005**, *46* (5), 1459–1465.

9. Kwolek, Stephanie L., and Paul W. Morgan. *J. Pol. Sci. Gen. Pap,* **1964**, *2.6*, 2693-2703.

10. Popa, Paul, et al. *Coatings Tech*, **2015**, *12.5.*

11. Cornille, A.; Auvergne, R.; Figovsky, O.; Boutevin, B.; Caillol, S. *Eur. Polym. J.* **2017**, *87*, 535–552.

12. Argyropoulos, JN., et al. "Ambient temperature curable isocyanate-free compositions for preparing crosslinked polyurethanes." U.S. Patent Application No. 15/068,823.

13. Anderson, Jeff R., et al. "Crosslinkable composition, a method of making the same and a crosslinked composition produced therefrom." U.S. Patent No. 9,580,622. 28 Feb. 2017.

14. Spilman, Gary E., et al. "Crosslinkable coating composition and method of producing the same." U.S. Patent No. 9,822,280. 21 Nov. 2017.

15. Popa, Paul J., et al. "Cross-linkable coating composition and method of producing the same." U.S. Patent No. 9,604,721. 28 Mar. 2017.

16. Kamber, Nahrain E., et al. "Ambient cure compositions for making coatings having humidity and corrosion resistance and methods of use." U.S. Patent Application No. 15/214,907.

17. Spilman, Gary E., et al. "Crosslinkable coating composition and method of producing the same." U.S. Patent No. 9,650,541. 16 May 2017.

18. Argyropoulos, John N., et al. "Ambient temperature curable isocyanate-free compositions for preparing crosslinked polyurethanes." U.S. Patent Application No. 15/068,823.

19. Amarasekara, A. S.; Green, D.; Williams, L. D. *Eur. Polym. J.* **2009**, *45*(2), 595–598.

20. Moreau, C.; Belgacem, M. N.; Gandini, A. *ChemInform* **2004**, *35* (31).

21. Jang, N. R.; Kim, H.-R.; Hou, C. T.; Kim, B. S. *Polym. Adv. Tech.* **2013**, *24* (9), 814–818.

22. Ikezaki, T.; Matsuoka, R.; Hatanaka, K.; Yoshie, N. *J. Polym. Sci., Part A: Polym. Chem.* **2013**, *52* (2), 216–222.

23. Pan, Xiao, Partha Sengupta, and Dean C. Webster. *Green Chem.*, **2011**, *13.4*, 965-975.

24. Pan, Xiao, Partha Sengupta, and Dean C. Webster. *Biomac.*, **2011,** *12.6*, 2416-2428.

25. Yan, Jingling, and Dean C. Webster. *Green Mat.*, **2014**, *2.3*, 132-143.

26. Kovash, C. S.; Pavlacky, E.; Selvakumar, S.; Sibi, M. P.; Webster, D. C. *ChemSusChem* **2014**, *7* (8), 2289–2294

27. Monono, E. M.; Webster, D. C.; Wiesenborn, D. P. *Ind. Crops and Prod., **2015**, 74, 987-997.*

28. Monono, E. M.; Bahr, J. A.; Pryor, S. W.; Webster, D. C.; Wiesenborn, D. P. *Org. Process Res. Dev.* **2015**, *19* (11), 1683–1692.

29. Nelson, TJ.; Masaki, B.; Morseth, Z.; Webster, DC. *J. Coat. Tech and Res.* **2013**, *10.6*, 757-767.

30. Adamopoulos, Lambrini. "Understanding the formation of sugar fatty acid esters." (2006).

31. Murillo, E. A.; Vallejo, P. P.; López, B. L. *Prog. Org. Coat.*, **2010**, *69.3*, 235-240.

32. Spasojević, P. M., et al. *Advances,* **2015**, *5.76*, 62273-62283.

33. Pan, Xiao, Webster, DC. *Chem. Sus. Chem.*, **2012**, *5.2*, 419-429.

34. Jones, Frank N., Mark E. Nichols, and Socrates Peter Pappas. Organic coatings: science and technology. John Wiley & Sons, 2017. Page 76.

CHAPTER 3. EXPLORATION OF BIO-BASED FUNCTIONALIZED SUCROSE ESTER

RESINS FOR ADDITIVE MANUFACTURING VIA STEREOLITHOGRAPHY

Introduction

Bio-derived alternatives to petrochemically-derived resins are being sought for a wide variety of applications. Among them is the growing field of stereolithographic printing (SLA). Stereolithography, or *vat polymerization,* involves a vat filled with prepolymer, a build platform, and an ultraviolet laser.[1] First, a computer-assisted design (CAD) file is translated into a number of slices depending on set print resolution. This build platform is lowered into the prepolymer vat and the laser beneath draws out, or cures, one of these slices from the file onto the build platform. The platform then raises at an angle before lowering into the vat again and the next slice drawn. This process continues until the 3D object is completed.[2]

Resin formulations in SLA must meet a wide variety of processing and curing parameters to ensure a successful print and not risk damaging the printer. Among these are considerations of viscosity, mechanical properties, and extent of cure of the formulation being compatible with the characteristics of the printer (laser power, infill rate, print resolution).[3-5] Bio-derived SLA resins such as from polylactic acid,[6] lignin,[7] hydroxyalkanoates,[8] cellulose,[9] and plant oils[10-12] have been explored as alternatives. The bio-derived material epoxidized sucrose soyate (ESS) is remarkable giving it contains flexible aliphatic chains, a rigid sucrose core, and numerous epoxy sites that can be easily modified.[13] Its analogues have been assessed for use in many high-performance thermosets cured by heat, UV-radiation, and under ambient conditions.[14-18] Polyacrylates of ESS with esters formed from acrylic and methacrylic acid have been synthesized and tested as UV-curable coatings and composites.[19] These resins show potential as a component of a stereolithographic resin. The purpose of this study was to carry out an initial

57

exploration of several poly(meth)acrylates from ESS, formulate them to be successful for SLA printing, and compare the mechanical and thermomechanical properties of the prints with resin prints with petrochemically-derived urethane acrylate resins.

Experimental Section

Materials

Epoxidized sucrose soyate (ESS, EEW: 253 g/eq, 99% solid was prepared from the pilot plant at North Dakota State University[20], dibutyltin oxide (DBTO), methacrylic anhydride (MA, 94%), acrylic acid (AA, 99%), butyric anhydride (BA, 98%), and hydroquinone (HQ, 99%) were received from Sigma Aldrich. Hexandedioldiacrylate (HDDA), Ebecryl 1290 (aliphatic urethane acrylate), Ebecryl 220 (aromatic urethane acrylate), and Ebecryl 150 (BPAEDA, bisphenol-a ethoxylate diacrylate) were kindly supplied by Allnex. Irgacure TPO-L (TPO-L, Ethyl(2,4,6-trimethylbenzoyl)-phenyl phosphinate) photoinitiator was received from BASF. The Peopoly Moai Blue resin was purchased from matterhackers.com.

Synthesis of (Meth)acrylated Resins from Epoxidized Sucrose Soyate

Three different resins were synthesized from epoxidized sucrose soyate (ESS) based on previously published procedures. AESS (acrylated ESS) is synthesized from the reaction of acrylic acid with ESS where 90% of the epoxy groups are reacted.[19] DMESS (dimethacrylated ESS) is synthesized from the reaction of methacrylic anhydride and methacrylic acid with ESS, where the epoxy and subsequent hydroxyl groups are reacted (2 eq acid: 1 eq oxirane, with an acid to anhydride molar ratio of 1:9).[22] MBSS (methacrylated-butylated ESS) is synthesized by reacting both methacrylic anhydride and butyric anhydride with ESS where the epoxy and subsequent hydroxyl groups are reacted (2 eq acid: 1 eq oxirane, with butyric anhydride to methacrylic anhydride molar ratio of 1:9).[21]

Preparation of Formulations for SLA Printing

In a 250 mL plastic container, TPO-L photoinitiator (1.18%), HDDA (7.41%) and

BPAEDA diluent (49.41%), and the respective resin (41.99%) was added before being mixed

vigorously with a tongue depressor for 10 minutes. The formulation was vortex-mixed for 15

minutes and let to sit until bubbles were no longer present before any analysis was completed.

Formulations were kept in the dark to prevent unintended polymerization before use or analysis.

The hexafunctional aliphatic and aromatic urethane acrylates Ebecryl 220 and Ebecryl 1290 were

chosen as comparison resins to the ESS-derived resins for the same formulations. As a further

comparison, Peopoly Moai Blue was tested alongside these formulations given it is a commercial

SLA ink specifically optimized for the Peopoly Moai SLA printer.

Rheological Analysis of the Resins and SLA Resin Formulations

Rheological analyses were completed on an ARES Parallel Plate Rheometer by TA

Instruments. Resin or formulation was pipetted onto the bottom plate and the gap set to 1 mm.

Excess resin running outside the plates was wiped away with a KimWipe™ before the plates

were rotated at a steady rate sweep from 1 rotation/second to 100 rotations/second.

Solids Content of the Resins

Approximately 1 g of resin was deposited in a tared aluminum pan and ~0.5 g of toluene

pipetted over it. The pan was then placed in a convection oven and heated to 150 °C and held at

that temperature for 1 hour. The resin weights were recorded, and the percent solids of the resin

determined from the pre and post resin weights. Assessments were completed in triplicate and

averaged.

Spectroscopic Analysis of the Resins

Resins were characterized using a 400 MHz Bruker Nuclear Magnetic Resonance Spectrometer (^{1}H-NMR). Resin samples were dissolved in deuterated chloroform (99.8%; one assessment with 1% TMS). Fourier Transform Infrared Spectroscopy (FTIR) was run on a a ThermoScientific Nicolet 8700. A thin layer of resin was deposited on a spectroscopic-grade KBr crystal for assessment.

Gel Permeation Chromatographic Analysis of the Resins

GPC analysis of the resins was run on an EcoSEC HLC-8320GPC from Tosoh Bioscience with a differential refractometer detector. 10 mg of sample was thoroughly dissolved in tetrahydrofuran (THF) in a vial. This was then filtered through a 0.45 mm PTFE filter before being assessment. The samples were eluted at flow rate 0f 0.35 mL/min. An EasiVial polystyrene standard obtained from Agilent was utilized for calibration.

Printing of Flexural and Tensile Samples with the SLA Resin Formulations

Samples were printed using a Peopoly Moai SLA Printer (Firmware version 1.6, with layer height set to 100 µm). Flexural and Tensile Samples were CAD files with dimensions in accordance with ASTM D790 and ASTM D438 respectively. The files were input into XYZ Nobel software and 10 mm supports added. The subsequent STL file was inputted into Ultimaker Cura software to translate to a GCODE file. All printing on the Moai used firmware version 1.6. Flexural and Tensile samples assessed were printed horizontal (**0x**) and normal (**90x**) to the build platform. The placement of the prints on the build platform were regularly moved to extend the lifespan of the PDMS layer in the vat. Post print, the samples required careful separation from the build platform with the use of a sharp tool provided with the Moai printer. The removed samples were washed in an ethanol bath for 5 minutes, dried, and then placed in a convection

oven with rotating chamber surrounded with 405 nm wavelength lights and heated to 50 ℃ for 2 hours for post-cure. The structural supports were first clipped and then the print was smoothed with sandpaper. Flexural samples were rectangular and with dimensions of 76.8 mm x 13 mm x 4 mm before the addition of supports. Tensile samples were Type IV dimensions as specified in ASTM D638.

Differential Scanning Calorimetry (DSC) of the Prints

Differential Scanning Calorimetry (DSC) was run on a TA Instruments Q1000 Modulated Differential Scanning Calorimeter. ~ 5 mg of coating was placed in a standard aluminum pan and run under a Heat-Cool-Heat regime first equilibrating at 30 °C, heating at 10 °C/min to 150 °C, cooling 10 °C/min to 20 °C, then reheating at 10 °C/min to 150 °C. T_g was determined as the mid-point of the inflection from the second heating.

Dynamic Mechanical Analysis (DMA) of the Prints

Dynamic Mechanical Analysis (DMA) was run on a TA-Instruments Q800 Dynamic Mechanical Analyzer. Printed samples of 70 mm x 13 mm x 4 mm (the same dimensions of flexural samples but carefully cut to fit completely in the clamp) thickness were prepared, washed in ethanol, postcured under 405 nm light and heated to 50 ℃ for 2 hours for post-cure. The scaffolding was carefully clipped from the samples and the sample gently sanded with sandpaper where the scaffolding once was. The sample was then locked in the calibrated dual cantilever DMA clamps at 2 lbs with a torque wrench. Samples were equilibrated at -40 °C before heating at 10 °C/min to 150 °C.

Tensile Assessment of the Prints

The tensile testing was completed on an Instron 5567 load frame (Instron, Norwood, MA), a 2 kN load cell, and 25.4 mm extensometer. Tensile testing was carried out in accordance

to ASTM D638 for a type IV sample. The samples were tested at a 1 mm/min crosshead rate withfailure typically occurring within 10 minutes. Five sample specimens were tested for each tensile assessment.

Flexural Assessment of the Prints

The flexural testing was also completed on the Instron 5567 load frame with a 2 kN load cell and the data collected the same as through tensile testing. Tensile testing was carried out in accordance with ASTM D790 with a three-point bending set-up using center loading. The span was set for a span-to-thickness ratio of 16:1 for the average thickness of 5 samples. Crosshead rate for testing was 5 mm/min.

Gel Content of the Prints

Samples of 1 g were taken from the post-cured prints. Each were wrapped in filter paper and placed upright (not stacked) in a paper thimble which was then inserted into a Soxhlet extractor. The extractor was inserted into a round bottom flask filled with dichloromethane and a reflux condenser attached to the top. The round bottom flask was then lowered into an oil bath with thermocouple and heated until dichloromethane was refluxing. Reflux was continued for 24 hours before the samples were removed from the thimble and dried in a vacuum oven for several hours. The final-initial/initial weights of the samples were taken and averaged to find the gel content of the prints.

Thermogravimetric Analysis (TGA) of the Prints

Thermogravimetric analysis (TGA) was completed on a TA Instruments Q500 Thermogravimetric Analyzer. Tared platinum pans were loaded with ~10-15 mg of the respective cured formulation before being heated from room temperature to 600 °C at 10 °C/minute.

Results and Discussion

The synthesis schemes for the functionalized bio-based resins, MBSS, DMESS, and AESS, are given in **Figure 3.1**. The resins had a similar greenish appearance due to the chromium-based AMC-2 catalyst. ^{1}H-NMR analysis of the (meth)acrylated resins in **Figure 3.2** show the depletion of the strong oxirane signals in ESS (2.8-3.2 ppm) and the appearance of -C=CH$_2$ protons (6.2 ppm). **Figure 3.3** supports this signal change through FTIR analysis where new C=O signals (1730 cm^{-1}) of the (meth)acrylate esters near the C=O stretching ester signals of the sucrose-fatty acid core (1750 cm^{-1}). The appearance of C=C stretching of the (meth)acrylates is also present (1690 cm^{-1}). AESS and MBSS show the presence of a broad O-H stretch (3600 cm^{-1}). ^{31}P-NMR method to determine hydroxyl content (method as specified elsewhere[23]) found an OHEW of 298 g/eq for AESS. The resins show O-H signals due to the secondary hydroxyls that were not esterified.

Gel Permeation Chromatographic Analysis and % solids of the resins are seen in **Figure 3.4** and **Table 3.1**. The distinct ESS signal at 2717 g/mol shows a lower elution time shift with AESS followed by DMESS and MBSS with similar elution time shifts indicating a trend of increasing molecular weights. Several broad signals at even lower elution times for AESS, DMESS, and MBSS indicate the presence of oligomers which likely formed due to hydroxyl-epoxy alkoxylation during synthesis.[21-22] The solids content of the resins show AESS, MBSS, and ESS to be very high, while DMESS is around 90%. This is most likely due to unreacted acrylate monomer since the reaction was stopped at an acid number of 15 to keep it consistent with the other resins and prevent gelation that could occur at longer reaction times.

Rheological analysis of the resins as well as the BPAEDA reactive diluent is seen in **Figure 3.5**. AESS shows the highest viscosity due to its highly hydroxylated structure resulting

in significant hydrogen bonding. This is followed by decreasing viscosity with DMESS and then MBSS. The lower viscosity of MBSS is attributed to its plasticizing butyl groups. ESS follows with even lower viscosity, being only slightly higher than BPAEDA.

Upon mixing the resins into their respective formulations, they were once again assessed for rheological behavior. The formulations compared the ESS-derived resins to tough aliphatic and aromatic urethane acrylates as well as a formulation specifically formulated for the Moai SLA printer. This analysis seen in **Figure 3.6** shows the Moai Resin to have the lowest viscosity while the next least viscous formulations contained DMESS and then MBSS. These were then followed by the formulations with the aliphatic urethane acrylate Ebecryl 220 and then the aromatic urethane acrylate Ebecryl 1290. The most viscous formulation contained AESS which once again was attributed to the high hydroxyl content present on AESS. All formulations were able to print successfully for flexural and tensile assessment even though they were much more viscous than the Moai Blue, however future prints of higher resolution may merit a lower viscosity.
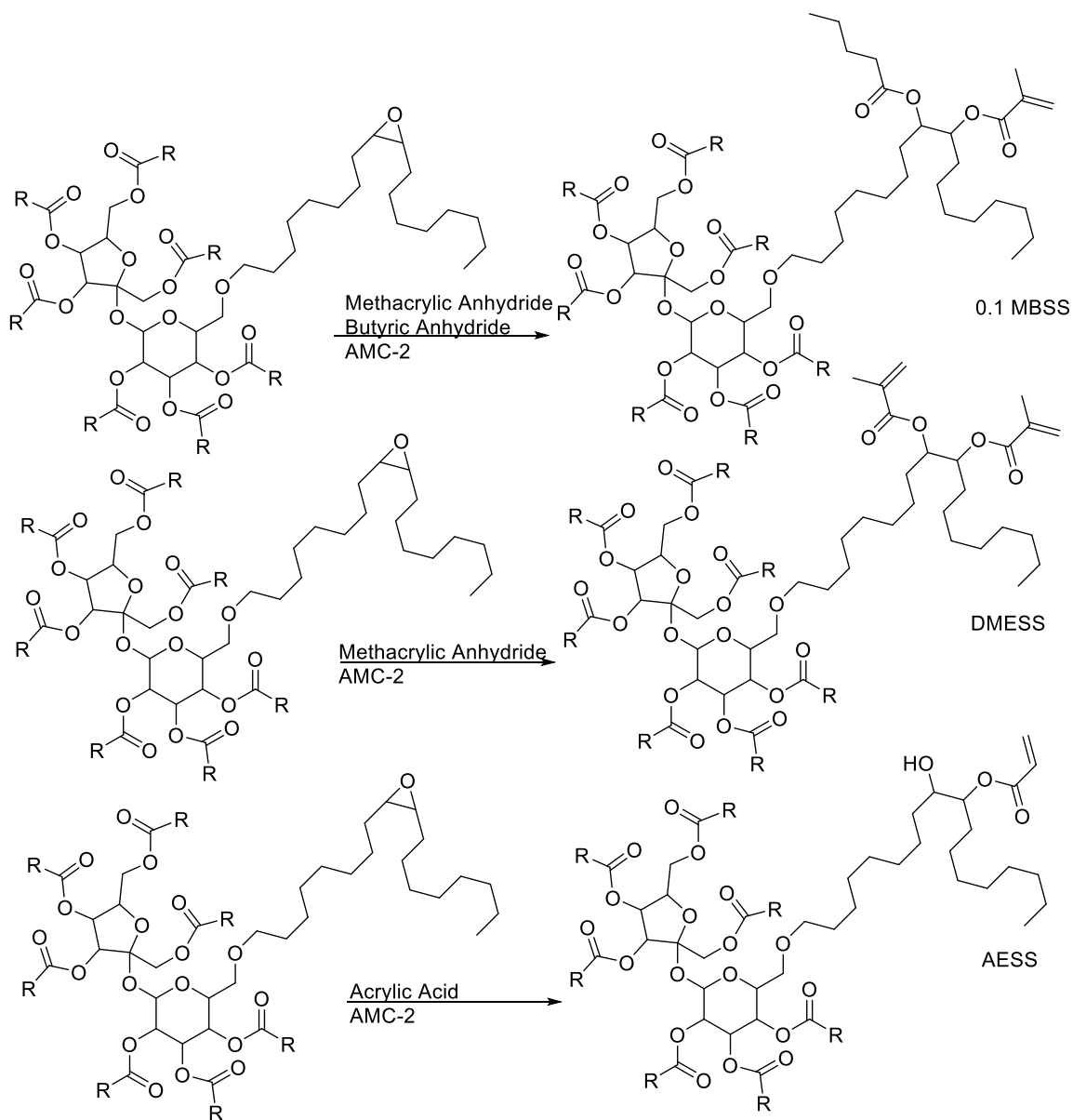
Figure 3.1. Representative Synthetic Scheme of MBSS, DMESS, and AESS
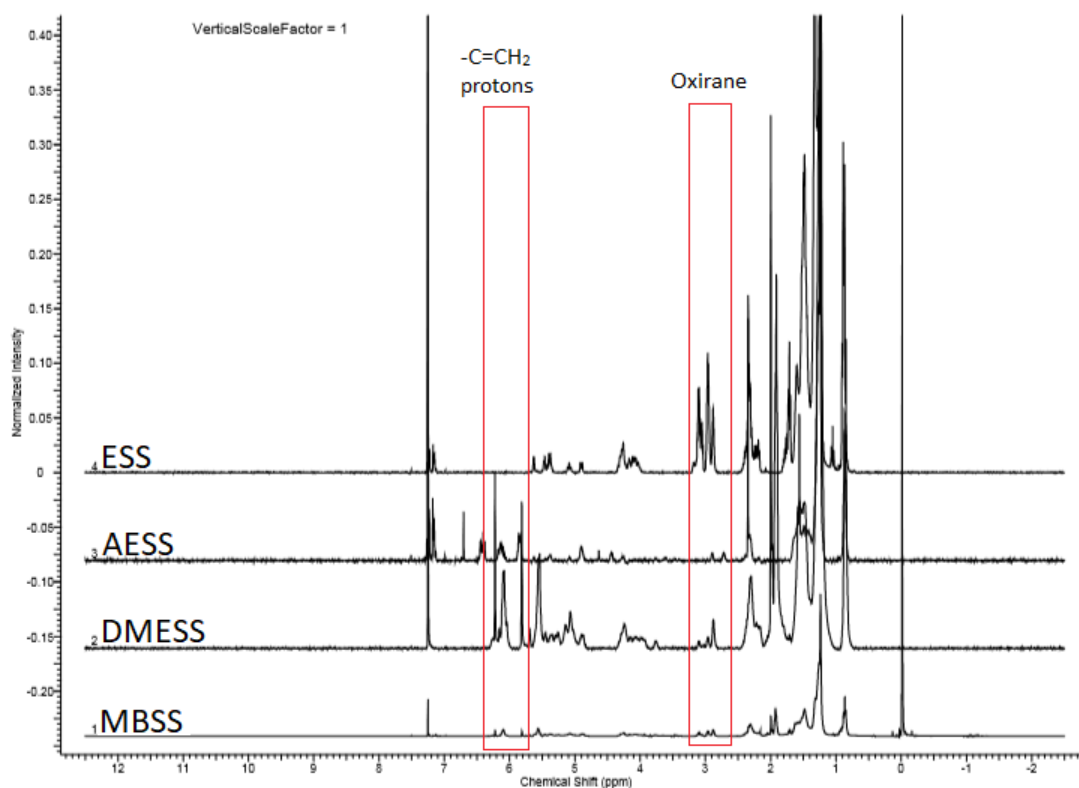
Figure 3.2. ^{1}H-NMR Spectroscopy of ESS, AESS, DMESS, and MBSS. Highlighted Areas Show Protons Corresponding to Oxirane and Vinyl Groups
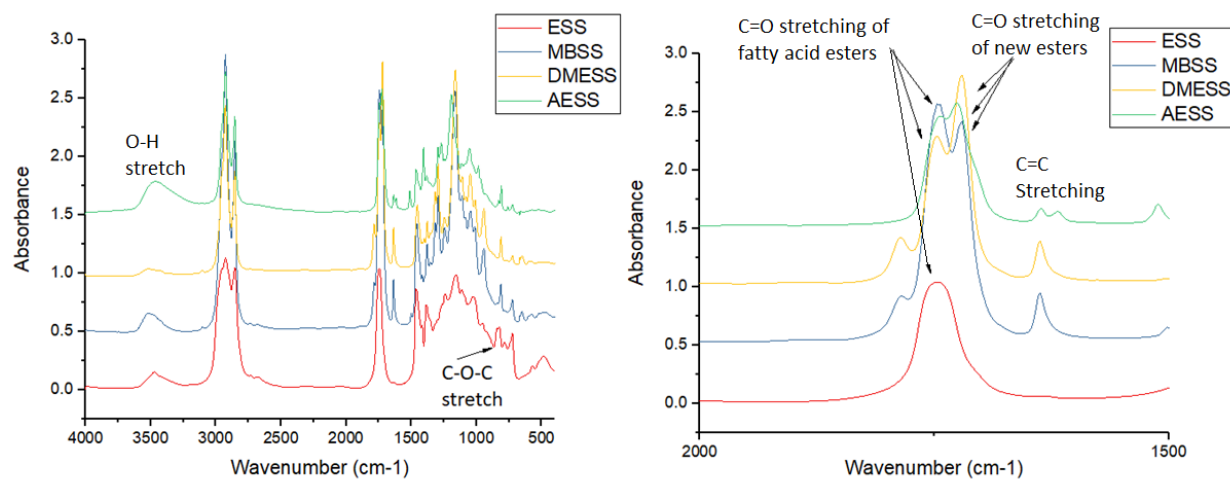
Figure 3.3. FTIR Analysis of ESS, MBSS, DMESS, and AESS. Left: Full Range of Spectra. Right: 2000-1500 cm^{-1} Range of Spectra to Highlight Carbonyl and Unsaturation Signals
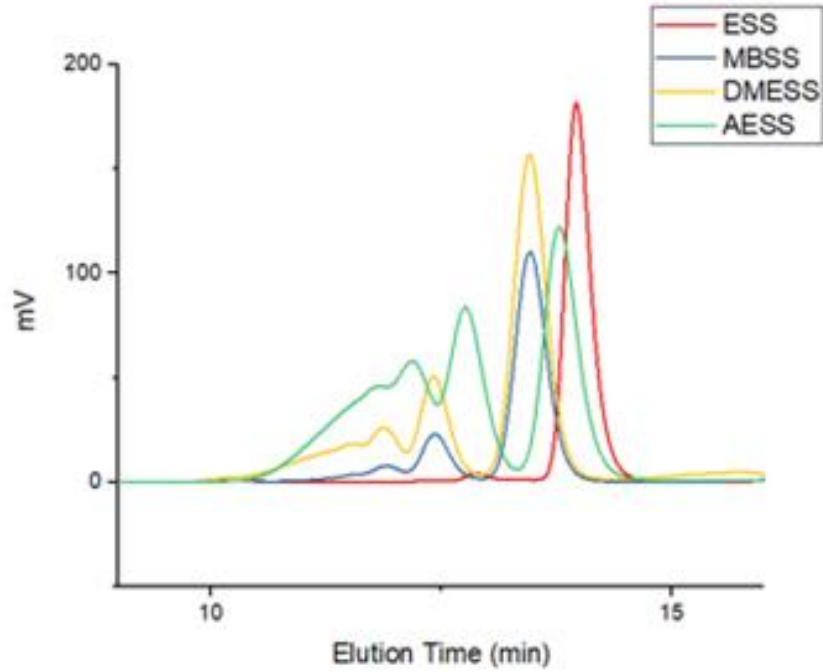
Figure 3.4. Gel Permeation Chromatographic Analysis of ESS, MBSS, DMESS, and AESS

Table 3.1. Gel Permeation Chromatographic Analysis and % Solids of ESS, MBSS, DMESS, and AESS

RESIN	M_n	M_w	PDI	% Solids
ESS	2717	2737	1.01	98.7
MBSS	4125	4415	1.07	97.0
DMESS	1430	6578	4.59	90.7
AESS	3091	7565	2.45	98.6
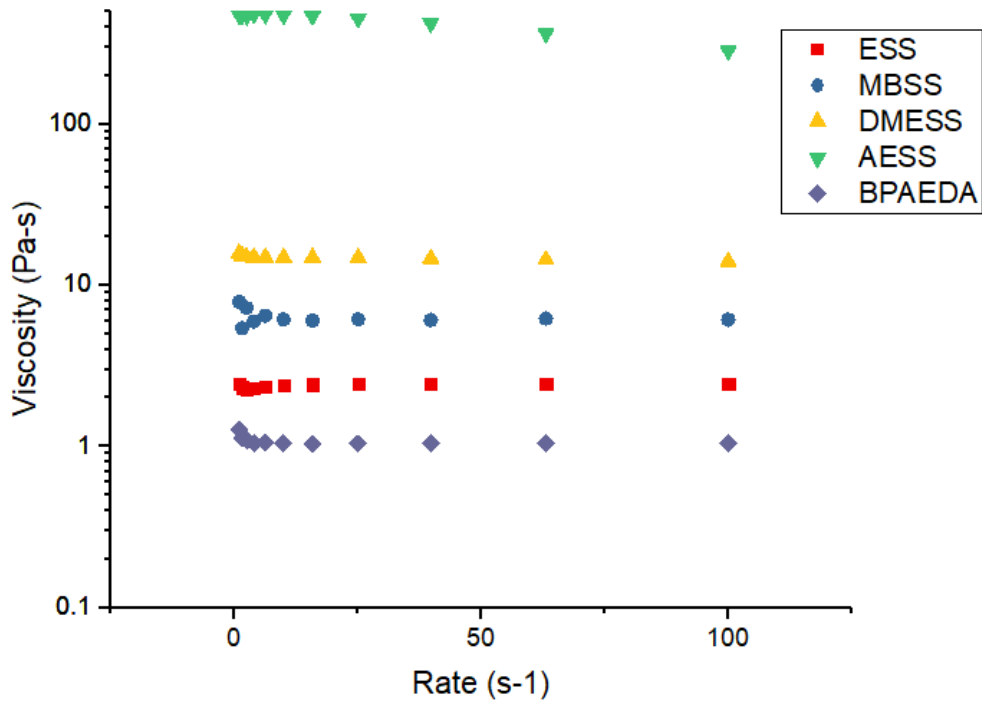
Figure 3.5. Rheological Analysis of ESS, MBSS, DMESS, AESS, and SLA Reactive Diluent BPAEDA
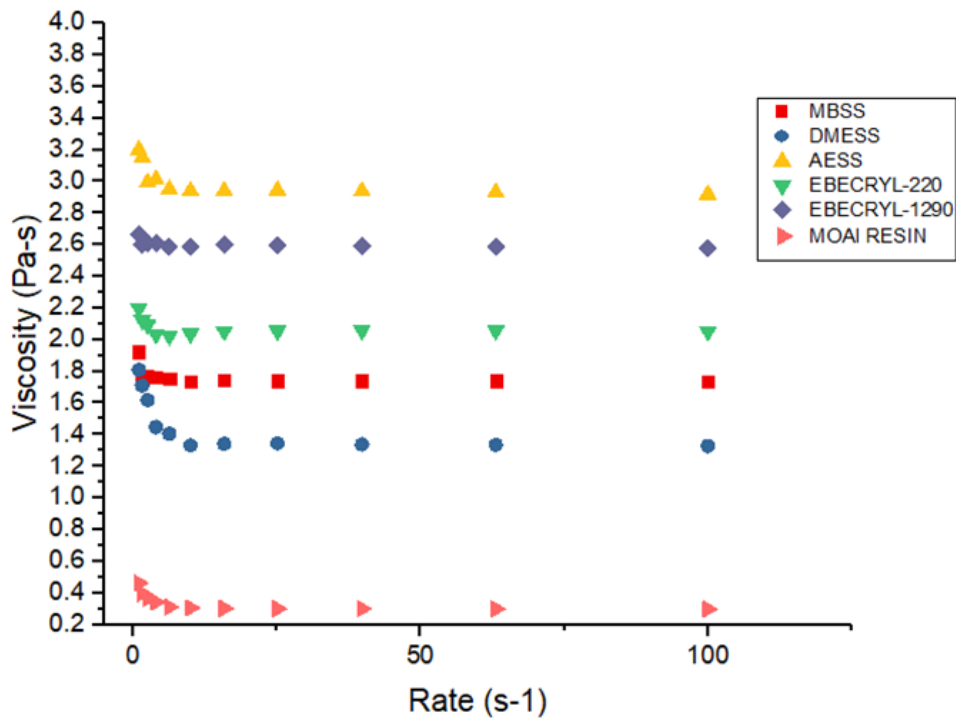
Figure 3.6. Rheological Analysis of Formulations with 41.99% MBSS, DMESS, AESS, Ebecryl-220, or Ebecryl-1290, and Commercial SLA Resin (Peopoly Moai Blue)

The appearance of 0x orientation tensile prints of MBSS formulations with supports and Moai Blue where the supports have been removed and the print sanded are shown in **Figure 3.7**. It is important to mention that the clipping and sanding process of the prints may impart stress histories that can impact the subsequent tensile and flexural measurements. Further, points where these supports meet the print may have different cure due to more laser exposure compared to the non-supported side. Therefore, the presence of the structural supports may impart stress concentrators. The green appearance of the prints is a result of the chromium-based catalyst used to synthesize the functionalized bio-based resins. There were some issues encountered during printing in the 90x orientation for each of the formulations where curing occurred in the PDMS layer and not upon the build platform. This was more of an issue with Ebecryl 1290 for flexural samples so flexural assessment of this formulation is not seen in this orientation.

Figure 3.7. 0x Tensile Prints of MBSS with Supports and Moai Blue with Supports Removed

The tensile properties of the prints are summarized in the following sections. The Moai Blue resin exhibited the highest tensile strength in either orientation followed by the urethane acrylate formulations. MBSS followed at slightly more than half the maximum tensile strength of the urethane acrylate formulations. The lowest tensile strengths were seen in the DMESS and

AESS formulations. Tensile strain measurements showed that AESS formulations deformed extensively at maximum stress for each printed orientation. MBSS formulation showed high strain to failure only when printed vertical to the build platform but low when printed horizontally. DMESS formulations exhibited the lowest strain to failure in both printed orientations. The urethane acrylate formulations had very low strain to failure at for 0x printed orientation, however the 90x prints had about twice the strain to failure.

The performance of DMESS, especially in comparison to MBSS formulations prompted a closer look which showed small cracks appearing in the prints which further developed over time when exposed to light. This is seen in **Figure 3.8**. To compare the tensile behavior for these formulations before the weakening due to the cracks is seen, the Young's Modulus, is presented in **Figure 3.9**. In both formulations, DMESS shows the highest modulus out of the ESS-derived formulations regardless of orientation. This was followed by MBSS and then AESS which was the lowest out of all the formulations. The Moai Blue and urethane acrylate formulations showed similar, high moduli to DMESS formulations. This shows that DMESS can make strong formulations, however its tensile strength is compromised due to the surface crack formation which can lead to initiation failure under stress. Methods of improving this situation are being explored.

Figure 3.8. Cracking Observed with the DMESS Printed Formulations
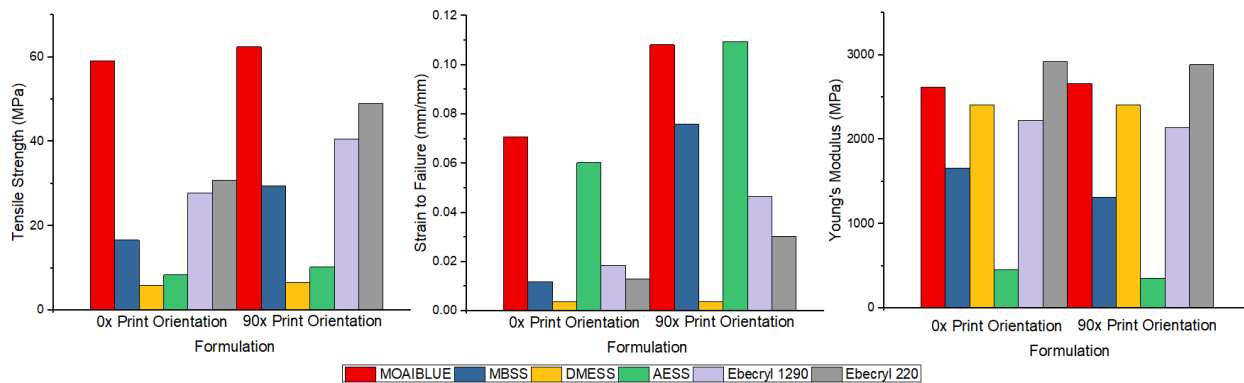
Figure 3.9. Tensile Strength (left), Tensile Strain to Failure (center), and Young's Modulus (right) of the Printed Formulations

The flexural behavior of the formulations showed similar results (**Figure 3.10**). The Moai Blue resin showed high flexural strength. The urethane acrylate formulations, particularly those with Ebecryl 220 showed high flexural strength, and high flexural modulus. Of the ESS-derived acrylate formulations, MBSS showed the highest flexural strength at around 2/3 the strength of the urethane acrylate formulations in several orientations. DMESS and AESS formulations were similar and yielded at low flexural strength. Flexural moduli of DMESS and MBSS were similar near 1000 MPa while AESS remained low around 200-250 MPa in each orientation.
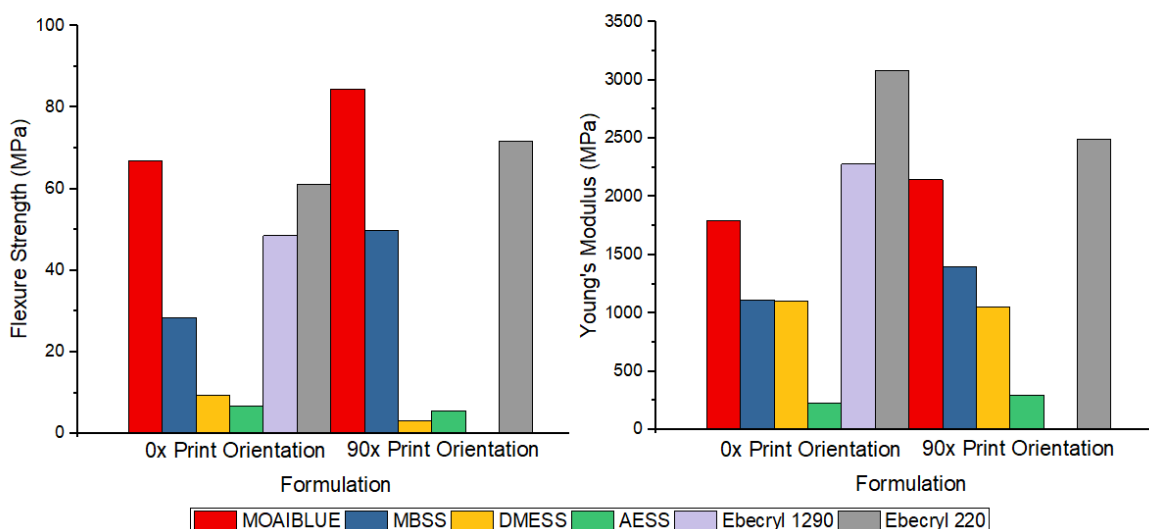
Figure 3.10. Flexural Strength (left) and Young's Modulus (right) of the Printed Formulations

Dynamic mechanical analysis of the print formulations is shown in **Figure 3.11**. and

Table 3.2 further elucidate some of this behavior. Storage modulus values for prints except for

the Moai Blue do not show a rubbery plateau and indicate that that the rubbery plateau is at a

higher temperature. For AESS and DMESS, there are drops at the end of the tan δ curves. This

may be due to the samples slipping in the clamp grips. Further optimization of post-cure

conditions for the prints will likely improve mechanical properties. The T_gs of the resins as

recorded through DMA and DSC showed Moai Blue had the highest T_g (averaged from both

thermal analytical methods) of 96.16 °C followed by 81.06 °C and 77.39 °C of Ebecryl 1290 and

Ebercyl 220 respectively. DMESS had the highest T_g of the ESS-derived formulations at 77.85

°C and followed by MBSS at 73.75 °C while AESS had the lowest T_g of all at 43.46 °C. The gel

content of the formulations was the lowest with DMESS at 92.25% followed by Ebercyl 220,

Ebercyl 1290, AESS, MBSS, and finally Moai Blue at 98.67%, respectively. These values when

related to the thermal analytical analysis demonstrate that the hydrogen-bonding of a urethane is

an incredibly important moiety to be present in the resin to imbue toughness. It also demonstrates

72

that the butyl group on the MBSS may have important contributions to tensile and flexural performance of the final print by mitigating cracking. This is due to the butyl groups preventing shrinkage of the parts during post-cure and causing stress cracking.
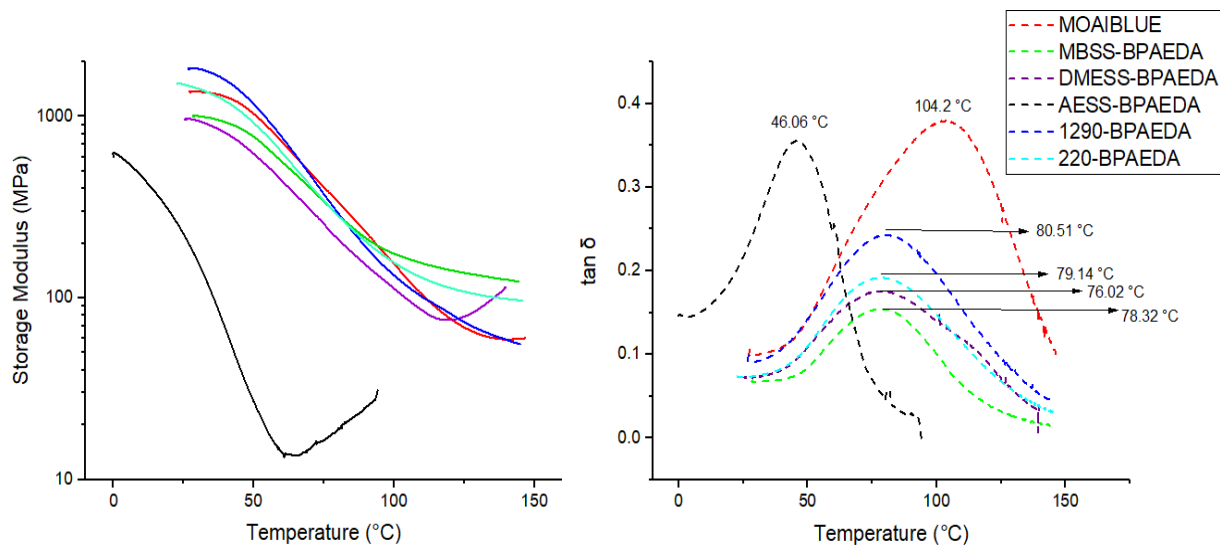
Figure 3.11. Dynamic Mechanical Analysis of the Printed SLA Formulations

Table 3.2. Gel Content and Glass Transition Temperatures of Printed Formulations

Formulation	Gel Content (%)	T_g (DSC, °C)	T_g (DMA, °C)
MOAIBLUE	98.67	88.12	104.2
MBSS-BPAEDA	98.59	69.17	78.32
DMESS-BPAEDA	92.25	79.73	76.02
AESS-BPAEDA	94.89	40.86	46.06
1290-BPAEDA	94.69	81.62	80.51
220-BPAEDA	93.27	75.63	79.14

Thermogravimetric analysis of the cured prints is seen in **Figure 3.12** and compiled values in **Table 3.3**. It is seen that the Moai Blue resin had the lowest temperature where the rate of decomposition was highest. These were followed by MBSS, DMESS, and AESS formulations before the urethane acrylate comparisons. The urethane acrylates had significantly higher $T_{5\%}$

73

and $T_{50\%}$ values. This demonstrates that urethane acrylates impart more thermal resistance than the bioderived resins.
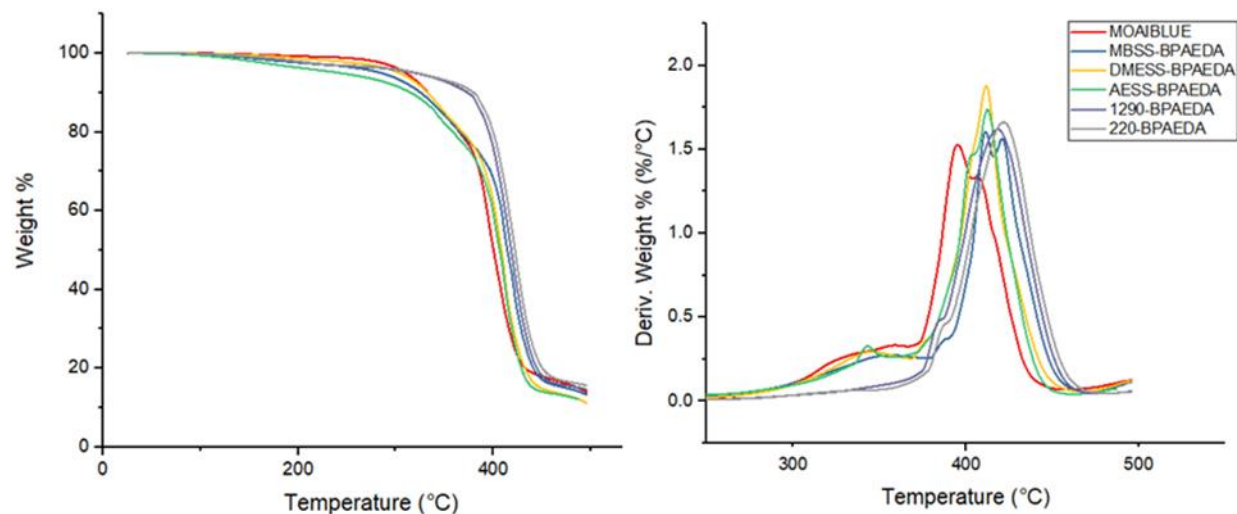
Figure 3.12. Thermogravimetric Analysis of Printed SLA Resin Formulations. Left: Weight % Loss, Right: Derivative Weight % Loss

Table 3.3. Summary of Thermogravimetric Analysis Results of SLA Prints

Formulation	Initial Decomposition Temp ($T_{5\%}$, °C)	Temperature of 50% Weight Loss ($T_{50\%}$, °C)	Temperature Maximum Decomposition Rate (T_{max}, °C)
MOAIBLUE	309.2	400.3	394.3
MBSS-BPAEDA	317.7	411.4	408.3
DMESS-BPAEDA	321.4	408.2	411.7
AESS-BPAEDA	338.1	414.6	420.2
1290-BPAEDA	385.5	418.5	418.5
220-BPAEDA	392.9	422.4	421.8

Conclusions

Resins made from derivatives of the bioderived material ESS were prepared, characterized, and formulated to make stereolithographic resins. For comparison, formulations were made with petrochemically-derived urethane acrylates replacing the ESS derivative

74

content. Another comparison was a commercial resin formulated for the SLA printer used. It was seen that hydroxy-functional acrylated ESS derivative not only was highly viscous due to its hydroxyl content but having lower crosslinking groups available resulted in weak tensile and flexural behavior. DMESS and MBSS showed similar glass transition temperatures to Ebecryl 1290 and Ebecryl 220 formulations. DMESS indicated a comparable tensile modulus to the urethane acrylate formulations, however its low tensile and flexural behavior were attributed to the onset of cracks. The best-performing of the ESS derivatives for flexural and tensile assessments, MBSS, was due to the small presence of plasticizing butyl groups that mitigated the occurrence of cracks. Comparison urethane acrylate resins and the commercial resins showed superior mechanical properties. The urethane acrylates also imparted thermal resistance to the prints. DMA indicated further crosslinking occurring when analyzing storage modulus for the ESS-derived resin formulations and the Ebecryl resins. This study demonstrates that a bioderived material can be modified and incorporated into an SLA formulation at significant amounts (41.99% weight). Improvements to tensile and flexural behavior to match or exceed urethane acrylates as well as the mitigation of cracking during the post-cure process are a concern. Potentially, the synthesis of an ESS derivative with hydrogen-bonding functional groups such as urethanes may create a prepolymer with stronger properties.

References

1. Griffey, Jason. *Library Technology Reports,* **2014**, *50*, 8-12

2. Lee, Jian-Yuan, Jia An, and Chee Kai Chua. *Applied Materials Today,* **2017**, *7*, 120-133.

3. Gibson, Ian, David Rosen, and Brent Stucker. *Additive Manufacturing Technologies*. Springer, New York, NY, 2015. 63-106.

4. Hofmann, Manfred. *ACS Macro Lett.* **2014**,*3*,4-382-386.

5. Rohner, Gottfried, et al. U.S. Patent No. 8,623,264. 7 Jan. 2014.

6. Voet, Vincent SD, et al. *ACS Omega,* **2018**, *3*, 1403-1408.

7. Sutton, Jordan T., et al. *ACS applied materials & interfaces,* **2018**, *10,* 36456-36463.

8. Yang, Elisa, et al. *Polymer Reviews,* **2018**, *58*, 668-687.

9. Sodian, Ralf, et al. *ASAIO journal,* **2002**, *48*, 12-16.

10. Markstedt, Kajsa, Johan Sundberg, and Paul Gatenholm. *3D Printing and Additive Manufacturing,* **2014**, *1*, 115-121.

11. Miao, Shida, et al. *Scientific reports,* **2016**, *6*, 27226.

12. Manapat, Jill Z., et al. *Macromolecular Materials and Engineering,* **2017**, *302*, 1600553.

13. Pan, Xiao, Partha Sengupta, and Dean C. Webster. *Green Chemistry,* **2011**, *13,* 965-975.

14. Kovash Jr, Curtiss S., et al. *ChemSusChem,* **2014**, *7*, 2289-2294.

15. Yan, Jingling, and Dean C. Webster. *Green Materials,* **2014**, *2*, 132-143.

16. Arvin, Z. Yu, AliReza Rahimi, and Dean C. Webster. *European Polymer Journal,* **2018**, *99,*202-211.

17. Pan, Xiao, and Dean C. Webster. *ChemSusChem,* **2012**, *5*, 419-429.

18. Nelson, Thomas J., et al. *Journal of Renewable Materials,* **2013**, *1.2*, 141-153.

19. A. Paramarta; X. Pan; C. Webster Dean. *Radtech Report,* **2013**, *27*, 26-32.

20. Monono, Ewumbua M., Dean C. Webster, and Dennis P. Wiesenborn. *Industrial Crops and Products,* **2015**, *74*, 987-997.

21. Arvin, Z. Yu, et al. *Reactive and Functional Polymers,* **2018**, *128*, 29-39.

22. Arvin, Z. Yu, Jonas M. Sahouani, and Dean C. Webster. *Progress in Organic Coatings,* **2018**, *122*, 219-228.

23. Archipov, Yuri, et al. *Carbohydrate research,* **1991**, *220*, 49-61.

CHAPTER 4. EFFECT OF INCORPORATION OF SUBSTITUTED POLYHEDRAL OLIGOMERIC SILSESQUIOXANES IN A BIO-BASED RESINS SYSTEM FOR STEREOLITHOGRAPHIC PRINTING

Introduction

Stereolithographic printing (SLA), or vat polymerization involves a container (or vat) filled with prepolymer and a build platform. The build platform lowers itself the vat and submerges in prepolymer. Below the vat a laser exposes prepolymer to UV radiation and cures a layer of thermoset onto the platform. The platform then raises from the vat and lowers again before another layer is cured. These layers are from a dissected CAD file and upon curing of every layer, a 3D object is printed. SLA, like other forms of 3D printing, is studied in academic and commercial settings for a variety of fields and products.[1-3]

Within a growing number of these fields, there is a desire to design bioderived materials for 3D printing processes. Given petrochemicals are a finite resource and its extraction and processing pose environmental and health concerns, derivatives from renewable plant feedstocks are an attractive alternative. However, challenges involve modifying plant derivatives to be competitive with conventional, petrochemically-derived materials so that they are competitive in performance and cost.[4] Further, in regards to SLA printing, there are processing parameters (Ex: laser wavelength and exposure time, compatibility aspects of vat with formulations, layer building rates, viscosity of formulation, print removal and post-cure processing) that must be met to ensure successful prints. In the submitted study "Exploration of Bio-based Functionalized Sucrose Ester Resins for Additive Manufacturing via Stereolithography" (Chapter 2), acrylate resins made from bioderived epoxidized sucrose soyate were synthesized and formulated into

SLA inks. Prints with high bioderived content were compared to commercial SLA resins and several improvements to the bioderived prints were sought.

Additives which can improve properties of thermosets with little amounts required are an important and growing industry. Compatibilization, appearance, strengthening, adhesion, and rheological control are but a few attributes for which additives are desired.[5-10] Families of additives based upon polyhedral oligomeric silsesquioxane (POSS) have been developed and studied for incorporation in variety of materials due to the remarkable properties they possess. These materials are unique given they are an inorganic-organic hybridization. The SiO core portion of the cage imparts thermal stability and high modulus (11.7 GPa), while organic (R) portions enable miscibility of these materials in organic systems as well as incorporation of reactive functionalities to covalently incorporate the nanoparticles into a thermoset.[11-14] **Figure 4.1** shows an octameric cage-like structure of POSS. The cage sizes can also be decameric and dodecameric and cage diameters can range from 1.5-3.0 nm. These large volumes have been attributed to the making formulation components more compatible by increasing the contact of the organic groups on the POSS with other organics in the formulation.[12-14] **Figure 4.2** shows Methacrylated POSS (m-POSS). With this functionality, POSS nanoparticles can be incorporated into a multitude of free-radically curing thermosets; this includes thermosets used in SLA printing.
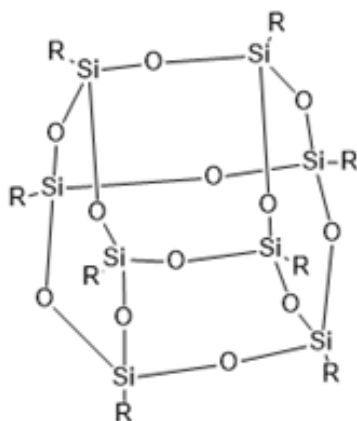
Figure 4.1. Representation of a POSS Nanoparticle with Octameric Core Structure

Epoxidized sucrose soyate (ESS), seen in **Figure 3.2**. is a polyester of flexible soybean oil fatty acids and a rigid sucrose core where the unsaturation of the fatty acids is converted to oxirane using peroxides.[15] With 9-14 modifiable oxiranes present in each molecule, many sites are available to participate and perform densely crosslinked networks. ESS and its derivatives have found use in polyurethanes, polyesters, acrylics while unmodified ESS has formed highly bioderived UV-curable coatings with hardness and solvent resistances.[15-21]
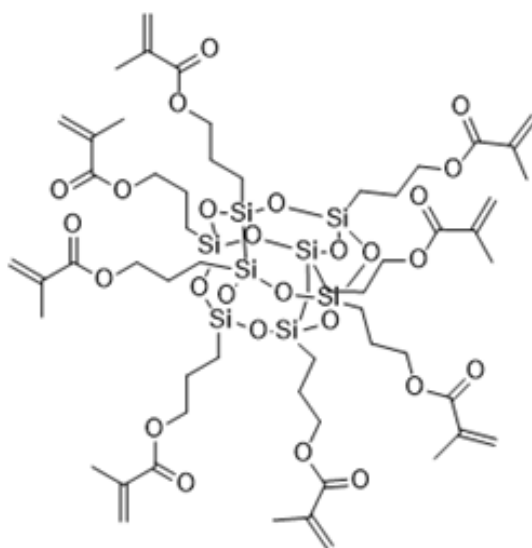
Figure 4.2. Structure of m-POSS

POSS nanoparticles have yet to be assessed for their incorporation into networks formed by ESS and its derivatives. Dimethacrylated ESS (DMESS, **Figure 4.3**) and other ESS derivatives were previously assessed as SLA inks, but there was interest in improving thermal and mechanical properties of the printed thermosets. This study investigates the structure-property relationships of *m*-POSS in thermosets with high DMESS content. These formulations specifically were made to ascertain whether POSS materials can successfully be incorporated with ESS derivatives and explore influence of the additive on rheology, thermal, and mechanical properties of the final thermosets. With significant improvements seen, not only does it expand the thermosets that can incorporate POSS nanoparticles, but it may improve the performance of thermosets with high bioderived content while using small additive amounts.
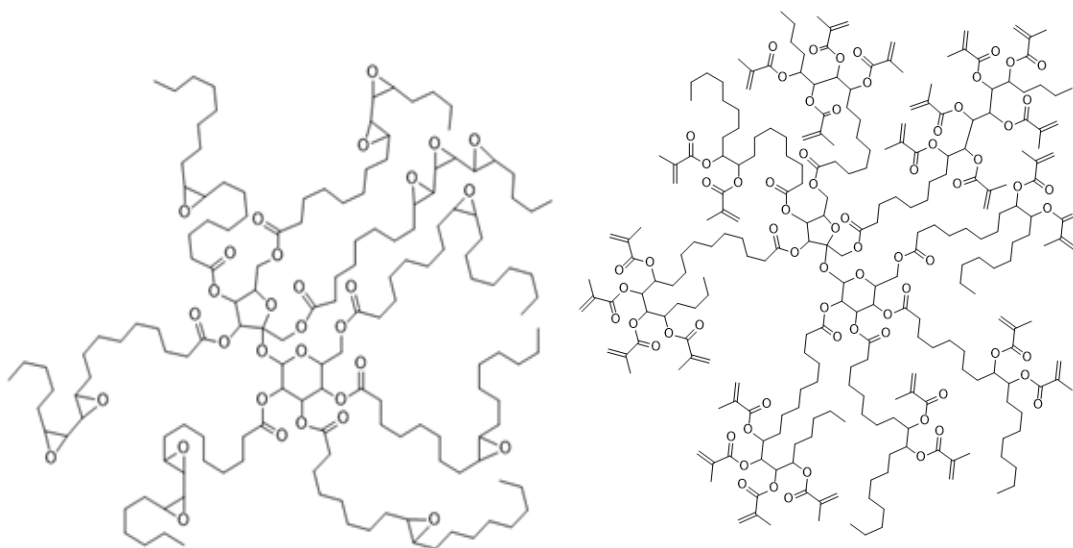
Figure 4.3. Representative Structure of Epoxidized Sucrose Soyate (ESS) and Dimethacrylated Sucrose Soyate (DMESS)

Experimental Section

Materials

Epoxidized sucrose soyate (>99% solids, 1000 cP, 236 g/eq. epoxy) was received from a pilot plant producing the material at North Dakota State University (Fargo, ND, USA).[15, 16]

Dimethacrylated epoxidized sucrose soyate (DMESS) was prepared according to an earlier method.[22] Methacrylated polyhedral oligomeric silsesquioxanes (*m*-POSS) was purchased from Hybrid Plastics (Hattiesburg, MS) and used as received. Dibutyltin oxide (DBTO), methacrylic anhydride (MA, 94%), and Hydroquinone (HQ, 99%) were purchased from Sigma Aldrich (St. Louis, MO, USA) and used as received. Steel panels were purchased from Q-Lab Corporation (Westlake, OH, USA). Hexandedioldiacrylate (HDDA) Ebecryl 150 (BPAEDA) were kindly supplied by Allnex. Ethyl(2,4,6-trimethylbenzoyl)-phenyl phosphinate (TPO-L) photoinitiator was received from BASF (Florham Park, NJ).

Formulations Assessed

The free-radical, UV-curable SLA formulation contained 41.99% DMESS, TPO-L photoinitiator (1.18%), HDDA (7.41%) and Ebecryl 150 (49.41%). To these, was added 0, 1, 3, 5, and 10% weight *m*-POSS. The respective formulations were made by pipetting each component into a plastic beaker, mixing by hand for 15 minutes, then vortex-mixing another 10 minutes. The formulations were let to sit out of the light for 30 minutes before their use to allow bubbles to settle out.

Rheological Analysis of the Resins and SLA Ink Formulations

Rheological analyses were done on an ARES Parallel Plate Rheometer by TA Instruments. Formulation was pipetted onto the bottom plate and the gap set to 1 mm. Excess resin outside the plates was carefully wiped away before the plates were rotated at a steady rate sweep from 1 rotation/second to 100 rotations/second.

Printing of Flexural and Tensile Samples with the SLA Ink Formulations

Samples were printed using a Peopoly Moai SLA Printer. Flexural and Tensile Samples were CAD files with dimensions in accordance with ASTM D790 and ASTM D438 respectively.

The files were inputted into XYZ Nobel software and supports added. The subsequent STL file was inputted into Ultimaker Cura software to translate to a GCODE file. All printing on the Moai used firmware version 1.6. Flexural and tensile samples assessed were printed horizontal (0x) to the build platform. The placement of the prints on the build platform were regularly moved to extend the lifespan of the PDMS layer in the vat. Post print, the samples required careful separation from the build platform with the use of a sharp tool provided with the Moai printer. The removed samples were washed in an ethanol bath, dried, and then placed in a convection oven with rotating chamber surrounded with 405 nm lights and heated to 50 °C for 2 hours for postcure. Flexural samples were rectangular and with dimensions of 76.8 mm x 13 mm x 4 mm before the addition of supports.

Dynamic Mechanical Analysis (DMA) of the Prints

Dynamic Mechanical Analysis (DMA) was run on a TA-Instruments Q800 Dynamic Mechanical Analyzer. For the SLA formulations, printed samples of 70 mm x 13 mm x 4 mm (the same dimensions of flexural samples but carefully cut to fit completely in the clamp). The scaffolding was carefully clipped from the samples and the sample gently sanded with sandpaper where the scaffolding once was. The sample was then locked in the calibrated dual cantilever DMA clamps at 2 lbs with a torque wrench. Samples were equilibrated at -40 °C before heating at 10 °C/min to 150 °C.

Thermogravimetric Analysis (TGA)

Thermogravimetric analysis (TGA) was completed on a TA Instruments Q500 Thermogravimetric Analyzer. Tared platinum pans were loaded with ~10-15 mg of the respective cured formulation before being heated from room temperature to 600 °C at 10 °C/minute.

Tensile Assessment of the Prints

The tensile testing was completed on an Instron 5567 load frame (Instron, Norwood, MA), a 2 kN load cell, and 25.4 mm extensometer. The samples were tested at a 1 mm/min crosshead rate so failure typically occurred within 10 minutes. Five sample specimens were tested for each tensile assessment.

Flexural Assessment of the Prints

The flexural testing was also completed on the Instron 5567 load frame with a 2 kN load cell. Flexural testing was carried out in accordance with ASTM D790 with a three-point bending set-up. The span was set for a span-to-thickness ratio of 16:1 for the average thickness of 5 samples. Crosshead rate for testing was 1 mm/min.

Gel Content of the Prints

1 g samples were taken from the post-cured prints. Each were wrapped in filter paper and placed upright (not stacked) in a paper thimble which was then inserted into a Soxhlet extractor. The extractor was inserted into a round bottom flask filled with dichloromethane and a reflux condenser attached to the top. The round bottom flask was then lowered into an oil bath with thermocouple and heated until dichloromethane was refluxing. Reflux was continued for 24 hours before the samples were removed from the thimble and dried in a vacuum oven for several hours. The final-initial/initial weights of the samples were taken and averaged to find the gel percent content of the prints.

Results and Discussion

Characterization of SLA Resin Formulation (DMESS-BPAEDA) and Prints with m-POSS

The rheological properties of the SLA resin formulations with *m*-POSS increments are shown in **Figure 4.4**. It is clear that even low amounts of 1% weight *m*-POSS significantly lower the viscosity of the formulation, but larger increments do not show much more of a change.
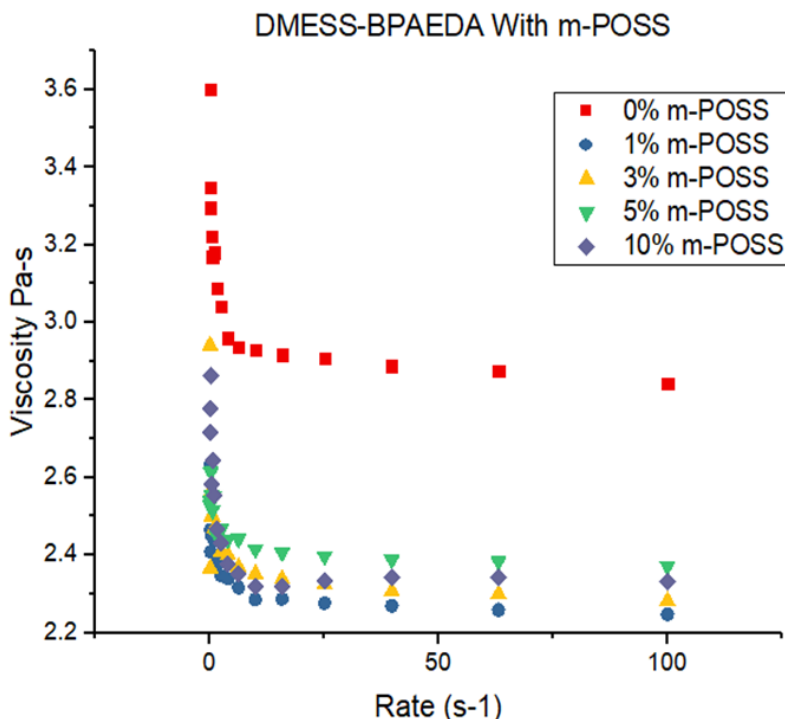
Figure 4.4. Rheological Properties of the DMESS-BPAEDA SLA Formulation with Addition of m-POSS

While the prints showed no difference in appearance with m-POSS addition, **Figure 4.5** shows thermomechanical differences as elucidated by DMA. The storage modulii at various temperatures and tan δ amplitudes were plotted in **Table 4.1** and used to calculate the crosslink densities (ν_e) of the networks. There is a distinct increase in rubbery modulus as more *m*-POSS is present in the formulations as well as glass transition temperatures elucidated from the amplitudes of the tan δ curves and the calculated M_cs and ν_es. This demonstrates that the *m*-POSS is contributing to the crosslinking and stiffness of the network. Gel content of the

respective prints show variation (st. dev: ± 4.95) in cured content. This variation is more likely due to inconsistencies in the post-curing procedure for thick, stereolithographically printed samples (washing sequence in ethanol and placement of samples in rotating UV oven) instead of differences in *m*-POSS being incorporated into the final network due to a lack of a trend seen in gel % of the formulations with different *m*-POSS amounts.
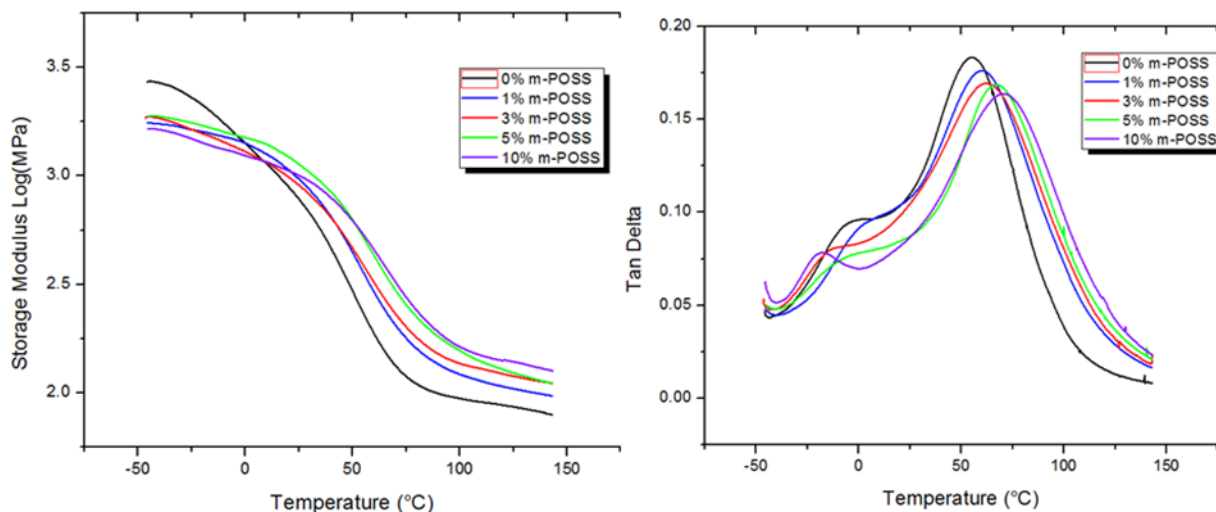
Figure 4.5. Dynamic Mechanical Analysis of the DMESS-BPAEDA m-POSS Formulations

Table 4.1. Storage Modulii, Glass Transition, Crosslink Density, and Gel % of the DMESS-BPAEDA m-POSS SLA Formulations

m-POSS Content	Tan δ Amplitude (°C)	E' Rubbery Modulus (at Tg + 60 °C, MPa	M_c (g/mol)	v_e (mol/m³)	Gel content (%)
0	55.38	89.50	108	9.24×10^3	93.8
1	60.27	107.0	91.7	1.09×10^2	88.4
3	62.54	121.0	81.3	1.23×10^2	94.3
5	67.22	122.1	81.9	1.22×10^2	98.6
10	70.55	135.4	74.1	1.35×10^2	84.4

Thermogravimetric analysis of the formulations was completed and weight loss and Derivative Weight Loss (DTG) plots are shown in **Figure 4.6**. A shoulder in the DTG graphs at 350 °C decreases as more m-POSS is introduced, indicating that the additive is aiding in diluting another component of the formulation which has a maximum decomposition rate at 350 °C.

Tabulated $T_{5\%}$, $T_{50\%}$, and maximum decomposition rates T_{Max} seen in **Table 4.2** show slight

increases in these values with the small *m*-POSS amounts added. However, the most notable

increase is the residual weight at 500 °C with incremental *m*-POSS addition. The flame

retardancy of POSS materials has been well-studied and is postulated to be due to an intumescent

char forming silicon network.[11] The differences in remaining mass indicate potential

improvement in fire retardancy imparted by the increasing *m*-POSS content.
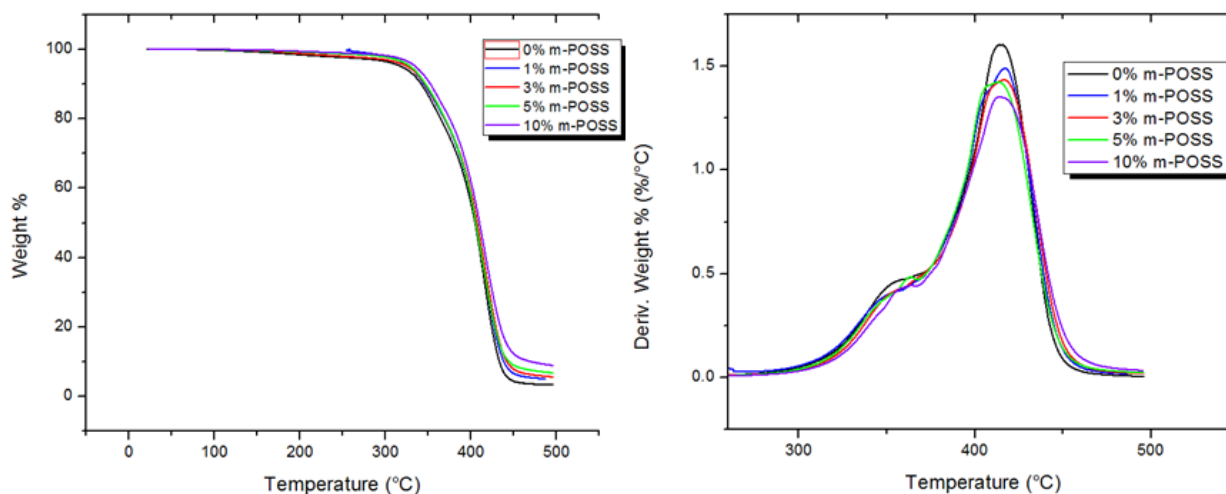
Figure 4.6. Thermogravimetic Analysis of the DMESS-BPAEDA m-POSS SLA Formulations

Table 4.2. $T_{5\%}$, $T_{50\%}$, and T_{max} of the DMESS-BPAEDA m-POSS SLA Formulations

m-POSS Content (%)	Initial Decomposition Temp (°C)	Temperature of 50% Weight Loss ($T_{50\%}$, °C)	Temperature Maximum Decomposition Rate (T_{max}, °C)	Residual Weight at 500 °C (%)
0	328.4	404.8	414.0	3.37
1	339.7	405.7	417.2	5.11
3	333.7	407.2	416.5	5.68
5	335.6	405.6	413.4	6.84
10	334.5	409.9	413.5	8.96

The mechanical contribution of 10% m-POSS in the printed DMESS-BPAEDA

formulation through tensile and flexural assessment is seen in **Table 4.3**. While there is a

decrease by around half in maximum tensile stress and tensile strain, there is around 24%

increase in modulus with the addition of 10% *m*-POSS. Flexural behavior shows mild increases

in load at maximum stress and stress but a 56% increase in modulus. These results are in

concurrence with DMA results indicating that the *m*-POSS addition is producing a stiffer

network.

Table 4.3. Tensile and Flexural Comparison of DMESS-BPAEDA SLA Ink Baseline and with 10% POSS Addition

DMESS-BPAEDA *m*-POSS Content (wt %)	Tensile Strength (MPa)	Strain to Failure (mm/mm	Young's Modulus (MPa)	Flexural Strength (MPa)	Flexural Modulus (MPa)
0%	12.99	0.028	574.6	23.27	515.3
10%	6.933	0.012	713.8	24.98	807.6

Conclusions

Methacrylated polyhedral oligomeric silsqueloxane (*m*-POSS) was incorporated into

significantly bioderived, stereolithographic resin formulations. Even 1% weight incorporation of

m-POSS decreased viscosity significantly. Larger amounts did not change the viscosity

significantly more than the 1% addition. The increasing *m*-POSS formulations showed a trend

increasing glass transition, network stiffness, and crosslink density of the cured prints. While

there were only slight improvements in decomposition temperatures of the network with the

additive, trends were seen with larger weight % of the residual char and indicate possible fire

retardancy being imparted by the POSS. Mechanical assessment of the formulation with no *m*-

POSS compared to the 10% weight *m*-POSS SLA ink showed improvements in tensile and

flexural modulus. There were mild improvements in maximum flexural stress with the additive

incorporated, however tensile stress and strain decreased. These results indicate that *m*-POSS is

able to improve the processing viscosity for an SLA application and create stiffer printed

networks. SLA requires a multitude of processing parameters to be met to print successfully. Further, there is much interest in bioderived materials that can be utilized in SLA inks to produce prints with desirable properties. Additives like *m*-POSS both aid in making bioresin-containing SLA inks meet such parameters while also improving properties of a thermoset with small additive amounts.

References

1. Camino, G., and L. Costa. *Pol. Deg. & Stab.,* **1988**, *20.3*, 271-294.

2. Pape, Peter G. "Adhesion Promoters." *Handbook of Adhesives and Surface Preparation*. William Andrew Publishing, 2011. 369-386.

3. Pritchard, Geoffrey. *Plastics additives: an AZ reference*. Vol. 1. Springer Science & Business Media, 2012.

4. Yezrielev, Albert Ilya, Vijay Swarup, and Konstantinos R. Rigopoulos. "Thermoset coating compositions having improved hardness." U.S. Patent No. 5,681,906. 28 Oct. 1997.

5. Deanin, Rudolph D., and Margaret A. Manion. *Plast. Eng. NY,* **1999**, 1-22.

6. Samarth, Nikesh B., and Prakash A. Mahanwar. *J. Org. Pol. Mat.*, **2015**, *5.01*, 1.

7. Li, Guizhi, et al. *J. Inorg. & Organomet. Pol.,* **2001**, *11.3*, 123-154.

8. Schwab, Joseph J., and Joseph D. Lichtenhan. *App., Organomet. Chem.,* **1998**, *12.1*, 707-713.

9. Tanaka, Kazuo, and Yoshiki Chujo. *J. Mat. Chem.,* **2012**, *22.5*, 1733-1746.

10. Amerio, Ezio, et al. *Macromol. Mat. & Eng.,* **2008**, *293.8*, 700-707.

11. Wang, Xin, et al. *Composites Part B: Engineering,* **2017**, *110*, 442-458.

12. Manapat, Jill Z., et al. *Macromol. Mat. & Eng.,* **2017**, *302.9*, 1600553.

13. Bhatia, Sujata K., and Krish W. Ramadurai. "3-Dimensional Printing and Rapid Device Prototyping." *3D Printing and Bio-Based Materials in Global Health.* Springer, Cham, 2017.

14. Meier, Michael AR, Jürgen O. Metzger, and Ulrich S. Schubert. *Chem. Soc. Rev.* **2007**, *36.11*, 1788-1802.

15. Monono, Ewumbua M., et al. *Org. Proc. Res. & Dev.,* **2015**, *19.11*, 1683-1692.

16. Yan, Jingling, and Dean C. Webster. *Green Mat.,* **2014**, *2.3*, 132-143.

17. Hosseini, Nassibeh, Dean C. Webster, and Chad Ulven. *Eur. Pol. J.,* **2016**, *79*, 63-71.

18. . Kovash Jr, Curtiss S., et al. *Chem. Sus. Chem.,* **2014**, *7.8*, 2289-2294.

19. Pan, Xiao, Partha Sengupta, and Dean C. Webster. *Biomacromol.,* **2011**, *12.6,* 2416-2428.

20. Nelson, Thomas J., et al. *J. Renew. Mat.*, **2013**, *1*, 141-153.

21. Arvin, Z. Yu, AliReza Rahimi, and Dean C. Webster. *Eur. Pol. J.*, **2018**, *99*, 202-211.

CHAPTER 5. CARDANOL GLYCIDYL ETHER AS A BIODERIVED DILUENT IN UV-CURABLE EPOXIDIZED SUCROSE SOYATE COATINGS

Introduction

UV-curable materials are of great interest in industrial and academic circles due to the benefits they provide to applications ranging from adhesives to dental materials to protective coatings.[1-3] Among these benefits are the ability to create low viscosity, high solids (and thus, low or no VOC), and room-temperature curable formulations in a matter of seconds with good mechanical properties. UV-curable processes can be divided into those cured cationically or by free-radical curing. The differences not only involve the monomeric species, but the photoinitiators utilized as well. Unlike free radical polymerization, where the reaction is propagated by transferring free radicals to monomers, cationic polymerization involves the transfer of a charge. This charge first comes from the cationic, or *photo-acid* photoinitiator; a material that converts to a strong acid species upon absorbing actinic UV radiation that is dependent on molecular configuration of the photoinitiator. Commonly, these types of photoinitators are sulfonium or iodonium salts. This species initiates the polymerization by reacting with the reactive groups on the monomer, such as an epoxy group. Cationic curing is cited for advantages over free-radical curing given the process is not sensitive to oxygen, curing is rapid, and shrinkage is low.[4-11]

Another aspect of UV-curing, the monomers, are being investigated for bio-derived alternatives to petrochemically-derived epoxies. Many studies have investigated the epoxidation and curing of plant oils.[12-17] Issues encountered with vegetable oils are the lack of modifiable sites for UV-curing, high viscosities, and the production of relatively soft coatings. Epoxidized sucrose soyate (ESS) seen in **Figure 5.1** is a bioderived material that mitigates several issues of

vegetable oils in thermosets. Soybean oil fatty acids esterified onto sucrose takes advantage of a

rigid core and flexible chains. The unsaturation of these chains modified to oxirane allow many

sites for further modification and dense crosslinking. Modification of these sites has allowed

studies to be completed on ESS to be incorporated in a multitude of thermosets; from

polyurethanes, to acrylics, to polyesters.[18-22]
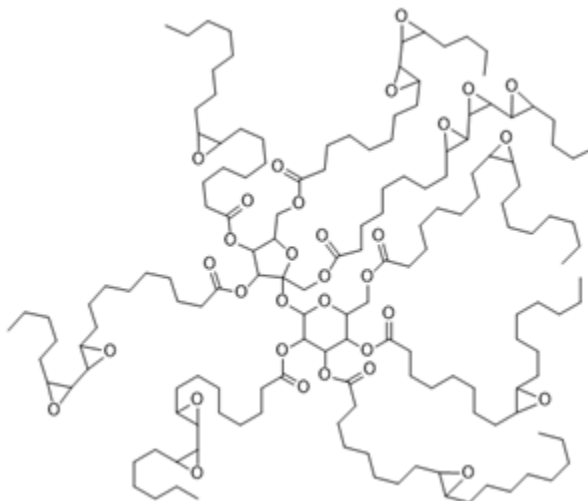
Figure 5.1. Representative Structure of Epoxidized Sucrose Soyate

ESS has been assessed as a UV-curable epoxy along with the reactive diluent 3,4-

epoxycyclohexylmethyl 3,4-epoxycyclohexanecarboxylate (CAE) and triarylsulfonium

hexafluoroantimonate salts (PI).[23] These coatings were able to cure rapidly, however, coatings

with high hardness and solvent resistance required a significant amount of this petrochemically-

derived diluent to achieve desirable mechanical properties.

Cashew nutshell biproduct cardanol has generated interest due to its production, cost, and

structure. The ancardic acid content undergoes a decarboxylation producing a mixture of

cardanol (60%), cardol (20%), methylcardol (trace), and some polymeric products (10%).

Vacuum distillation yields cardanol.[24] While there a host of modifications have been pursued for

cardanol, epoxidation of the phenylhydroxyl with epichlorohydrin produces cardanol glycidyl

91

ether (CGE) (**Figure 5.2**). This material can be further modified with acrylate for free-radical curing as well as incorporated into cationically-cured epoxy thermosets.[25-29] This study investigates the changes in mechanical properties of UV-curable epoxy coatings with ESS and CGE as a co-diluent and bioderived replacement diluent to CAE.
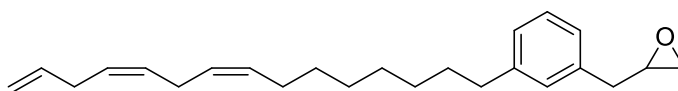
Figure 5.2. Representative Structure of Glycidyl Cardanol with Bi-Unsaturation

Experimental Section

Materials

Epoxidized Sucrose Soyate (>99% solids, 1000 cP, 236 g/eq epoxy) was received from a pilot plant producing the material at North Dakota State University (Fargo, ND, USA)[28]. Epoxycyclohexylmethyl 3,4-epoxycyclohexanecarboxylate (CAE, >99%) and triarylsulfonium hexafluoroantimonate salts (PI, 50% in propylene carbonate), and 2-butanone (>99%) were purchased from Sigma Aldrich (St. Louis, MO, USA) and used as received. Ultra LITE 513 (cardanol glycidyl ether >99%, 25 centipoise at 25 °C, EEW: <450 g/eq.) was kindly provided as a sample from Cardolite Corporation (Bristol, PA, USA) and used as received. Cold-rolled steel panels were purchased from Q-Lab Corporation (Westlake, OH, USA).

Coating Formulation and Curing

Coatings were made by measuring out each component into a 20 mL vial and first mixing by hand for 10 minutes before vortex mixing for 20 minutes to ensure full dispersion. Formulations were based on a 60 phr ESS, 40 phr CAE, and 4 phr PI base formulation denoted 0%-CGE. Subsequent formulations introduced 5 (5%-CGE), 10 (10%-CGE), 25 (25%-CGE), 50 (50%-CGE), 75 (75%-CGE), and 100% (100%-CGE) replacement of the CAE content of the

base formulation. Formulations were let to sit 15 minutes before further curing or analysis. Each formulation was then drawn down on cold-rolled steel panels and glass panels previously cleaned with hexanes and KimWipe^{TM} at 6 MILs wet film thickness in a fume hood. Coated substrates were then placed on the conveyor of a LC6B Benchtop Conveyor^{TM} from Fusion UV. The irradiation of the UV bulb as elucidated by radiometer puck before curing is seen in **Table 12**. Conveyor speed was modified to change exposure time to the UV source. This time was recorded for each formulation when the emerged coating passed tack free testing where a glove thumb pressed on the coating and twisted 90° did not leave a mark.

Table 5.1. UV Signals of UV Curing Apparatus Before Curing

UV Signal	Energy Density (mJ/cm^2)	Peak Irradiance (mW/cm^2)
UVA	3706	1393
UVB	1010	410
UVC	169	73
UVV	3232	1209

Characterization

Rheological Analysis

Formulations were characterized for viscosity with an ARES Parallel-Plate Rheometer (TA Instruments). Around 1 gram of formulation was deposited on the lower plate and the gap between plates was set at 1 mm. Excess formulation exuding from the plates was carefully wiped away. The plates were rotated at a steady rate sweep from 1 rotation/second to 100 rotations per second. Viscosity and shear rate were plotted.

Thermomechanical Analysis

Differential Scanning Calorimetry (DSC) was run on a TA Instruments Q1000 Modulated Differential Scanning Calorimeter. Approximately 5 mg of coating was placed in a

standard aluminum pan and run under a Heat-Cool-Heat regime first equilibrating at 30 °C, heating at 10 °C/min to 150 °C, cooling 10 °C/min to 20 °C, then reheating at 10 °C/min to 150 °C. Dynamic Mechanical Analysis (DMA) was run on a TA-Instruments Q800 Dynamic Mechanical Analyzer. Samples removed from glass panels and cut into dimensions ~15 mm x 8 mm x 0.07 mm were prepared. Samples were measured with the tension clamp and carefully locked in place under 4 lb torque with torque wrench. The assessment consisted equilibrating the sample at -40 °C before heating at 10 °C/min to 150 °C with 1 Hz oscillation.

Thermogravimetric analysis (TGA) was completed on a TA Instruments Q500 Thermogravimetric Analyzer. Tared platinum pans were loaded with ~10-15 mg of the respective cured formulation before being heated from room temperature to 600 °C at 10 °C/minute.

Standard Coating Assessments

Dry coating film thickness was measured with a QNIX 8500 Paint/Coating Thickness Gauge calibrated to steel substrates with an average of 10 measurements per coating reported. König hardness was completed in accordance with ASTM D4366 with a Gardco Pendulum Hardness Tester with an average of 3 measurements per coating. Rapid impact resistance was completed in accordance with ASTM D2794 with an average of 3 measurements per coating, with frontal and back assessments. Mandrel bend flexibility test was completed in accordance with ASTM D522 with 1 panel per assessment. Pencil hardness was completed in accordance with ASTM D3363 with gauge point recorded. Crosshatch adhesion of the coatings was completed in accordance with ASTM D3359 with 3 measurements per coating and an average taken of the 0B-5B scale. ASTM D5402 was followed to assess solvent resistance of the coatings with 1 panel per assessment.

Results and Discussion

   Rheological behavior of the formulations is seen in **Figure 5.3**. Initially, 5%-CGE has a

similar viscosity to 0%-CGE. 10%-CGE shows a mild increase in viscosity while 25%, 50%,

75%, and 100% show a consistently decreasing viscosity due to the plasticizing effect of the

CGE. Ultra LITE 315 is more viscous (1000 cP) than CAE (400 cP) which may explain this

initial increase but viscosity decreases when a larger amount of CGE is added. A beginning

undershoot is seen in thse curves which is attributed to no pre-assessment normalizing shear

being completed.
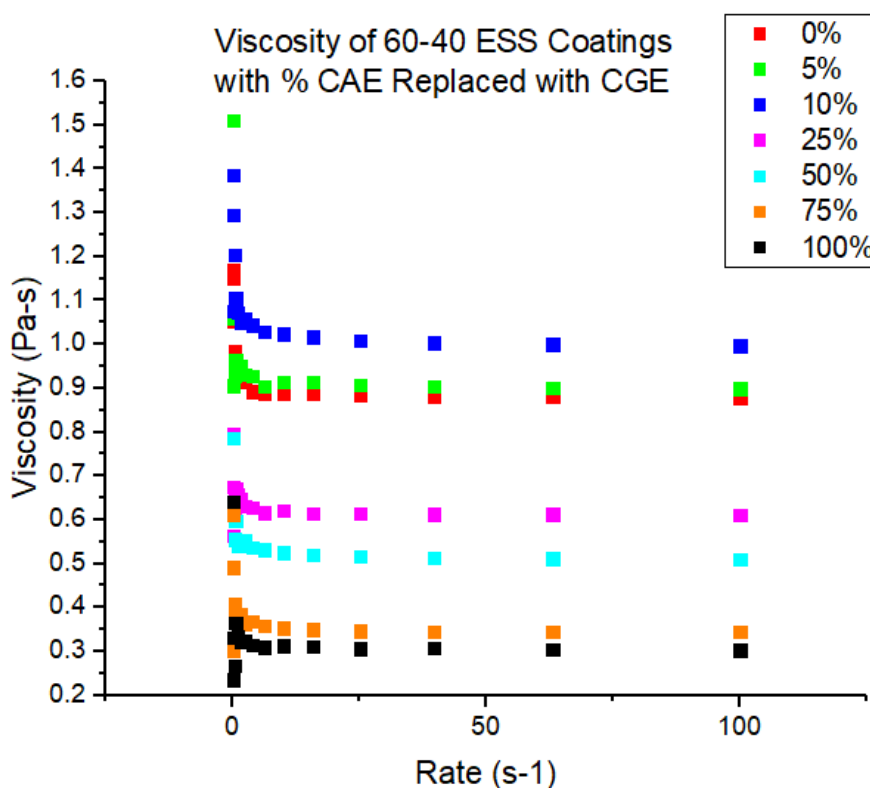
Figure 5.3. Rheological Assessment of ESS-CAE Coatings with Gradual Replacement of CAE
with CGE

   DSC curves of the cured formulations from the 2nd heating cycle and the determined glass

transition temperatures are seen in **Figure 5.4**. It is seen that small formulation substitutions of

CGE (5-10%) for CAE slightly lower the glass transition temperature. This decreasing trend

from the original formulation continues with a 22% T_g decease for the transition at 25%

replacement, 47% T_g decrease for 50% replacement, 76% T_g decrease for 75% replacement, and

a 108% T_g decrease at complete replacement of CGE with CAE. Due to the softness of the 100%

replacement formulation, it was omitted from tension DMA analysis.

Storage modulus and tan δ Curves from DMA analysis of the cured films are seen in

Figure 5.5. A similar trend is seen where 5 and 10% CGE replacement have similar storage

modulus, tan δ peak heights, and peak maximums (T_gs) while 25% replacement shows a more

pronounced decrease followed by drastic decreases at 50 and 75% replacement. These results

indicate that there is less crosslinking present with monofunctional glycidyl cardanol replacing

the difunctional epoxy diluent. The glycidyl cardanol also has a plasticizing effect which is

lowering the glass transition, while the decreasing peak heights indicate that networks with more

glycidyl cardanol have more of an elastic response to an applied force than those without or little

amounts of the diluent.

Calculations of the molecular weights between crosslinks (M_c) and crosslink densities

(v_e) were completed using the equation $E' = 3RT\rho M_c = 3RT\rho/v_e$ from Rubber Elasticity Theory

where E' is the storage modulus in the rubbery plateau region, R is the gas constant, T is the

temperature at which E' is taken (T_g + 60 °C, T_g being an average of DSC and DMA T_g values

elucidated, and ρ is the density of the cured formulation (assumed to be 1). These calculations

are compiled in **Table 5.2**. Remarkably, M_c is seen to decrease and v_e increase with increasing

CGE content with a very slight reverse of the trend at 75% replacement. This may be due to a

sharp increase in chain entanglements by introducing the glycidyl cardanol. These chain

entanglements, such as those with the long aliphatic chains present on the CGE may require

more energy before the onset of long-range molecular motion in the cured network.
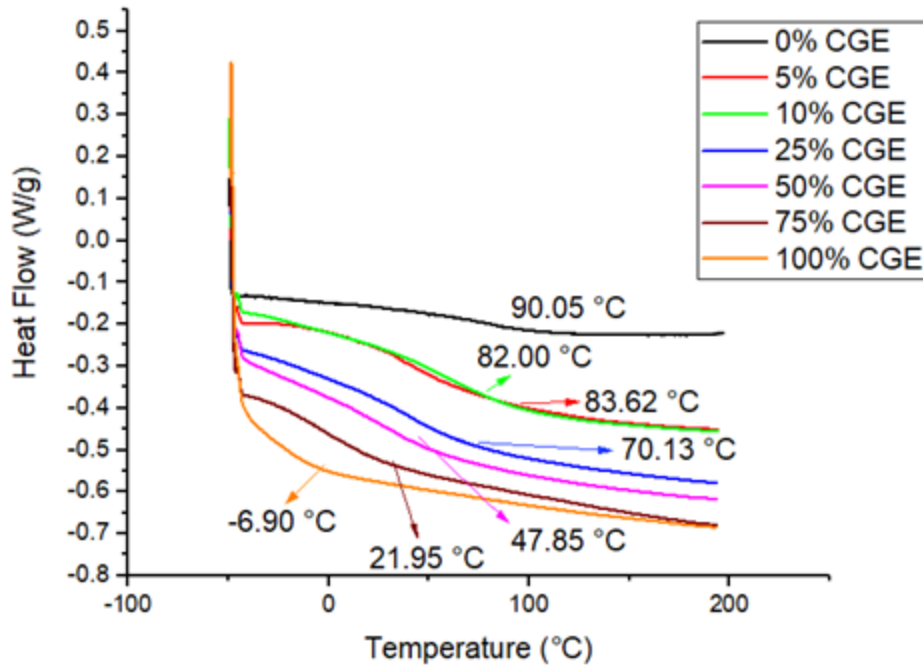
Figure 5.4. DSC Curves of 60-40 ESS-CAE UV-Curable Coatings with % CGE Weight Replacement of CAE Diluent
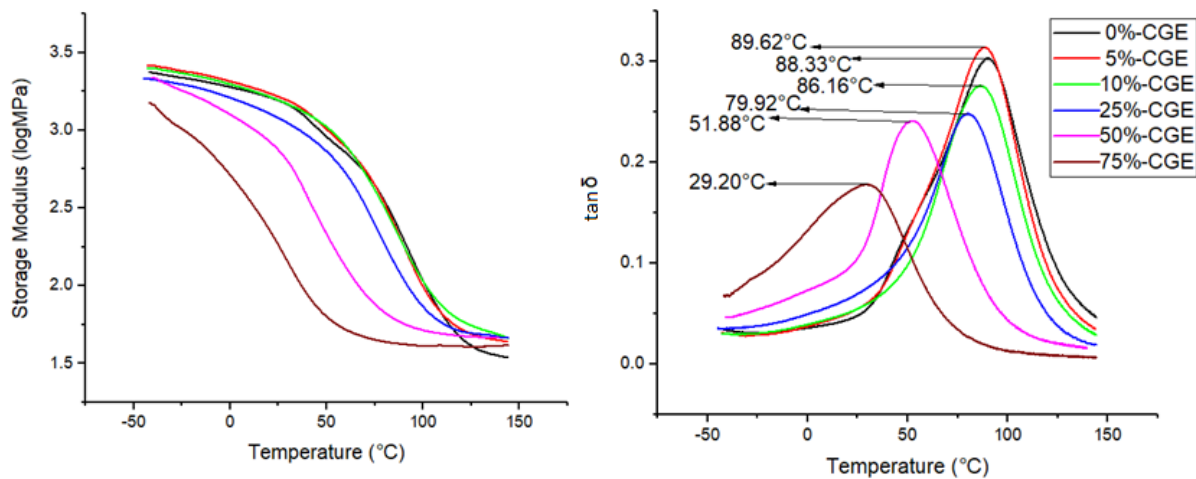
Figure 5.5. Tension DMA Storage Modulus (E') and Tan δ Curves of 60-40 ESS-CAE UV-Curable Coatings with % CGE Weight Replacement of CAE Diluent

To evaluate the thermal resistance properties of the coatings with increasing CGE replacement, thermogravimetric analysis was completed. The weight changes of the formulations and the derivative weight percent (DTG) overlays are seen in **Figure 5.6** with values presented in **Table 5.3**. It is apparent that the maximum decomposition rate signal at 373 °C relates to the

97

ESS-CAE network. However, as CGE content in the network increases, another signal at higher temperature, 421 °C, also increases. Slight increases in the initial decomposition temperature and 50% decomposition temperature ($T_{5\%}$ and $T_{50\%}$) are seen with CGE replacement increases. These increases are due to the aromatic ring structure in cardanol which has been attributed for its thermal resistivity properties.[25-27]

Coatings properties are compiled in **Table 5.4**. CGE replacement in the ESS-CAE formulations slightly increased the tack-free times for the coatings, however even full replacement of the CAE with CGE produced tack-free coatings in 20 seconds. A slight decrease in König hardness corresponded with 5, 10, and 25% CGE replacement while the decrease became sharper in greater amounts. This was initially seen in pencil hardness too, however 50% and 75% replacements produced harder coatings. CGE replacement did not show improvement in adhesion to the ESS-CAE formulation given crosshatch adhesion remained poor. There was not much of an improvement in forward impact resistance except for complete CGE replacement of CAE given the coating was far more flexible. Remarkably, even a large increase in CGE up until full replacement resulted in highly solvent resistant coatings. While this may be unexpected given a monofunctional epoxy is replacing a difunctional one in the network, the many functional groups present on ESS as well as chain entanglements of the glycidyl cardanol may be responsible for the high solvent resistances.

Table 5.2. Molecular Weight between Crosslinks (Mc) and Crosslink Density (ve) Calculations of the 60-40 ESS-CAE UV-Curable Coatings with % CGE Weight Replacement of CAE Diluent

60-40-ESS-CAE Formulation, % CGE Replacement of CAE	T_g (DSC, °C)	T_g (DMA, °C)	E' Rubbery Modulus (at T_g + 60 °C, MPa)	M_c (g/mol)	v_e [x10³ mol mm⁻³]
0%	90.05	89.62	34.63	305	3.28
5%	82.00	88.33	43.74	239	4.19
10%	83.12	86.16	46.01	227	4.41
25%	70.13	79.92	48.03	212	4.72
50%	47.85	51.88	49.08	195	5.13
75%	21.95	29.20	42.52	210	4.75
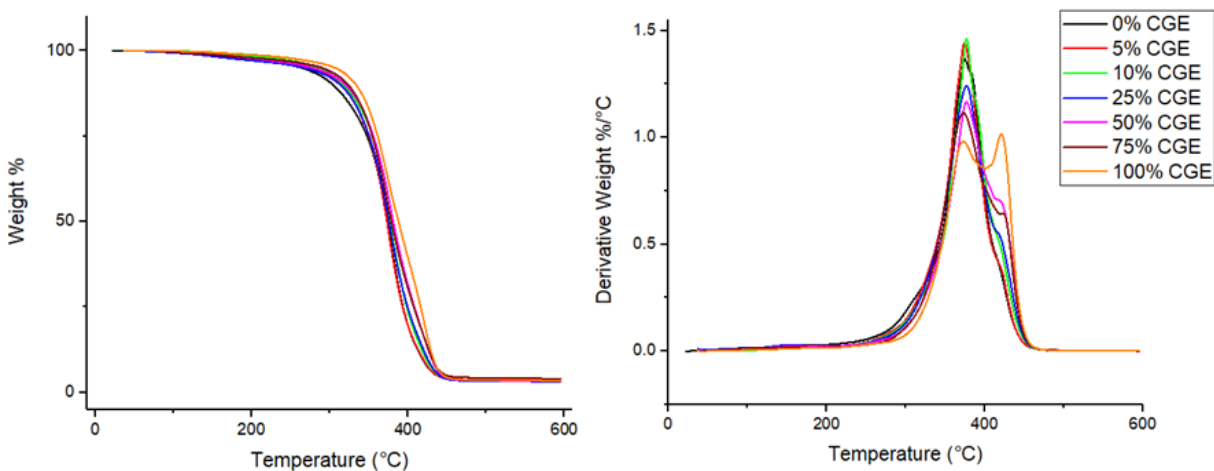
Figure 5.6. Weight % Change and Derivative Weight % Change (DTG) of 60-40 ESS-CAE UV-Curable Coatings with % CGE Weight Replacement of CAE Diluent

Table 5.3. Thermogravimetric Properties of 60-40 ESS-CAE UV-Curable Coatings with % CGE Weight Replacement of CAE Diluent

60-40-ESS-CAE Formulation, % CGE Replacement of CAE	Initial Decomposition Temp ($T_{5\%}$, °C)	Temperature of 50% Weight Loss ($T_{50\%}$, °C)	Temperature Maximum Decomposition Rate (T_{max}, °C)
0%	263	374	375
5%	280	373	374
10%	284	377	377
25%	267	376	377, 419
50%	277	381	377, 419
75%	289	379	373, 423
100%	306	388	373, 421

Table 5.4. Cure Time and Coating Characterizations of the 60-40 ESS-CAE UV-Curable Coatings with % CGE Weight Replacement of CAE Diluent

Formulation (60-40 ESS-CAE, % CGE Replacement of CAE)	UV Exposure Time Until Tack Free (s)	Thickness (μm, avg 5)	König Pendulum Hardness (s)	Pencil Hardness	Crosshatch Adhesion	MEK Double Rubs	Rapid Impact (reverse, in-lbs,)
0% CGE	10	122	175	H	0B	>400	27.4
5% CGE	10	105	169	HB	0B	>400	35.3
10% CGE	20	97.5	159	B	0B	>400	23.5
25% CGE	20	87.9	145	HB	0B	>400	23.5
50% CGE	20	101	95.7	2H	0B	>400	27.4
75% CGE	20	103	50.7	F	0B	>400	39.2
100% CGE	20	99.9	33.3	8B	0B	300	137

Conclusions

Glycidyl cardanol was incorporated into a cationic, UV-curable, soybean oil-derived epoxy coating with petrochemically-derived diluent. The bioderived diluent gradually replaced the petrochemically-derived diluent until complete replacement. Coatings were made and cured successfully with little increase in UV exposure time. Mild increases in CGE lowered the viscosities of the formulations and produced hard coatings while slightly lowering the T_gs of the cured coatings in comparison to the original formulation. Larger % CGE replacements resulted in lower T_g, softer coatings. However, large increases in CGE content did not hinder solvent resistances of the coatings and an increase in thermal resistance of the coating occurred. This study demonstrates the incorporation and structure-property relationships of a material produced from a bioderived biproduct, into a formulation with high bio-derived content.

References

1. Raghavachar, Ramya, et al. *J. Coat. Tech.,* **2000**, *72*, 125-133.

2. Thames, Shelby F., and H. Yu. *Surf. & Coat. Tech.,* **1999**, *115*, 208-214.

3. Chen, Zhigang, et al. *J. Coat. Tech. & Res.,* **2010**, *7.5*, 603-613.

4. Crivello, James V., and Marco Sangermano. *J. Pol. Sci. Part A: Pol. Chem.,* **2001**, *39*.3, 343-356.

5. Hoyle, Charles E., and James F. Kinstle. "Radiation curing of polymeric materials." *Radiation Curing of Polymeric Materials/Volume 417 of ACS Symposium Series, Eds. Charles E Hoyle and James F Kinstle. Washington DC: American Chemical Society, c1990..* Vol. 417. 1990.

6. Sangermano, Marco, Nicolò Razza, and James Vincent Crivello. *Macromol. Mat. & Eng.,* **2014**, *299*, 775-793.

7. Rosli, WD Wan, et al. *Euro. Pol. J.,* **2003**, *39.3*, 593-600.

8. Wu, Shaobing, et al. *Pol.*, **1999**, *40.2*, 5675-5686.

9. Allen, Norman S. *J. Photochem. & Photobio. Chem.,* **1996**, *100.1*, 101-107.

10. Decker, Christian. *Surf. Coat. Int. Part B: Coatings Transactions,* **2005**, *88.1*, 9-17.

11. Stone, Edward, et al. "Low VOC cationic curable lithographic printing inks." U.S. Patent No. 6,489,375. 3 Dec. 2002.

12. Rosli, WD Wan, et al. *Eur. Pol. J.,* **2003**, *39.3*, 593-600.

13. Thames, Shelby F., Haibin Yu, and Ramesh Subramanian. *J. Appl. Pol. Sci.,* **2000**, *77.1*, 8-13.

14. Zou, Kunrong, and Mark D. Soucek. *Macromol. Chem. & Phys.*, **2005**, *206.9*, 967-975.

15. Ahn, B. Kollbe, et al. *Pol. Int.,* **2013**, *62.9*, 1293-1301.

16. Alam, Samim, and Bret J. Chisholm. *J. Coat. Tech. & Res.,* **2011**, *8.6*, 671-683.

17. Rengasamy, Senthilkumar, and Vijay Mannari. *Prog. in Org. Coat.*, **2013**, *76.1*, 78-85.

18. Monono, Ewumbua M., Dean C. Webster, and Dennis P. Wiesenborn. *Indust. Crop. & Prod.*, **2015**, *74*, 987-997.

19. Yan, Jingling, and Dean C. Webster. *Green Mat.,* **2014**, *2.3*, 132-143.

20. Kovash Jr, Curtiss S., et al. *Chem. Sus. Chem.*, **2014**, *7.8*, 2289-2294.

21. Arvin, Z. Yu, AliReza Rahimi, and Dean C. Webster. *Eur. Pol. J.,* **2018**, *99*, 202-211.

22. Arvin, Z. Yu, et al. *J. Coat. Tech. & Res.,* **2019**, *16.1*, 41-57.

23. P.P. Sengupta, X. Pan, T.J. Nelson, A. Paramarta, D.C. Webster, *PMSE Prepr.*, **2010**, *102*, 888-889.

24. Balachandran, Vijai Shankar, et al. *Chem. Soc. Rev.*, **2013**, *42.2*, 427-438.

25. Voirin, Coline, et al. *Pol. Chem.,* **2014**, *5.9*, 3142-3162.

26. Chen, Jie, et al. *ACS Sus. Chem. & Eng.,* **2015**, *3.6*, 1164-1171.

27. Chen, Jie, et al. *RSC Adv.,* **2015**, *5.69*, 56171-56180.

28. Jaillet, Fanny, et al. *Eur. J. Lip. Sci. & Tech.,* **2014**, *116.1*, 63-73.

29. Monono, Ewumbua M., Dean C. Webster, and Dennis P. Wiesenborn. *Indust. Cr. & Prod.*, **2015**, *74*, 987-997.

CHAPTER 6. IMPROVEMENT OF SUBSTRATE ADHESION OF CATIONIC, UV-CURABLE EPOXY COATINGS

Introduction

Coatings on metal surfaces not only are valued for contributions to appearance but are an important barrier layer to prevent phenomena such as corrosion. In order for a coating to be an effective layer over a metal substrate it must, above all, demonstrate good adhesion. Adhesion is not explained by a single theory; however, several basic definitions have been used to explain mechanisms of adhesion. These definitions are adhesion by chemical interactions, mechanical interlocking, and adsorption. Chemical interaction in this context refers to ionic or covalent bonding between the binder and substrate, mechanical interlocking refers to when binder flows and cures in voids of the substrate (thus *interlocking* within it); this can also include diffusion adhesion for polymeric materials where chains are both soluble and mobile to diffuse and entangle, and adsorption refers to interactions where the forces are non-covalent, weaker intermolecular forces (IMFs).[1] These are illustrated in **Figure 6.1**.
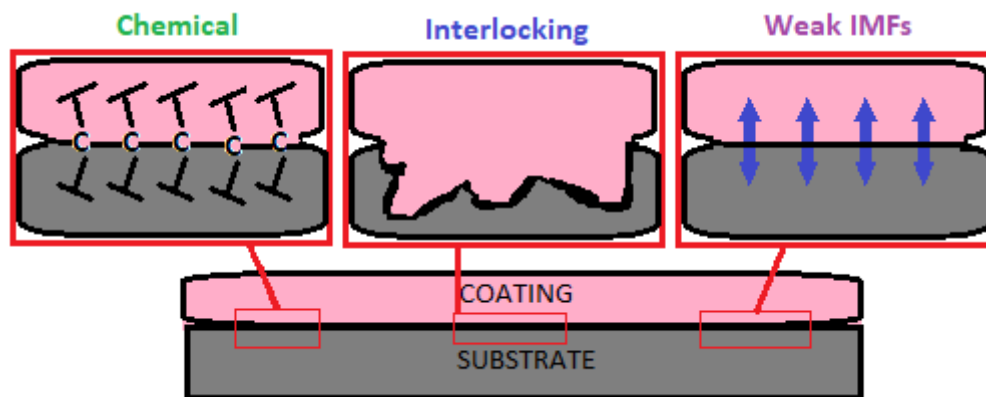
Figure 6.1. Illustrated Mechanisms of Adhesion

There are a multitude of strategies to improve adhesion between thermosets and metal substrates. When focus is on modifying the substrate, physical or chemical etching can be carried

out to aid in the previously mentioned mechanisms.[2,3] When focus is on the thermoset, both the prepolymer processing and chemistry of the thermoset can be modified. For example, making the prepolymer less viscous allows it to flow into more crevices and increase mechanical interlocking. Another example is to modify the prepolymer with functional groups that may covalently bond or adsorb onto the metal substrate.[4]

Adhesion-promoting groups are an extensive field of study. As green chemistry is guiding in hosts of bioderived alternatives, there is increasing interest in incorporating such groups into biobased materials. Among groups that have been studied are phosphonates given they can chemically react with certain metal substrates, for example, surface metal oxide layers of titanium, aluminum, or magnesium substrates.[5-6] For incorporation of phosphonates into bioderived materials, Stratmann et al found that phosphorylation of cellulose was seen to improve adhesion to aluminum substrates.[7]

Another adhesive functional group of great interest comes from a natural inspiration: mussels. Mussels create *L*-DOPA, a catecholic amino acid that has been found to possess strong metal chelating and hydrogen-bonding properties.[8-9] The tough adhesive, plant-derived lacquer urushiol also has had its adhesive properties attributed to catechols.[10] Since understanding the importance of catechols in adhesion to metals, a wide array of studies looking at biomimetic adhesives by incorporation of catechol moieties have been produced.[10-14]

One bioderived platform that has yet to be investigated for incorporation of adhesion-promoting groups is epoxidized sucrose soyate (ESS). ESS is a material made from soybean oil fatty acids esterified onto sucrose and the unsaturation of the fatty acids converted to epoxy. Its combination of flexible and rigid components alongside a multitude of oxirane sites which can

be modified with various functional groups has resulted in a versatile material that can produce unique thermosets.[15-17]

Initially, ESS was investigated to form UV-cured epoxy coatings when mixed with the epoxy diluent 3,4-epoxycyclohexylmethyl 3,4-epoxycyclohexanecarboxylate (CAE) and the cationic photoinitiator triarylsulfonium hexafluoroantimonate salts (PI).[18] The structures of these materials are seen in **Figure 6.2**. A gradient of ratios of ESS and CAE were examined while the PI amount was 4 phr ESS. The coatings showed good solvent resistance, increasing hardness with increasing amounts of CAE, however, had poor adhesion to metal substrates. While the coatings demonstrated several desirable qualities, their poor adhesion was a point for improvement. Thus, this study further investigated modifications of ESS oxirane with phosphonate and a series of benzoic acid esters, with and without catechol functionalities, to see if adhesion of the UV-curable coatings to metal substrates could be improved.
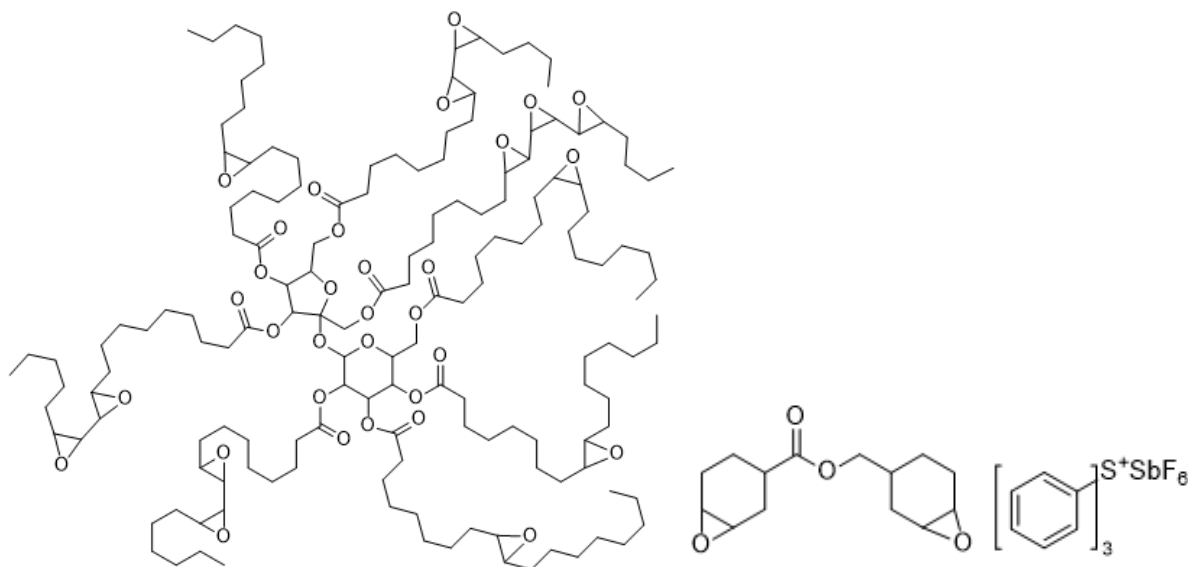
Figure 6.2. From Left: Epoxidized Sucrose Soyate, 3,4-Epoxycyclohexylmethyl 3,4-epoxycyclohexanecarboxylate, Triarylsulfonium Hexafluoroantimonate Salts

Experimental Section

Materials

Epoxidized Sucrose Soyate (>99% solids, 236 g/eq epoxy, M_n:2717) was synthesized as previously reported.[18,19] Phosphonated epoxidized sucrose soyate (PESS, >99% solids, 1500 g/eq) was prepared by Raphael Menard at the University of Montpelier in France in accordance with a previous method.[20] Epoxycyclohexylmethyl 3,4-epoxycyclohexanecarboxylate (CAE, >99%), triarylsulfonium hexafluoroantimonate salts (PI, 50% in propylene carbonate), benzoic acid (BA, >99%), 4-hydroxybenzoic acid (MHBA, >99%), 3,4-dihydroxybenzoic acid (PA, >99%), and 3,5-dihydroxybenzoic acid (DHBA, >99%) were purchased from Sigma Aldrich (St. Louis, MO, USA) and used as received. Cold-rolled steel, aluminum and aluminum 2024, and phosphated steel panels were purchased from Q-Lab (Westlake, OH). Alodine 5700™ pretreatment wipes were purchased from Henkel (Cleveland, OH).

Synthesis of Phenolic ESS-Esters

The capping of epoxy materials with hydroxybenzoic acids is based upon a procedure reported in literature.[20] ESS derivatives BA-ESS, MHBA-ESS, PA-ESS, and DHBA-ESS refer to ESS resins where 10% of epoxy on ESS (based up 236 g/mol epoxy as elucidated by ASTM D1652) was reacted with BA, MHBA, PA, or DHBA respectively. An example reaction for BA (122.12 g/mol) producing BA-ESS is as follows: To a 250 mL round bottom flask equipped with a mechanical stirrer, thermocouple, and oil bath was added 100 g of ESS (1 eq epoxy), 5.1746 g of BA (0.1 eq), and 7.6266 g H_2O (1.5 eq). The mixture was heated to 90 ℃ and stirred for 24 hours. The water was removed by vacuum oven upon completion. The epoxy equivalent weights (EEWs) of the resins were assessed in accordance with ASTM D1652 with an average of 3 sample titration results per resin.

Formulations Assessed

Initial screening formulations of ESS and CAE were made at 90-10, 80-20, 75-25, 60-40, 40-60, 20-80, and 0-100 ESS:CAE content by weight. All of the formulations contained 4 phr PI. Formulations containing PESS were made where 3, 5, and 10% weight of the ESS content in 75-25, 80-20, and 90-10 ESS-CAE formulations with 4 phr PI was replaced with PESS. For the 10% phenolic ester ESS resins, 5, 10, 25, and 50% of the ESS in a 60-40 ESS-CAE formulation with 4 phr was replaced with BA-ESS, MHBA-ESS, DHBA-ESS, and PA-ESS respectively. The respective formulations were made by pipetting each component into a beaker and mixing by hand for 15 minutes before vortex-mixing another 10 minutes. The formulations were let to sit out of the light for 24 hours before their respective use.

UV-Curing of the Formulations

Each formulation was drawn down on aluminum, Alodine[TM] pre-treated aluminum (aluminum panels wiped with Alodine[TM] wipes and dried 24 hours ambiently), steel, phosphate steel, and glass panels previously cleaned with hexanes and KimWipe[TM] at 6 MILs wet film thickness in a fume hood. Coated substrates were then placed on the conveyor of a LC6B Benchtop Conveyor[TM] with a Fusion UV model F300S lamp system from Fusion UV. The irradiation of the UV bulb as elucidated by a UVICURE ® Plus II radiometer puck from EIT before curing is seen in **Table 12**. Conveyor speed was modified to change exposure time to the UV source. This time was recorded for each formulation when the emerged coating passed tack free testing where a glove thumb pressed on the coating and twisted 90° did not leave a mark and no resistance to removal from the coating surface was felt.

Spectroscopic Analysis of the Resins

Fourier Transform Infrared Spectroscopy (FTIR) analyses of the 10% phenolic ESS ester resins were run on a ThermoScientific Nicolet 8700 in transmission using a spectroscopic-grade KBr crystal. A blank spectrum of solely the KBr crystal was first run before a thin layer of each respective resin was deposited on the crystal with a pipet and analyzed.

Gel-Permeation Chromatography

GPC analysis of the resins was completed on an EcoSEC HLC-8320GPC from Tosoh Bioscience with a UV-8320 (wavelength range: 195-350 nm) detector. Around 10 mg of sample was dissolved in 1.5-2 mL of tetrahydrofuran (THF). This was then filtered through a 0.45 mm PTFE filter before being run. THF was used to elute the samples at flow rate of 0.35 mL/min. An EasiVial polystyrene standard obtained from Agilent was utilized for calibration.

Rheological Analysis of the Resins and SLA Ink Formulations

Rheological analyses were completed on an ARES Parallel Plate Rheometer by TA Instruments. Formulation was pipetted onto the bottom plate and the gap set to 1 mm. The plates were rotated at a steady rate sweep from 1 rotation/second to 100 rotations/second.

Coatings Property Assessments

Dry coating film thickness was measured with a QNIX 8500 Paint/Coating Thickness Gauge calibrated to steel (Fe) or non-steel (N-Fe) substrates with an average of 10 measurements per coating reported. König hardness was completed in accordance with ASTM D4366 with a Gardco Pendulum Hardness Tester with an average of 3 measurements per coating. Rapid impact resistance was completed in accordance with ASTM D2794 with an average of 3 measurements per coating, with forward and reverse assessments. Pencil hardness was completed in accordance with ASTM D3363 with gauge point recorded. Crosshatch adhesion of the coatings was

completed in accordance with ASTM D3359 with 3 measurements per coating and assessments made using the 0B-5B scale. ASTM D5402 was followed to assess solvent resistance of the coatings with 1 panel per assessment.

Dynamic Mechanical Analysis of the Cured Coatings

Dynamic Mechanical Analysis (DMA) was run on a TA-Instruments Q800 Dynamic Mechanical Analyzer. Samples removed from glass panels and cut into dimensions ~15 mm x 8 mm x 0.07 mm were prepared. Samples were placed in the tension clamp and carefully locked in place under 4 lb torque with torque wrench. The assessment also consisted of equilibrating the sample at -40 °C before heating at 10 °C/min to 150 °C with 1 Hz oscillation.

Results and Discussion

The initial screening results of ESS-CAE coatings are seen in **Table 6.1**. The coatings show high hardness and solvent resistance, however poor crosshatch adhesion and impact resistance. This indicates that the coatings are brittle and poorly adhesive to aluminum substrates regardless of the ESS or CAE ratio.

Table 6.1. Properties of Initial UV-Cured Epoxy Coating Formulations on Aluminum Panels

Formulation (ESS:CAE Weight Ration with 4 PHR PI)	Film Thickness (ave 5, μm)	Pencil Hardness (gage)	Konig Hardness (ave 3)	Crosshatch Adhesion	Reverse Impact (in-lbs)	MEK Double Rubs
90-10	56.5 ± 11	F	92.3 ± 2	0B	<3.92	>400
80-20	44.9 ± 2	H	123 ± 2	0B	<3.92	>400
75-25	52.8 ± 11	B	108 ± 12	0B	<3.92	>400
60-40	64.8 ± 2	H	161 ± 1	0B	<3.92	>400
40-60	47.7 ± 4	H	183 ± 6	0B	<3.92	>400
20-80	41.3 ± 2	H	190 ± 10	0B	<3.92	>400
0-100	43.9 ± 4	2H	197 ± 10	0B	<3.92	300

To improve the adhesion of the coatings to metal substrates, modifications of ESS were carried out. The synthetic schemes to produce PESS is seen in **Figure 6.3** and for BA-ESS, MHBA-ESS, DHBA-ESS, and PA-ESS are seen in **Figure 6.4**.
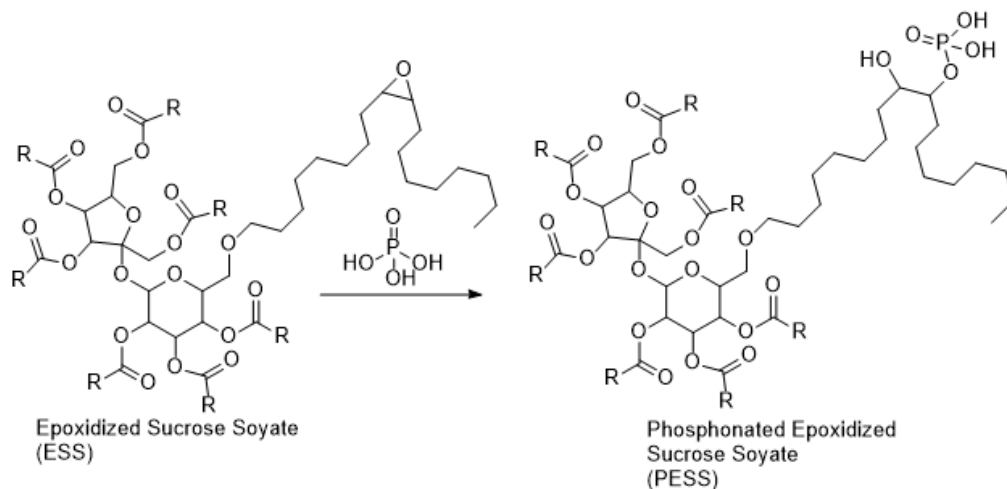
Figure 6.3. Representative Structure of the Synthesis of Phosphonated Epoxidized Sucrose Soyate (PESS)
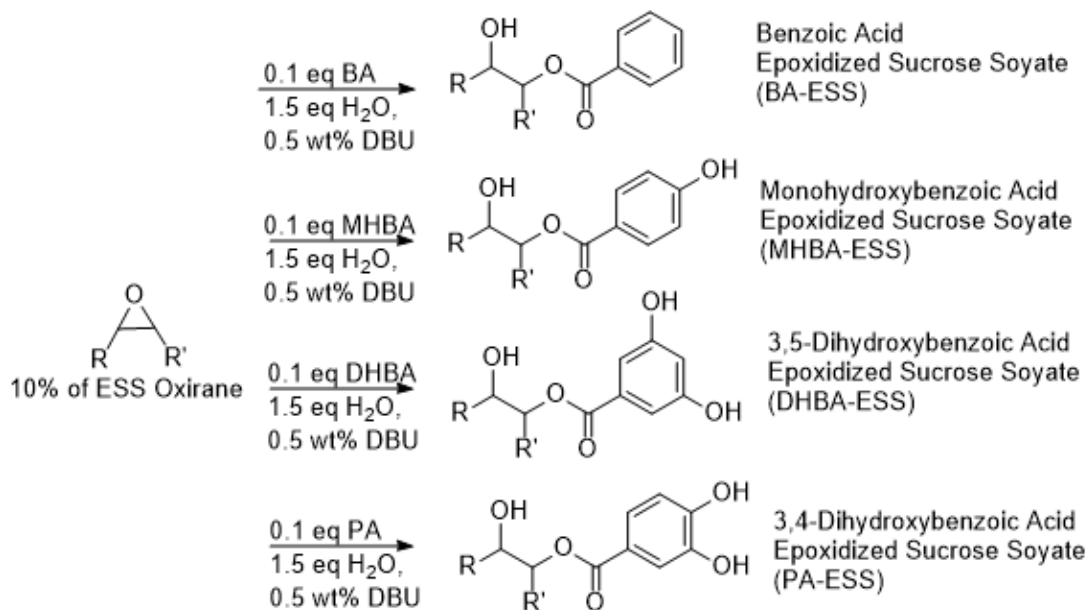
Figure 6.4. Synthetic Scheme to Produce ESS Catecholic Resins

The solids and epoxy equivalent weights of the modified ESS resins are seen in **Table 6.2**. The epoxy equivalent weight of the ESS used to make these resins is 236 g/eq. The new

EEWs show that more than 10% of the epoxies of ESS have been consumed and the non-volatile content is high. FTIR analysis in **Figure 6.5** showed signals corresponding to the appearance of new hydroxyl content (3500-3700 cm^{-1}), esters (1730-1750 cm^{-1}), aromatics (1585-1600 cm^{-1}), and residual epoxy (830 cm^{-1}).
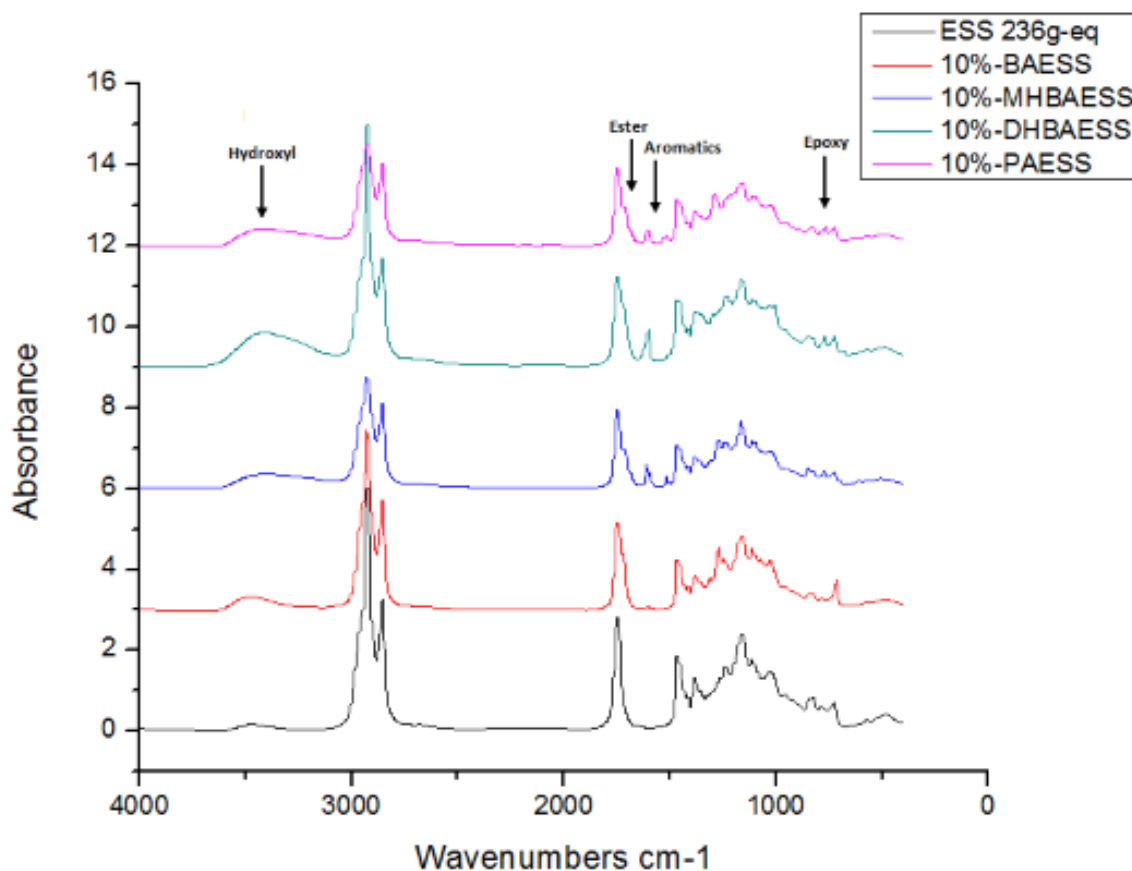
Figure 6.5. FTIR Analysis of ESS and the 10% Phenolic ESS Ester Resins

GPC analysis using a UV detector was carried out to see whether the adduct was formed and is presented in **Figure 6.6**. Ultraviolet adsorption is not seen in ESS, however UV absorption appears in the novel phenol ESS ester resins and corresponds to specific molecular weights. The molecular weight of the ESS utilized is 2717 g/mol and the molecular weights where UV absorption are seen show increases consistent with adduct formation. The UV absorption signals

occurring at larger molecular weights are oligomers formed as side reactions (hydroxyl-epoxy) during the functionalization step.

The rheological profiles of the phenolic ESS ester resins are seen in **Figure 6.7**. ESS and BA-ESS show similar rheological profiles while a slight increase is seen in MHBA-ESS. There is a large increase in viscosity with DHBA-ESS and PA-ESS. Upon higher shear rate, the dihydroxybenzoic ESS resins level at a similar viscosity. The increases in viscosity can be attributed to the hydroxyl content either or both from a vicinal hydroxyl to the new ester after ring-opening of the epoxide and phenolic hydroxyls. PESS had a viscosity at use of 1000 Pa-s. Its high viscosity is also due to hydroxyl content from both phosphonate content and a vicinal hydroxyl.

The appearances of the resins are seen in **Figure 6.8**. The phenolic ESS esters show significant color development given ESS is a transparent, colorless resin. BA-ESS took on an amber appearance, MHBA-ESS appeared light yellow, DHBA-ESS showed a remarkable dark brown color, and PA-ESS took on an amber appearance. Each of the resins remained transparent. This color difference is a remarkable instance where the minimal addition of chromophores with slightly different structures result in starkly different appearances.
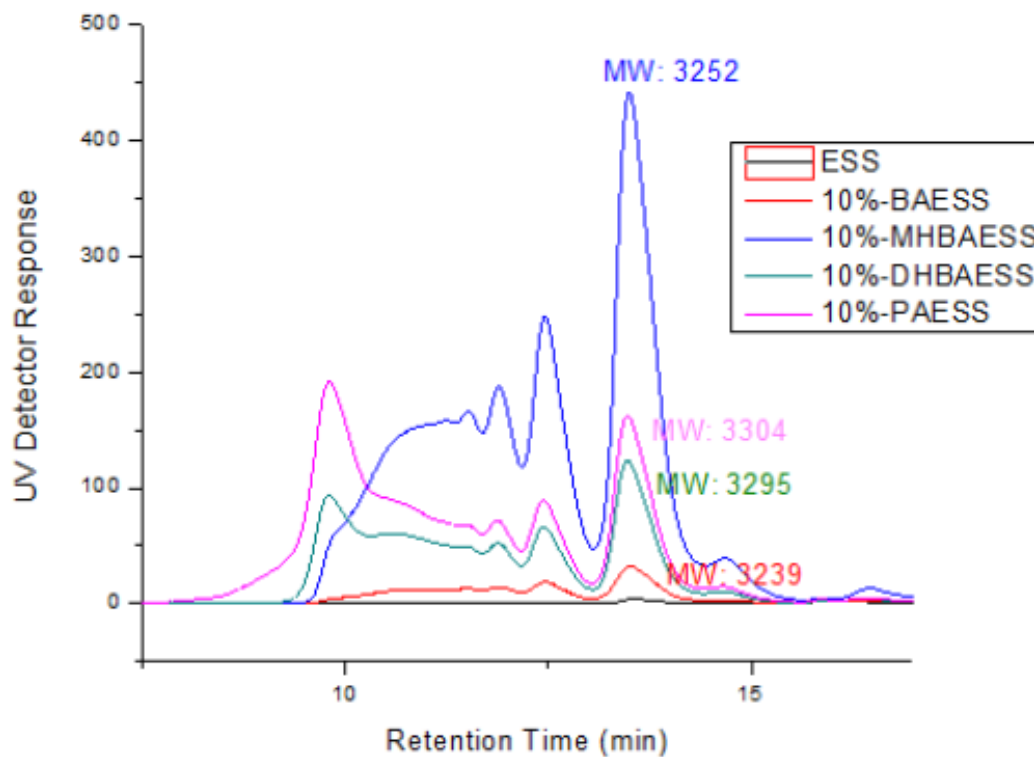
Figure 6.6. GPC Analysis Using a UV Detector of the Phenolic ESS Ester Resins
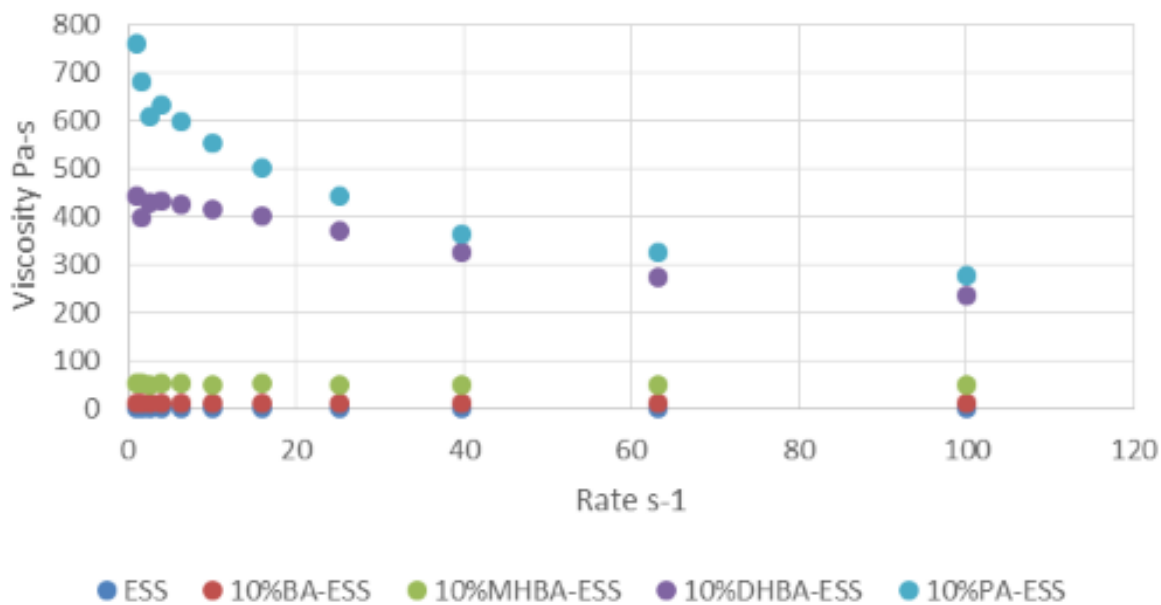
Figure 6.7. Rheological Analysis of ESS and the Phenolic ESS Ester Resins

114

Table 6.2. Percent Solids and Epoxy Equivalent Weights of the Phenolic ESS Ester Resins

Resin	10% BA-ESS	10% MHBA-ESS	10% DHBA-ESS	10% PA-ESS
% Solids	98.91	98.19	96.24	98.37
EEW (g/eq)	380.8	312.9	362.9	341.6
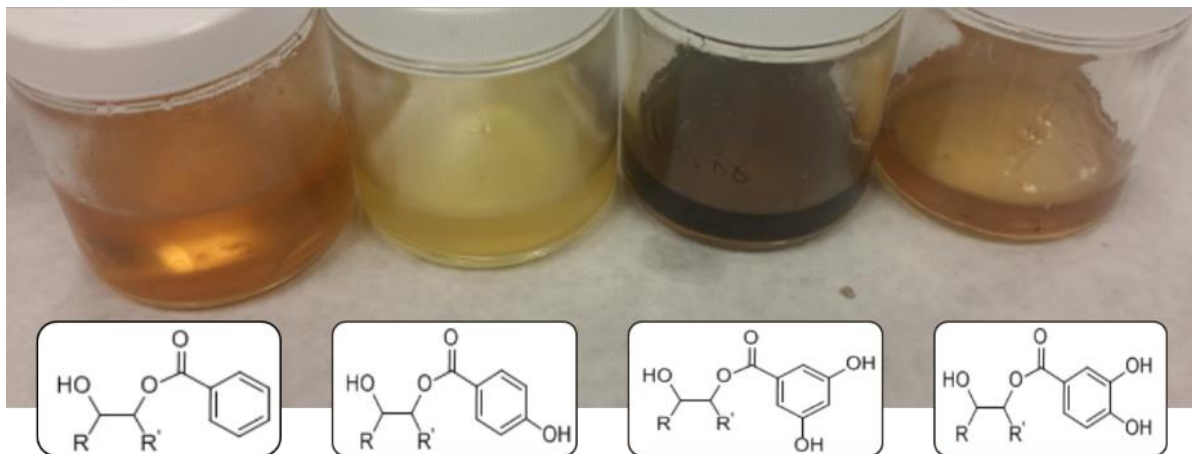
Figure 6.8. Appearances of the ESS-Derived Resins. Left to Right: 10% BA-ESS, 10% MHBA-ESS, 10% DHBA-ESS, 10% PA-ESS

The phenolic ESS ester resins were then incorporated into a 60-40 PHR ESS-CAE formulation (4 PHR photoinitiator) where 5, 10, 25, and 50% weight of the ESS added was replaced with each of the 4 resins. All coatings were tack free in a matter of seconds after UV exposure. All the coatings surpassed 400 MEK double rubs indicating that modifying some of the epoxies on ESS did not hinder solvent resistance, even when 50% weight of the ESS was replaced by the phenolic ESS ester resins The adhesion characterization via crosshatch adhesion of the resultant coatings on a variety of substrates are visible in **Figure 6.9**. The 5 and 10% replacements of ESS with phenolic ESS ester resins are not shown given there was no improvement to adhesion regardless of substrate.

It is apparent that for 25-50% amounts of ESS replaced with not only the catechol-containing ESS resin, there is an adhesion improvement on phosphated steel. In some cases, such

as for BA-ESS and DHBA-ESS, adhesion improvement was also seen on alodine-pretreated aluminum. It must be kept in mind that these resins only modified 10% of ESS epoxy content and are further diluted in the formulation given they are also mixed with ESS.

To see how incorporation of a large portion of these phenolic ESS resins into the formulation impact thermomechanical properties of the coating, DMA analysis was completed. The formulations with 50% weight replacement of ESS with the phenolic ESS ester resin were compared to a control 60-40 ESS-CAE formulation. Storage modulus (E') and tan δ curves are compiled in **Figure 6.10** as well as glass transition temperatures elucidated from the amplitude of the tan δ curves. The E' curve of the PA-ESS formulation shows an increase in storage modulus from between 50-100 °C. This indicates that further curing is occurring and is possibly due the vicinal hydroxyls on the aromatic ring. This is not seen in the MHBA-ESS and DHBA-ESS resins which also contain hydroxyls on the aromatic ring. MHBA-ESS shows a sharp decrease in E' at 140-150 °C. While further curing may be occurring during heating, the T_gs determined from the tan δ curves show that there is small increase in T_g for the formulations with BA-ESS, MHBA-ESS, and DHBA-ESS and a small decrease in T_g for PA-ESS indicating that even with a 50% weight replacement of ESS with the modified resins, T_g of the cured coatings is not impacted immensely.
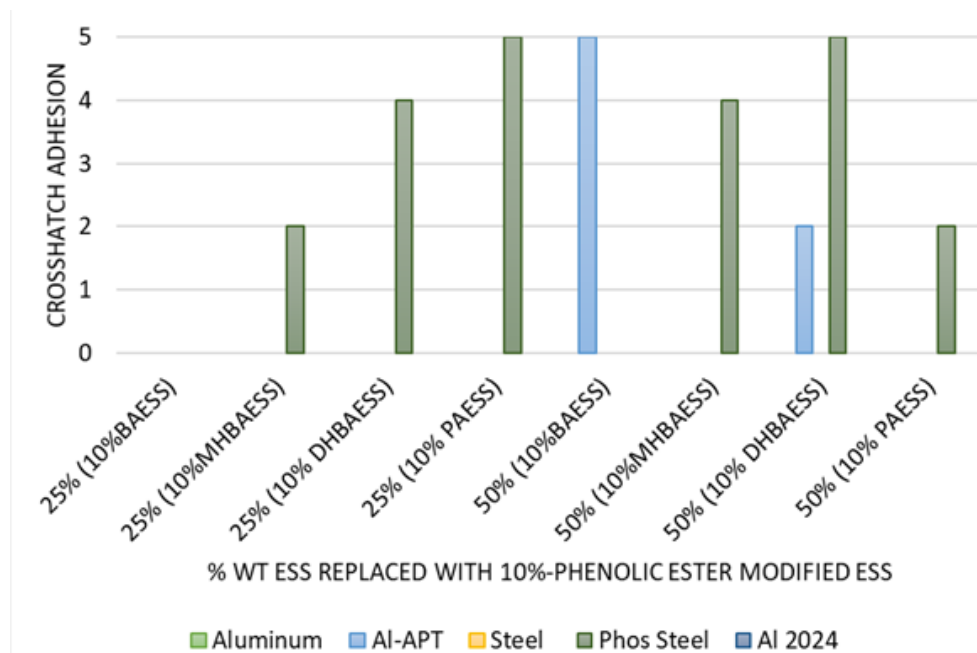
Figure 6.9. Crosshatch Adhesion of the 60-40 ESS-CAE Formulations with 25-50% Weight Replacement of ESS with 10% Phenolic Ester Modified ESS Resins
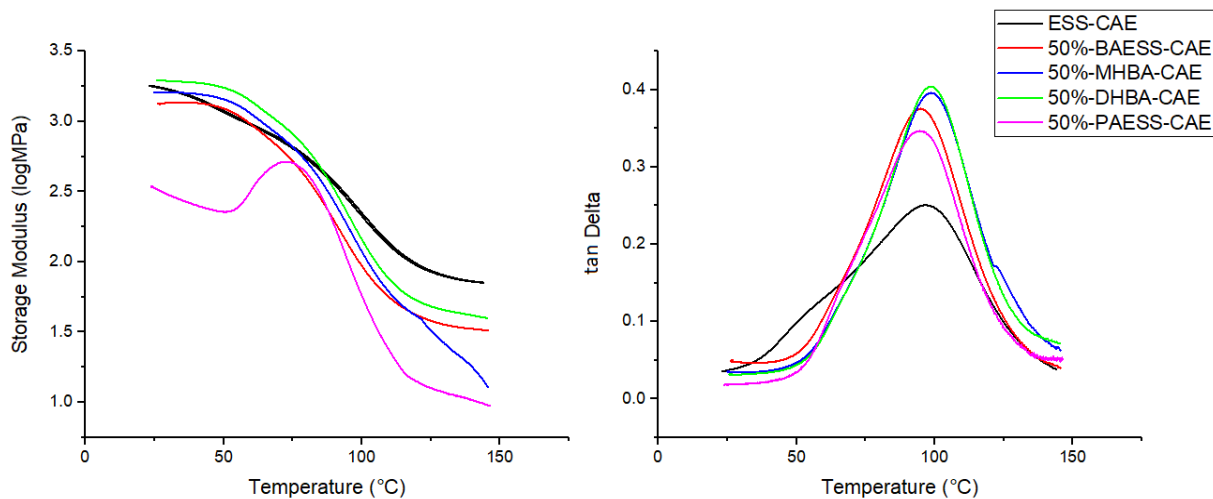
Resin 50% Weight Replacement of ESS in 60-40 ESS-CAE Formulation	Control	BA-ESS	MHBA-ESS	DHBA-ESS	PA-ESS
T_g (°C)	95.77	96.36	98.74	98.49	94.57

Figure 6.10. Storage Modulus (E') and Tan δ Curves of the 60-40 ESS-CAE Formulation with 50% Weight of the ESS Replaced with Phenolic ESS Ester Resin and T_gs (°C) Found via Tan δ Curves

PESS formulations and analysis were completed on 75-25, 80-20, and 90-10 ESS-CAE formulations where 3, 5, and 10% weight ESS was replaced with PESS given any higher replacement did not produce coatings that became tack free after long UV exposure. The adhesion of the PESS-coatings presented in **Figure 6.11** show that the best adhesion was seen at 5%-10% weight PESS regardless of the ESS-CAE ratio on Alodine-pretreated aluminum substrates. Further characterizations of the coatings are compiled in **Table 6.3**. It is seen that small amounts of PESS substitution result in softer coatings; significantly so with König hardness. There are mild improvements to rapid impact resistance, however the values still indicate very brittle coatings. Solvent resistance also decreases, in some cases almost by half with 5% PESS replacement. These results indicate that while adhesion to Alodine pretreated aluminum increases with small amounts of PESS replacement in the formulation, the coatings also become softer and less solvent resistant. This is likely due to less crosslinking available to make the network given there is less epoxy available on PESS.
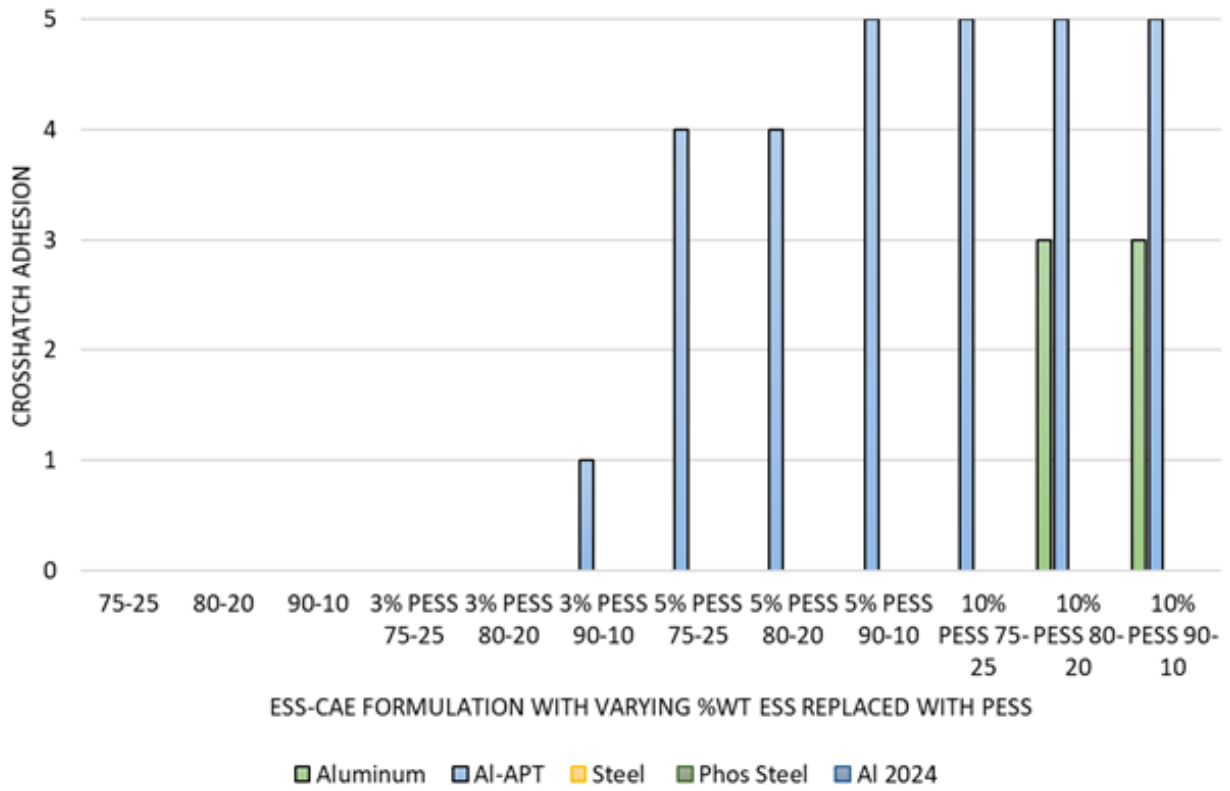
Figure 6.11. Crosshatch Adhesion of the ESS-CAE Formulations with Varying % Weight ESS replaced with PESS

Table 6.3. Properties of PESS and ESS-CAE Coatings on Alodine Pretreated Aluminum

Formulation ESS-CAE Ratio	% wt ESS Replaced with PESS	Film Thickness (ave 5, μm)	Pencil Hardness (gage)	Konig Hardness (ave 3)	Reverse Impact (in-lbs)	MEK DRs
75-25	0	52.8 ± 11	B	108 ± 12	<3.92	>400
80-20	0	44.9 ± 2	H	123 ± 2	<3.92	>400
90-10	0	56.5 ± 11	F	92.3 ± 2	<3.92	>400
75-25	3	60.2 ± 9	B	118 ± 13	<3.92	>400
80-20	3	57.2 ± 10	2B	105 ± 3	<3.92	>400
90-10	3	49.7 ± 10	2B	65 ± 5	<3.92	325
75-25	5	54 ± 12	HB	66.7 ± 9	5.88	380
80-20	5	47.3 ± 10	B	76 ± 6	<3.92	150
90-10	5	54.2 ± 13	B	45.7 ± 4	<3.92	210
75-25	10	58 ± 8	B	50.2 ± 9	5.88	400
80-20	10	43.1 ± 9	F	59 ± 6	5.88	310
90-10	10	73.7 ± 7	2B	54.7 ± 2	7.06	>400

Conclusions

Epoxidized sucrose soyate was shown to be able to be modified with phenolic ESS ester resins. These viscous resins were incorporated into an ESS-CAE UV-curable coating formulation and tested for crosshatch adhesion on a variety of substrates. While the coatings cured quickly under UV-exposure, showed high solvent resistance, and similar T_gs to the control, adhesion improvement was seen with several of the phenolic ESS ester resins with 25-50% weight replacement of ESS in the formulations when applied to phosphated steel. Larger amounts of replacement of ESS with these resins is of interest as well as further investigation of the adhesion improvement given it was not only the catechol-containing resin demonstrated adhesion improvement.

Phosphonated ESS was also incorporated into several ESS-CAE formulations. At amounts larger than 10% incorporation, the coatings were unable to become tack free after long UV exposure. It was seen that at 5-10% PESS replacement there was adhesion improvement to Alodine pretreated aluminum substrates, however the coatings became softer and less solvent resistant.

References

1. Kim, Won-Seock, et al. *I. J. Adh. & Add.,* **2010**, *30.6*, 408-417.

2. Alfano, Marco, et al. *J. of Adh.,* **2014**, *90.5*, 384-400.

3. Khramov, A. N., and J. A. Johnson. *Prog. Org. Coat.,* **2009**, *65.3*, 381-385.

4. Wapner, K., M. Stratmann, and G. Grundmeier. *Int. J. Adh. & Add.,* **2008**, *28.1*, 59-70.

5. Illy, Nicolas, et al. *Pol. Chem.,* **2015**, *6.35*, 6257-6291.

6. T. Kowalik , H. J. P. Adler , A. Plagge and M. Stratmann , *Macromol. Chem. Phys.*, 2000, **201** , 2064 -2069

7. Silverman, Heather G., and Francisco F. Roberto. *Mar. Biotech.*, **2007**, *9.6, 661-681.*

8. Crisp, D. J., et al. *J. Coll. Int. Sci.,* **1985**, *104.1*, 40-50.

9. Bandara, Nandika, Hongbo Zeng, and Jianping Wu. *J. Adh. Sci. & Tech.,* **2013**, *18*, 2139-2162.

10. Watanabe, Hirohmi, et al. *Lang.,* **2016**, *32.18*, 4619-4623.

11. Lee, Bruce P., et al. *Ann. Rev. Mat. Res.*, **2011**, *41*, 99-132.

12. Lee, Haeshin, et al. *Sci.,* **2007**, *318.5849*, 426-430.

13. Faure, Emilie, et al. *Prog. Pol. Sci.,* **2013**, *38.1*, 236-270.

14. Pan, Xiao, Partha Sengupta, and Dean C. Webster. *Green Chem,* **2011**, *13.4*, 965-975.

15. Pan, Xiao, Partha Sengupta, and Dean C. Webster. *Biomac.,* **2011**, *12.6*, 2416-2428.

16. Arvin, Z. Yu, Jonas M. Sahouani, and Dean C. Webster. *Prog. Org. Coat.*, **2018**, *122*, 219-228.

17. Paramarta, Adlina, Xiao Pan, and Dean C. Webster. *Radtech Rep.,* **2013**, *1*, 26-32.

18. P.P. Sengupta, X. Pan, T.J. Nelson, A. Paramarta, D.C. Webster, PMSE Prepr. **2010**, *102*, 888-889.

19. Nelson, Thomas J., et al. *J. Renew. Mat.,* **2013**, *1.2*, 141-153.

20. Yan, J, Webster, DC. *Green Mat.*, **2014**, *2.3*, 132-143.

21. Taft, D., and R. Schmidt. "Novel cured compositions prepared from the reaction of a polyisocyanate and a hydroxybenzoic acid capped epoxide-containing material." U.S. Patent No. 3,789,044. 29 Jan. 1974.

22. Ménard, Raphaël, et al. *RSC Adv.,* **2015**, *5.87*, 70856-70867.

CHAPTER 7. FUTURE DIRECTIONS

The Projected Future of Bioderived Alternatives

The interest in bio-derived polymers has and continues to grow as alternatives are sought for fossil fuel-based polymers. On top of innovative research and customer demands for biobased materials, government initiatives such as *BioPreferred* strive to increase the number of biobased products being purchased and utilized by manufacturers and consumers. This USDA program (started in 2002 and expanded under the 2014 Agricultural Act) looked to "spur economic development, create new jobs and provide new markets for farm commodities." Further justification came from the potential increase in use from renewables, reduction of harmful environmental and health impacts, and a lessened reliance of the USA on petroleum products as a result of the initiative. Specifically, the initiative works to reach its goals by emplacing mandatory purchasing requirements for government agencies (and their contractors) of bioderived products. Also, to allow consumers to be more aware of sustainable options, a voluntary labeling initiative where a business' verified product can display a USDA Certified Biobased Product label was implemented.[1]

While initiatives such as these are encouraging, broader implementation lies within cost and performance to the extent that large-scale processing and development of bioderived alternatives are more attractive than currently established petrochemical processes. Currently, oil prices have not risen to the extent to encourage this shift and bioreneweable polymers carry a low market share (<5%). However, as the innovation and price of large-scale biorefineries decrease, and material performances increase, alternatives may prove more competitive and share will increase concurrently.[2]

While there are many encouraging signs that bioderived feedstocks will increase in the future, the utilization of alternatives is not without its own environmental concerns. Issues can be exacerbated or mitigated depending on the choice of crops and how they are cultivated. For example, issues that arise from monocrop development can infringe on crops going towards consumables, increases in soil erosion, increase in transporting vehicles that utilize petrofuels, nutrients and pesticides can leach into waters, and the harm to biodiversity and natural lands to be developed for agriculture.[3]

It can be argued that the most environmentally friendly elements in designing products involve engineering maximum performance with the absolute minimum material used, minimum or no waste generated, and the smallest impact on the environment. These ideas compose the growing field of *sustainable design*.[4] Aspects of sustainable design can be applied to a material such as ESS. The studies mentioned not only vamped up the renewable sources to produce ESS, but also stressed the versatility of the material through its functionalization and incorporation into a variety of thermosets. Future work and directions for ESS will further strive to make it an attractive material for sustainable design of products. This will involve improvements to the mentioned studies and other possible thermosets where ESS and derivatives can be incorporated.

ESS in Non-Isocyanate Polyurethanes

The benefits concluded in the Chapter 2 study are that a safer route for an ambiently curable, non-isocyanate polyurethane can be made from bioderived polycarbamates and dialdehydes where the precursors do not involve the use of phosgene. Not only did this demonstrate that ESS derivatives can be functionalized to be a polycarbamate, it expanded the array of dialdehyde crosslinkers over the conventional 1,3 and 1,4-cyclohexanedicarboxaldehyde. To even further expand this thermosetting technology, it was

mentioned in **Figure 7.1** the synthetic route to make less viscous ESS polyols by using longer-

chain alcohols during alkoxylation. These derivatives can in turn be modified to make less

viscous polycarbamates. Further studying ESS polyols and their subsequent transcarbamoylation

and assessment is merited. However, designing and assessing an even more expanded library of

dialdehyde crosslinkers should be the focus. Natural products from biomass contain unique

structures which are not feasible to obtain through chemical synthesis. Thus, there are a plethora

of bioderived materials that can introduce unique and potentially advantageous properties to the

NIPUs. While aldehydes from HMF dimers with additions of groups on their carbon bridge were

made and tested alongside aldehydes with lignin-derived aromatic structures, saturation of the

furan rings to saturated furanics or hybrid dialdehydes of benzo-furanic structures are further

routes to explore. Examples of these options are seen in **Figure 7.2**.
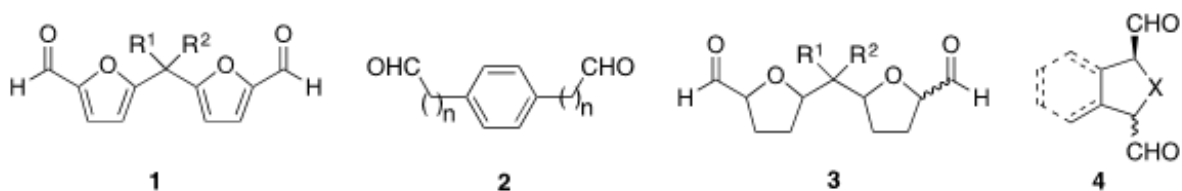
Figure 7.1. Examples of Dialdehyde Structures which can Expand the Library of Carbamate-
Aldehyde Crosslinking to Produce NIPUs. 1. Difuranic Aldehydes with Modifications at the
Carbon Bridge. 2. Lignin Derivative Dialdehydes with Extended Aldehyde Chains

While introducing a variety of novel structures into the thermoset will expand the

structure-function relationship understandings of bulk, a deeper understanding of the

crosslinking chemistry is equally valuable. Notably, there has not been much scrutiny of the

difference between the crosslinking of a cycloaliphatic and an aromatic dialdehyde. While DFF

was able to successfully participate in NIPU formation like CHDA, the properties of the coatings

may not only be different because of the structure of the dialdehydes, but *how* the dialdehydes

crosslink. CHDA, as shown in **Figure 2.1**, has been determined by *Argyropoulos et al* to form

full aminal, hemiaminal, and u-olefin linkages through ^{13}C-NMR studies.[4] The crosslinks

occurring with DFF and polycarbamate are currently being investigated by Mukund Sibi's group

at NDSU Chemistry through ^{1}H-NMR studies. Initial conclusions show a starkly different

process than CHDA; DFF reacts twice with polycarbamate on *one* side. This is illustrated in

Figure 7.2. Better understanding the aromatic character of DFF (and other aromatic, bioderived

aldehyde crosslinkers) and its contribution to the kinetics of the reaction may lead to precision

engineering of structures to create thermosets that have optimum bulk properties but also aspects

of processing and handling.
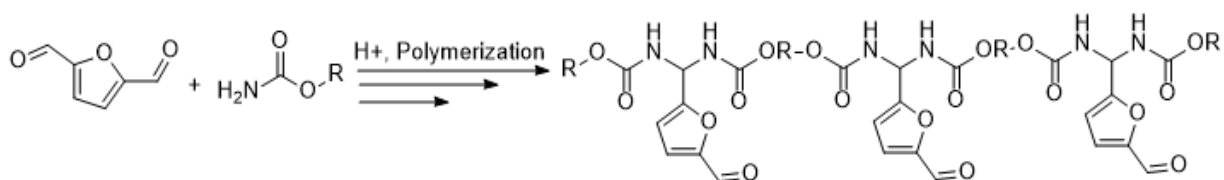
Figure 7.2. DFF Reaction with Polycarbamate

ESS in Stereolithographic Inks and Additives

Improving the properties of ESS derivatives in stereolithographic inks can involve other

acrylate structures by exploring a wider variety of acrylic acids and anhydrides. Further, there

has not been a study investigating a wider variety of photoinitiators compatible with the 405 nm

SLA printer's laser. Optimization of the cure and post-cure regimes for the formulations

including ESS acrylics is also necessary given cracking was observed in several thermosets.

Strengthening additives to build upon what was seen with *m*-POSS can also be explored to make

stronger or more easily processable prints. Cardolite, the supplier of bioderived CGE in the UV-

curable coatings study, also is in development of a cardanol acrylate which may be a valuable

plasticizing additive that can reduce cracking in prints. The Ulven group at NDSU Engineering is

currently exploring SLA thermosets with oriented structural reinforcement that comes from

carbon fiber. They are also investigating ESS acrylics in their studies.

Another avenue that can be investigated is the field of interpenetrating networks (IPNs) in stereolithography. IPNs are made when different prepolymers are polymerized using orthogonal (or non-interfering) initiators. In stereolithography, IPNs are of interest where acrylic and epoxy prepolymers are combined.[5-8] The acrylic contains a photoinitiator free-radical propagating mechanism while the epoxy progresses through cationic ring-opening. ESS and its derivatives have been seen to be polymerizable with both mechanisms, so it may be possible to combine ESS, ESS acrylics, and other epoxy or acrylic resins/additives into the formulation with different photoinitiators to make an IPN SLA ink. The challenge with cationic ring-opening photoinitiators, particularly those from iodonium salts, are that they are not actinic at the wavelength of the SLA printer's laser. This may necessitate the addition of a sensitizer such as isopropylthioxanthone which is actinic at that wavelength and in its excited state can then activate the cationic photoinitiator.[9] However, the implementation of a 2-stage curing process may also suffice. That is, printing the material so that the acrylic is able to cure and act as a scaffold for the uncured epoxy resin. Then, the print will be placed in a UV chamber that can activate the epoxy photoinitiator and fully cure the network. This route will need optimization to prevent issues of shrinkage and strain on the network during each curing cycle that can result in cracking. Likewise, the issue of thick prints being fully cured (aside from just at the surface) is a concern.

ESS in UV-Curable Coatings

There has not been an expanded look at UV-initiated crosslinking of ESS with other reactive diluents than CAE and photoinitiators for coatings. There have been studies accumulating libraries of biobased epoxy crosslinkers from such as furan-based and vanillyl alcohol glycidyl crosslinkers.[10-12] It is of utmost important to either modify existing architectures

or find epoxy resin alternatives which can be liquid at room temperature. This will ensure that the UV-curable formulation has facile processing, does not necessitate solvents and VOCs, and can ensure a high-solids process.

Other ESS and Life-Cycle Assessments

Recent publications show that ESS has expanded its use in the field of biotechnology through its use as a slow-release drug encapsulator.[13] While its utility in a variety of fields continues to be demonstrated, assessing the environmental impact of ESS and its incorporation in thermosets have not been determined. Life-cycle analysis (LCA) is field of study where a cradle-to-grave analysis is completed for a material to assess its environmental balance. Specifically, it compiles the impact from raw material extraction (which can include land development for crops on top of aspects of harvest), how it is processed, transported, manufactured, distributed, maintained/replaced, and recycled or disposed of.[14] An LCA analysis comparing ESS thermosets to a petrochemically-derived counterpart may further encourage consumers or businesses to adopt ESS materials or it may elucidate where there is room for improvement to make bioderived products more attractive from an environmental standpoint.

References

1. United States Department of Agriculture. About the BioPreferred Program. https://www.biopreferred.gov/BioPreferred/faces/pages/AboutBioPreferred.xhtml, Accessed 8/12/19.

2. Lligadas, Gerard, et al. *Mat. T.,* **2013**, *16.9*, 337-343.

3. Parris, Kevin. *Agriculture, biomass, sustainability and policy: an overview.* OECD Publication Service, Paris, 2004. Page 30-36.

4. Attributes John Argyropoulos, Nahrain Kamber, David Pierce, Paul Popa, Yanxiang Li and Paul Foley, "Isocyanate Free Polyurethane Coatings – Fundamental Chemistry and Performance Attributes", *European Coatings Congress*. April 21, 2015 presentation.

5. Li, W., et al. *Exp. Pol. Lett.,* **2016**, *10.12*.

6. Nowers, Joseph R., and Balaji Narasimhan. *Pol.,* **2006**, *47.4*, 1108-1118.

7. Kuang, Xiao, et al. *Macro. Rap. Comm.*, **2018**, *39.7*: 1700809.

8. Zhao, Yining, et al. "Preparation of a hybrid photopolymer for stereolithography." *5th International Conference on Advanced Design and Manufacturing Engineering*. Atlantis Press, 2015.

9. Barker, Ian A., and Andrew P. Dove. *Chem. Comm.,* **2013**, *49.12*, 1205-1207.

10. Hernandez, Eric D., et al. *ACS Sus. Chem. & Eng.,* **2016**, *4.8*, 4328-4339.

11. Stanzione III, Joseph F., et al. *Green Chem.,* **2012**, *14.8*, 2346-2352.

12. Hu, Fengshuo, et al. *Macromol.,* **2014**, *47.1*, 3332-3342.

13. Chitemere, Ruvimbo, et al. *Pol.,* **2018**, *10.6*, 583.

14. Grabowski, Alix, et al. *Int. J. LCA,* **2015**, *20.5*, 584-596.